12-2016

# Assessing fuel burn inefficiencies in oceanic airspace

Stephen Builta
*Purdue University*

# ASSESSING FUEL BURN INEFFICIENCIES IN OCEANIC AIRSPACE

by

**Stephen Builta**

**A Thesis**

*Submitted to the Faculty of Purdue University*

*In Partial Fulfillment of the Requirements for the degree of*

**Master of Science in Aeronautics and Astronautics**


Department of Aeronautics and Astronautics

West Lafayette, Indiana

December 2016

# THE PURDUE UNIVERSITY GRADUATE SCHOOL
# STATEMENT OF THESIS APPROVAL

Dr. Karen Marais, Chair

Department of Aeronautics and Astronautics

Dr. William A. Crossley

Department of Aeronautics and Astronautics

Dr. Steven Landry

Department of Industrial Engineering

**Approved by:**

Dr. Weinong W. Chen

Head of the Departmental Graduate Program

*Dedicated to my parents, Kevin and Denise*

# ACKNOWLEDGMENTS

First, I would like to thank my advisor, Dr. Marais, for her endless advice and encouragement. She provided opportunities for growth which have help me immensely.

The PTM project leads at NASA Langley, Michael Koch, Jennifer Kibler, and Ryan Chartrand have been essential in assisting my research through timely feedback and domain knowledge.

Fellow grad students such as Arjun, Nicoletta, Divya, Rakshit, and George have provided great all-around support, from reviewing documents to alerting me to relevant papers to being enjoyable conversationalists. Dreary nights in the office were made better by their presence.

Many thanks to Harish for seeing one of my problems and connecting it to work done in a completely different field. His domain expertise enabled me to build a better solution for optimizing trajectories.

Finally, I thank my parents for their wise counsel, emotional support, and technical advice. They have been, and will always be, a foundational element to my success.

Truly, Soli Deo gloria.

This research was partially funded by the National Aeronautics and Space Administration (NASA) through the National Institute of Aeronautics (NIA) under contract # NNL13AA08B-NNL15AC17T

# TABLE OF CONTENTS

# LIST OF TABLES

# LIST OF FIGURES

# NOMENCLATURE

| | |
|---|---|
| $C_{D0}$ | BADA Parasitic drag coefficient |
| $C_{D2}$ | BADA Induced drag coefficient |
| $C_{f1}$ | BADA 1st thrust specific fuel consumption coefficient |
| $C_{f2}$ | BADA 2st thrust specific fuel consumption coefficient |
| $C_{fr}$ | BADA cruise fuel flow correction coefficient |
| $D$ | Drag |
| $\delta$ | Ratio of pressure to sea-level ISA standard |
| $\eta$ | Thrust specific fuel consumption |
| $\dot{f}$ | Fuel burn rate |
| $g_0$ | Gravitational Acceleration |
| $h_{Geod}$ | Geodetic Altitude |
| $h_{geop}$ | Geopotential Altitude |
| $h_{press}$ | Pressure Altitude |
| $M$ | Mach number |
| $m$ | Aircraft mass |
| $P$ | Pressure |
| $T$ | Thrust |
| $t$ | Time |
| $\tau$ | Ratio of thrust to sea-level maximum thrust |
| $\theta$ | Ratio of temperature to sea-level ISA standard |
| $V_{TAS}$ | True Airspeed |

# ABSTRACT

Author: Builta, Stephen, M. MSAAE
Institution: Purdue University
Degree Received: December 2016
Title: Assessing Fuel Burn Inefficiencies in Oceanic Airspace
Major Professor: Karen Marais

Increasing the efficiency of aircraft operations offers a shorter term solution to decreasing aircraft fuel burn than fleet replacement. By estimating the current airspace inefficiency, we can get an idea of the upper limit of savings. Oceanic airspace presents a unique opportunity for savings due to increased separation differences vs. overland flight.

We assess fuel burn inefficiency by comparing estimated fuel burn for real world flights with the estimated optimal fuel burn. For computing fuel burn, we use the Base of Aircraft Data (BADA) with corrections based on research by Yoder (2005). Our fuel burn results show general agreement with Yoder's results.

Optimal operation depends on flying 4-D trajectories that use the least amount of fuel. We decompose optimal 4-D trajectories into vertical and horizontal components and analyze the inefficiencies of each separately.

We use the concept of Specific Ground Range [Jensen, 2011], to find optimal altitudes and speeds. We combine the optimal altitudes and speeds with an aircraft proximity algorithm to find pairs of aircraft in a vertical blocking situations.

To find the fuel optimal horizontal track in a wind field, we use methods from the field of Optimal Control. The original problem formulation can be transformed into a Two Point Boundary Value problem which we solve using MATLAB's bvp4c function.

From our set of flights, we hypothesized a scenario where aircraft stack in such a way that they cannot climb to their optimal altitudes because of separations standards. Using aircraft

positions we find when aircraft were within separation standards and were blocked from climbing or descending to their optimal altitude. We split our inefficiency results into a blocked and non-blocked set to see if blocking had an effect on mean inefficiency.

Our set of flights consisted of real world flights that flew through WATRS and CEP airspace regions during the month of April 2016. Using the optimal altitude for actual flight Mach profiles, we compute a mean inefficiency of 4.75% in WATRS and 4.50% in CEP, both of which are roughly 2 to 2.5 percentage points higher than studies using proprietary performance models and data. BADA overestimates optimal altitudes, leading to an overestimate in inefficiency. Inefficiency due to off-optimal speed for WATRS is 2.18% vs. 1.86% in CEP.

Blocking events result in a 2.59 percentage point increase in mean inefficiency due to off-optimal altitude in WATRS flights, and a 1.21 percentage point increase in mean inefficiency due to off-optimal altitude in CEP flights.

Using wind-optimal horizontal tracks gave a 1.24% mean inefficiency in WATRS, and a 0.41% mean inefficiency in CEP.

The results indicate that, in total, flights through WATRS and CEP have approximately the same inefficiency due to off-optimal altitudes, but that blocking effects are more prevalent in WATRS. In addition, flights through WATRS are farther from their wind-optimal horizontal tracks than flights in CEP.

# CHAPTER 1. INTRODUCTION

## 1.1 Introduction

Burning fuel in aircraft engines is expensive and results in pollutants, such as soot, nitrous oxide, and greenhouse gases. There are three main ways to reduce fuel burn: (1) use more fuel-efficient aircraft, (2) fly less, and (3) fly more fuel efficiently. The first option has the potential for the most long-term impact, but, because aircraft tend to be long-lived assets, it will take several decades before all the older, less fuel-efficient aircraft are replaced. The second strategy is unlikely to be possible, given that the world's population is both growing and becoming more affluent and therefore more likely to fly. The third option has the potential for near-term improvements in the single digit percentage range.

Many researchers have considered ways of flying more efficiently, see Marais et al. (2012) for a review of operational improvements. Here, our focus is on the fuel-efficiency of one particular type of operations: oceanic flight. Oceanic flight may offer the potential for significant fuel efficiency improvements because aircraft tend to be spaced much more widely than over the land, where there is near 100% surveillance. As a result, researchers have proposed ways of identifying fuel-optimal trajectories (e.g., Ng et al. (2014), Sridhar et al. (2015), Grabbe et al. (2006), Dalmau et al. (2015)) and efforts are underway to provide oceanic surveillance (e.g., space-based ADS-B).

But just how inefficient are these operations? And how much potential do they actually offer for improvement in practice? Currently, estimating inefficiency is either done on an individual flight level, or, for whole sets of routes using highly sophisticated simulation tools, or, in-house by airlines using closely guarded data. We develop a method for estimating inefficiency of flights through oceanic airspace using public data to research the effectiveness of an alternate source to closed data and to investigate the fuel burn inefficiency in select airspaces. This method allows us to compute the inefficiencies due to

flying off optimal altitudes, speeds, and horizontal tracks in the presence of winds. Figure 1 graphically represents the process for computing inefficiency.

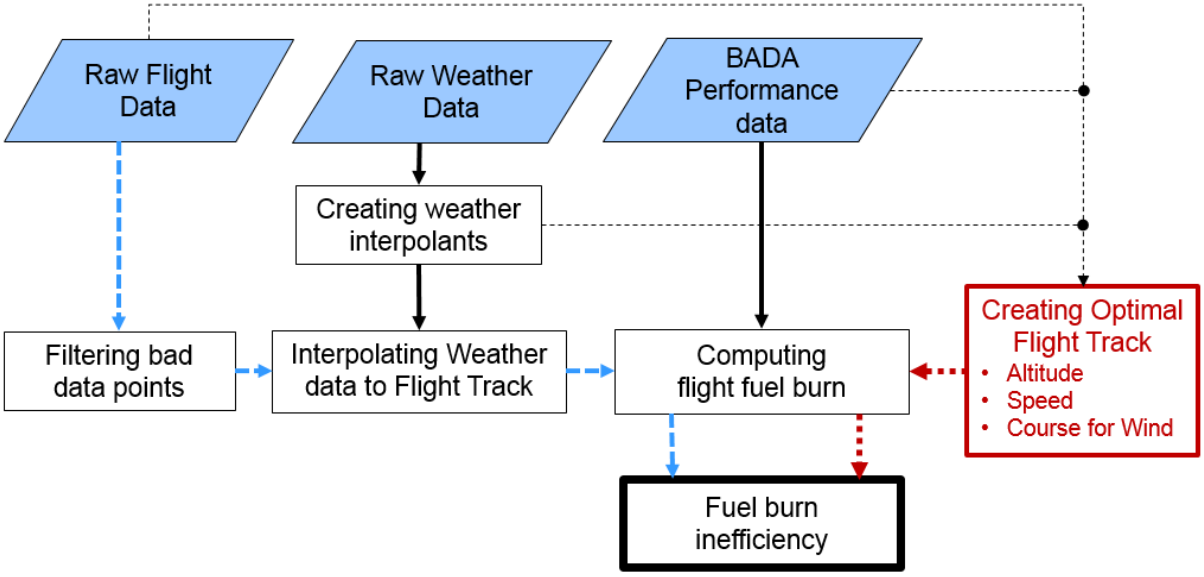


Figure 1: Process flowchart

## 1.2 Thesis Outline

We use Chapter 2 to discuss research done on the various types of inefficiencies. Chapters 3, 4, and 5 contain the methods we use to investigate horizontal, vertical and speed, and blocking inefficiencies respectively. Chapter 6 describes how we estimate fuel burn. We apply the methods on selected segments of oceanic airspace in Chapter 7 and then discuss conclusions and future work in Chapter 8.

# CHAPTER 2. BACKGROUND

At its core, inefficiency is a comparison of an actual state against an optimal state. The choice of optimal state will set the sense of the inefficiency metric. For example, airlines generally aim to maximize profit, which translates to goals of minimizing cost and maximizing revenue. Fuel burn makes up a significant part of airline operating costs so reduction of fuel burn is a priority. Figure 2 shows the trend in total fuel cost and percent of operating expense to worldwide airlines.

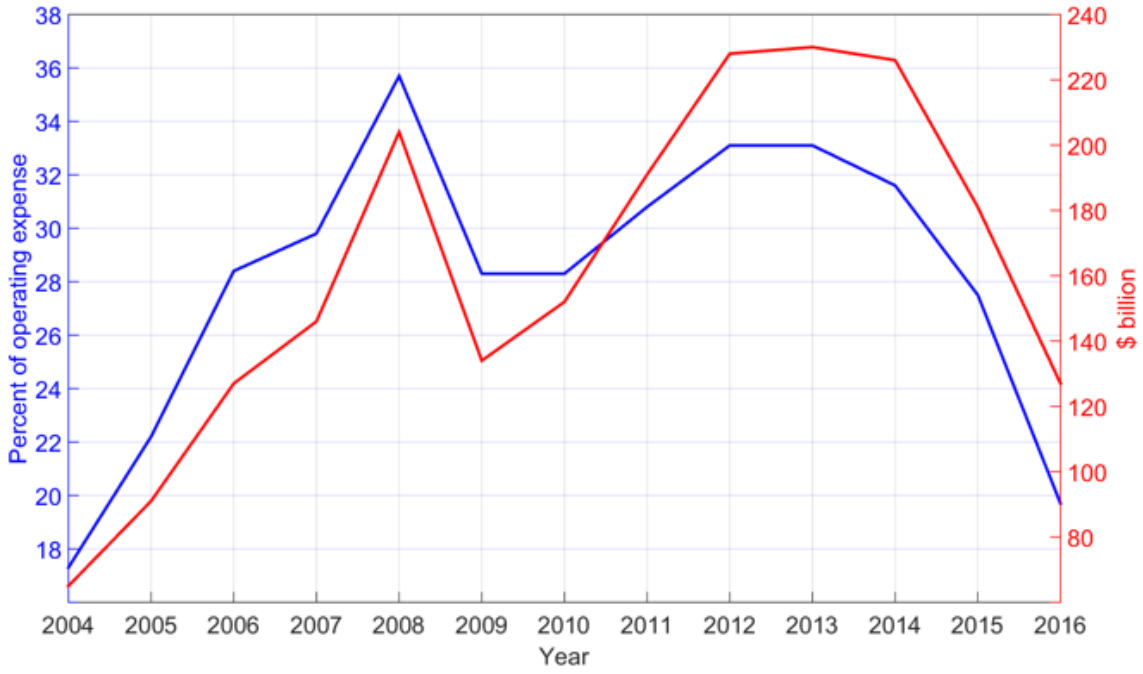


Figure 2: Fuel cost to airlines worldwide (IATA, 2016)

Demand shows a sensitivity to travel time, where slower flights show decreased demand, especially among business travelers [Belobaba, 2009]. Airlines take the tradeoffs between time and cost into consideration by planning flights around a metric called the “cost index”. Cook et. al. (2007) describe cost index as a sliding scale between maximum fuel savings and maximum time savings. For our research, we considered inefficiency against maximum fuel savings.

## 2.1 Inefficiency Sources

Marais et al. (2012) considered different sources of inefficiencies, each arising from different phases and aspects of a flight. Here, we discuss inefficiencies that we suspect are significant in cruise flight through oceanic airspace.

### 2.1.1 Minimum Separation Standards Inefficiencies

To maintain safety, aircraft are separated by minimum distances at all times, depending on the phases of operation and the capabilities of air traffic control. During takeoff and landing, aircraft are separated to avoid wake turbulence and to allow each aircraft to clear the runway. During cruise, lateral, longitudinal, and vertical separations are defined to allow air traffic control enough time to intervene in the event of loss of separation. Over the land, horizontal separation can be as little as 3 nm, but in spaces without surveillance, like most of the oceanic airspaces, separation is at least 30 nm. Vertical separation is usually 1000 ft or 2000 ft, depending on the location, as discussed next.

### 2.1.2 Vertical Separation

Vertical spacing is important because aircraft cruise most efficiently at their optimal altitudes and spend the most time at cruise. One way to improve fuel efficiency during cruise is to open more cruise altitudes for aircraft in a scheme called Reduced Vertical Separation Minimums (RVSM). RVSM reduced the vertical spacing at cruise altitudes to 1000ft between aircraft.

A Eurocontrol study found that RVSM provided fuel savings of 1.6 to 2.3% to RVSM [Jelinek, 2002]. Malwitz et al. (2007) examined the impact of RVSM on fleet wide fuel burn by computing fuel burn for a sample of flights before and after the implementation of RVSM. They found that while BADA's specific fuel consumption (SFC) value is good for fleet-wide performance estimates (e.g., total fleet fuel burn), it is not accurate for sensing small changes in operations, such as RVSM. They used Cockpit Flight Data Recorder (CFDR) data to improve the BADA suggested method for computing specific fuel

consumption. They found that RVSM led to savings of 1.8% ± 0.5%, in line with the Eurocontrol study.

### 2.1.3 Lateral and Longitudinal Separation

Reducing minimum separation can reduce inefficiency by allowing more aircraft onto great circle or wind optimal routes. In the North Atlantic, Williams & Greenfeld (2006) showed fuel savings benefits on the order of 0.1%. However, because this benefit is so small, it only yields significant total fuel savings when applied across many flights. The net saving per flight can be less than $100.

### 2.1.4 Cruise Altitude and Speed Inefficiencies

At each point in time, aircraft have fuel-optimal cruise speeds and altitude based on their mass. Ideally, aircraft should gradually increase their altitude and airspeed as they burn fuel. Unfortunately, air traffic restrictions will often prevent aircraft from flying in this way. In particular, while aircraft may be able to fly at an "average" good altitude and speed, cruise climb is difficult to implement. Step climbs, whereby aircraft increase their altitude in discrete steps, are a reasonable approximation to true cruise climb. Steps climbs are theoretically possible under current airspace rules, provided the steps are selected to correspond to permitted flight levels (even or odd flight levels depending on flight direction).

Ng et al. (2014) found that step climbs could reduce fuel burn by 1–3% on a subset of Pacific transcontinental flights compared to using a fixed cruise altitude. They used the BADA standard specific fuel consumption model (see Section 6.2). In turn, Dalmau and Prats (2015) found that cruise climbs could save 0.5–2.0% fuel compared to step climbs. They had engine performance data from Airbus and could therefore get more accurate results than is possible using BADA. Finally, Jensen (2014), estimated that the maximum average benefit due to altitude optimization alone (i.e., no speed optimization) was 1.94%.

The preceding studies suggest that not allowing aircraft to perform step or cruise climbs imposes a maximum fuel burn penalty of about 2%.

## 2.2 Trajectory-related Inefficiencies

Smart usage of winds can increase fuel efficiency. While many aircraft currently use jet streams and great circle routes, these routes are not always feasible due to factors like airspace restrictions, traffic, and weather. The exact savings from taking wind-optimal routes for a flight depends on the characteristics of that flight. For example, a delayed flight could regain some time by taking the wind-optimal routes. On the other hand, a normal flight may not want a faster than planned trip because of scheduling concerns (e.g. gate or runway not available). Larger and heavier aircraft may gain more benefit from wind-optimal routes than smaller and lighter aircraft.

One of the first considerations of optimization of an aircraft's trajectory through a wind field was given by Ernst Zermelo in 1930. In 1975, Bryson and Ho elaborated on the Zermelo problem in their text on optimal control where they presented an example of a minimum flight time trajectory in a wind field, assuming a flat Earth.

Sridhar et al. (2011) removed the flat-earth assumption from the optimal control approach and added a term to the cost function penalizing contrail generation, in addition to flight time and fuel burn. They found 6-8% extra fuel consumption was needed to reduce contrail formation time from 55 minutes to 20 minutes. They further modified their method using different cost functions in Ng et al. (2011, and 2014).

Jardin and Bryson (2012) revisited the problem from Bryson and Ho, extending the problem to a spherical earth and solving by using two different numerical approaches. Comparing trajectories between SFO and JFK, they found a 1 to 19 minutes travel time difference between trajectories generated by the two algorithms.

Bijlsma (2009) took a theoretical approach to computing optimal trajectories in general wind fields. He combined graph theory and calculus of variations to solve the problem, rather than an iterative method, which could result in a local minimum.

Campbell et al. (2013) used mixed-integer linear programming (MILP) to find flight trajectories that minimized contrail formation and fuel burn. They found that complete elimination of contrails would incur a 6.2% increase in fuel consumption.

### 2.2.1 Schedule-related Inefficiencies

The North Atlantic air traffic system is strongly tidal due to the combined effects of the total flight time and the difference in time zones (Attwooll, 1986). The peak traffic crosses the 30$^{o}$ W longitude between 1130 UTC and 1900 UTC for *westbound flow* departing from Europe, and between 0100 UTC and 0800 UTC for *eastbound flow* departing from North America (Rodionova et al., 2014). Such concentration of unidirectional traffic results in "rush hour congestion" and exacerbates many aspects of oceanic flight inefficiency.

Moving some traffic to "non-rush" periods can reduce congestion, but it is not always feasible for some routes. Rodionova et al. (2014) explained the "rush hour" effect as a result of passenger demand, time zone differences and airport noise restrictions. For example, the time zone difference between Eastern US and England creates two windows for flights from New York to London: Departing in the morning and arriving at night, or departing at night and arriving in the morning. In practice, the majority of flights from New York to London depart between 18:00 and 23:00 Eastern Time because: 1) Passengers save their time by spending the night on the plane and arrive at their destination at a "useful" time. 2) It provides sufficient time for transfer to subsequent domestic or international flights. Flights from London to New York have fewer restrictions because they land "about two hours" after takeoff. Some routes from non-hub to non-hub airports (for example BOS – ROM) have more flexibility on schedule because fewer passengers transfer. Rescheduling flights can reduce congestion, but it could defeat airlines' attempts to schedule their flights to maximize profit.

Gwiggner and Nagaoka (2014) used radar data to characterize the traffic flow into terminal airspace and found that the major sources of metering delays are spontaneous traffic peaks from an unknown source.

Hansen et. al. (2009) used a stochastic and deterministic queuing model to estimate the impact of 4D trajectory navigation on time delays of flights in the National Airspace System. They found that 4D navigation decreased delays by about 35% compared to the current traffic flow.

Using wind-optimal user preferred routes creates a problem where routes overlap in space and time. Grabbe et al. (2007) proposed a solution to the problem by using a job shop method to schedule flights through the Central Eastern Pacific (CEP) airspace. Using wind optimal routes generated in one of their previous papers (Grabbe, 2006), they cast flights as jobs and split the airspace up into grid segments to act as machines. Using the job-shop model allowed for tradeoffs between delays, time-savings, and residual trajectory conflicts. Their model yielded time savings from 1.8 to 4.6 minutes for flights in CEP.

### 2.2.2 Oceanic/Domestic Sector Transition Inefficiencies

When aircraft exit oceanic airspace they are routed into domestic airspace. Usually, aircraft enter domestic sectors at one of a few points, to simplify controllers' tasks. These points can become bottlenecks, and may also require aircraft to deviate from their optimal trajectories. In the case of WATRS airspace, restricted airspace on the East Coast limits access to domestic airspace.

Korn et al. (2009) created a simple simulation of sector-less airspace in German airspace. Their focus was to show the feasibility of such an airspace in terms of controller workload. Wan and Roy (2008) developed abstractions for flow-restriction procedures to enable better air traffic network evaluation and design. They use an abstracted model to pose a flow management problem for an airspace network. Flows toward other boundaries are

made by splitting/merging flows in the region. They designed their abstracted model to be able to examine generic traffic flows.

## 2.3 Congestion Metrics

Congestion may also aggravate inefficiency. Similar to how traffic causes delay on roads, airspace congestion forces air traffic management systems to reroute or prevent aircraft from flying their most efficient path. Congestion can show up as bottlenecking at sector transitions, en route delay, terminal delay, or altitude and route restrictions. One view of congestion is that a space is congested if traffic becomes backed up, such as at a bottleneck. The traffic may still be manageable, aircraft are merely delayed. Alternatively, one could view an airspace as becoming congested only when traffic becomes unmanageable, and aircraft must be diverted or departures delayed.

Laudeman et al. (1998) introduced Dynamic Density as a way to combine multiple factors relevant to the workload of a controller, compared to a simple measurement of traffic density. They performed a regression analysis with observed controller workload and the computed Dynamic Density to create weights for the relevant factors. Masalonis et al. (2003) assessed the applicability of Dynamic Density to the Traffic Flow Management decision making process. They suggest a multidimensional depiction of predicted workload may be more useful than reducing factors into a single metric.

Lee et al. (2007) used an "input-output" approach to create complexity maps of traffic situations. The input-output approach attempts to model the amount of "control activity" necessary to resolve a certain traffic situation when a new aircraft is introduced to the situation. The complexity maps show the control activity as a function of the entering aircraft bearing and position angle to the sector center.

Green et al. (2001) created a congestion metric designed to be independent of fixed airspace sector boundaries. The metric, *Gaggle Density*, requires automatic identification of aircraft

clusters, for which Bilimoria and Lee (2005) created an algorithm. They described Gaggle Density as being an "airspace independent" analog to Dynamic Density."

Prandini et al. (2011) reviewed complexity metrics, including input-output and Dynamic Density. They concluded that researchers have not considered time-dependency. Puechmorel and Delahaye (2009) uses Lyapunov exponents to model the air traffic system as a set of aircraft velocity vectors. This method is applicable to future ATM systems because it explicitly handles 4-D trajectories.

## 2.4 Inefficiency Metrics

Reynolds (2009) employed the idea of a general inefficiency metric formulated as follows:

$$Inefficiency = \frac{Actual - Optimal}{Optimal} * 100\% \qquad (1)$$

Where $Actual$ and $Optimal$ represent measures of some quantity related to a flight.

Reynolds gives some sample actual and optimal quantities based on lateral distance, vertical distance, speed, and fuel burn, as shown in Table 1. In practice, he found that geometry-based metrics were the easiest to implement, but that they could significantly underestimate fuel burn inefficiency. Fuel-based metrics, while more effective, are significantly more difficult to compute due to the lack of available data, but should provide the most relevant result.

Given the current research using estimated fuel burn for analyzing system characteristics (Yoder, Chatterji, Ng) and the availability of public performance models, we chose to measure inefficiency in terms of fuel.

$$Fuel\ Burn\ Inefficiency = \frac{f_{Actual} - f_{Optimal}}{f_{Optimal}} * 100\% \qquad (2)$$

Table 1: Inefficiency Metrics. From Reynolds (2009, Table 1)

| Dimension | Sample "Actual" | Sample "Optimal" | Advantages | Disadvantages |
|---|---|---|---|---|
| **Dimension** | **Sample "actual"** | **Sample "optimal"** | **Advantages** | **Disadvantages** |
| **Lateral** | Flown ground distance | Minimum ground distance (great circle) | Easy to measure and interpret Flown ground distance readily available (radar surveillance)<br>Minimum ground distance simple to calculate (great circle equation) | Does not capture vertical and speed elements<br>Great circle distance is not shortest in presence of wind |
| | Flown air distance | Minimum air distance | Minimum air distance is better "optimal" measure in the presence of wind | Need accurate wind field information to determine air distance for all flights |
| **Vertical** | Flown vertical profile | Optimal vertical profile | Captures vertical elements<br>Flown vertical profile readily available (transponder altitude) | Does not capture lateral and speed elements<br>Optimal vertical profile requires info not currently available from surveillance (e.g., aircraft weight, winds) |
| **Speed(also surrogate for Time)** | Flown speed profile | Optimal speed profile | Captures speed elements<br>Ground speed readily inferred (radar surveillance) | Does not capture lateral and vertical elements<br>Optimal speed profile requires info not currently available from surveillance (e.g., aircraft weight, winds) |
| **Fuel** | Flown block fuel | Optimal block fuel | Captures lateral, vertical and speed elements<br>Gives excess fuel burn, hence compatible with key environmental performance assessments (e.g., proportional to carbon dioxide emissions) | Actual and Optimal fuel burn requires info not currently available from surveillance (e.g., aircraft weight, winds) |

# CHAPTER 3. HORIZONTAL TRACK INEFFICIENCY

Organized route structures emerged from the use of ground based navigation technology. Pilots would file flight plans made up of chains of fixes. Now, the rise of global satellite navigation has opened up the capability of aircraft to fly arbitrary routes over land and sea, but air traffic control still requires aircraft to fly fixed routes due to the increased complexity of providing separation between aircraft flying arbitrary trajectories.

To save the most fuel and time, aircraft should fly near the highest tailwinds and away from headwinds. Only in rare circumstances will an existing fixed route structure allow aircraft to fly along the best winds. In this section, we develop a method to compute wind optimal horizontal tracks.

Section 3.1 is where we briefly discuss the theory of Optimal Control, before applying the theory to our problem in section 3.2. We used a MATLAB-based numerical algorithm to solve the resulting equations in section 3.3 and we discuss limitations of the solver in section 3.4.

## 3.1 Optimal Control

Finding optimal trajectories is a tricky problem because of the infinite number of sub-problems resulting from the continuous nature of time. The field of Optimal Control provides methods to tackle the problem by leveraging theorems from the Calculus of Variations. The basic idea of Optimal Control is to minimize or maximize a cost function that changes with time by solving for the time histories of control variables.

Deriving necessary conditions for optimality using the Euler-Lagrange equations and Pontryagin's Maximum principle leads to the use of indirect methods to solve the problem. Garcia-Heras (2016) provides a summary of indirect methods as well as direct and dynamic programming methods.

## 3.2 Problem Formulation

In the case of our problem, we want to minimize the total fuel burn. Following similar formulations by Ng (2014), Burrows (1983), and Dalmau (2015) we set up our cost function as follows:

$$J = \int_{t_0}^{t_f} \frac{f}{m_0}\, dt \tag{3}$$

Where $f$ is the fuel burn rate, $m_0$ is the initial mass, and $t_0$ and $t_f$ are the initial and final times respectively. We use fuel flow divided by initial mass as the objective, rather than fuel flow, to scale the problem so that it is easier to solve numerically. We use the same scaling on mass:

$$m^* = -\frac{m}{m_0} \tag{4}$$

Where $m^*$ is scaled mass and $m$ is actual mass. Anywhere $m$ shows up in our equations, we replace it with $m^* * m_0$.

The other states that define the problem are the latitude and longitude of the aircraft. Following Ng (2014) we set our aircraft dynamics for fixed-speed, fixed-altitude flight over a spherical Earth. The only aircraft control we allow to be adjusted is heading angle. The rate equations for the coordinates are:

$$\dot{\phi} = \frac{V_{TAS,i} * \cos(\psi) + u}{R} \tag{5}$$

$$\dot{\theta} = \frac{V_{TAS,i} * \sin(\psi) + v}{R\cos(\phi)} \tag{6}$$

Where $\psi$ is aircraft heading clockwise positive from due north, $\phi$ is latitude, $\theta$ is longitude, $u$ is the easterly wind component, $v$ is the northerly wind component, $R$ is the Earth's radius, and $V_{TAS,i}$ is the airspeed selected for the problem.

Formally, we state the optimization problem as follows:

$Minimize$:

$$J = \int_{t_0}^{t_f} \frac{f(\phi, \theta, m, V_{TAS,i}, h_i)}{m_0}\, dt \tag{7}$$

$subject\ to$:

$$\dot{\phi} = \frac{V_{TAS,i}\cos(\psi) + u(\phi, \theta, h)}{R} \tag{8}$$

$$\dot{\theta} = \frac{V_{TAS,i}\sin(\psi) + v(\phi, \theta, h)}{Rcos(\phi)} \tag{9}$$

$$\dot{m}^* = -\frac{f(\phi, \theta, m, V_{TAS,i}, h_i)}{m_0} \tag{10}$$

$with\ B.C.s$:

$$\phi(t_0) = \phi_0 \tag{11}$$

$$\theta(t_0) = \theta_0 \tag{12}$$

$$\phi(t_f) = \phi_f \tag{13}$$

$$\theta(t_f) = \theta_f \tag{14}$$

$$m^*(t_0) = 1 \tag{15}$$

Where $h_i$ is the altitude of the aircraft in segment $i$. For our analysis, we restricted the solver to a single segment.

The calculus of variations provides the techniques to minimize our cost function, ultimately reducing the root problem to a Two Point Boundary Value Problem (TPBVP), which is solvable using MATLAB routines [Longuski, 2014]. The Euler Lagrange Theorem provides the necessary conditions for minimization in the form of Ordinary Differential Equations (ODEs). The necessary conditions include the Hamiltonian, a function comprised of the cost function integrand and the equations of the state dynamics multiplied by time-variable coefficients called co-states:

$$H = \frac{f}{m_0} + \lambda_\phi \frac{V_{TAS}\cos(\psi) + u}{R} + \lambda_\theta \frac{V_{TAS} * \sin(\psi) + v}{Rcos(\phi)} + \lambda_{m^*}\left(-\frac{f}{m_0}\right) \tag{16}$$

Where $\lambda_\phi$, $\lambda_\theta$, and $\lambda_{m^*}$ are the costates for latitude, longitude, and scaled mass respectively. The Euler-Lagrange equations provide further necessary conditions:

$$\dot{\lambda}_\phi = -\frac{\partial H}{\partial \phi} \tag{17}$$

$$\dot{\lambda}_\theta = -\frac{\partial H}{\partial \theta} \tag{18}$$

$$\dot{\lambda}_{m^*} = -\frac{\partial H}{\partial m^*} \tag{19}$$

$$\frac{\partial H}{\partial \psi} = 0 = -\lambda_\phi \frac{V_{TAS}\sin(\psi)}{R} + \lambda_\theta \frac{V_{TAS}\cos(\psi)}{Rcos(\phi)} \tag{20}$$

Solving eqn. 3.20 for $\psi$ gives us an expression for our control,

$$\psi = \tan^{-1}\frac{\lambda_\theta}{\lambda_\phi \cos(\phi)} \tag{21}$$

Another necessary condition, Legendre-Clebsch, is based on Pontryagin's Minimum Principle. The purpose of the condition is to uniquely set $\psi$ after computing the inverse tangent.

$$H^*_{uu} \geq 0 \tag{22}$$

Or, the second derivative of the optimal Hamiltonian with respect to the control, in our case $\psi$, has to be greater than or equal to zero. We apply the condition to get a unique solution for $\psi$:

$$If\ H^*_{\psi\psi} \geq 0\ then\ \psi = \tan^{-1}\frac{\lambda_\theta}{\lambda_\phi \cos(\phi)}\ ;\ otherwise\ add\ \pi\ to\ \psi \tag{23}$$

In order to have a well-posed TPBVP, we need enough boundary conditions to satisfy the ODEs. Currently, we have six boundary conditions, short of the eight necessary because

we do not know final time or scaled mass. We obtain the remaining two boundary conditions using the transversality condition:

$$H_f dt_f - \lambda_{\phi_f} d\phi_f - \lambda_{\theta_f} d\theta_f - \lambda_{m_f^*} dm_f^* = 0 \tag{24}$$

Where $H_f, \lambda_{\phi_f}, \lambda_{\theta_f}, \lambda_{m_f^*}$ are the final values of the Hamiltonian and the states, and $dt_f, d\phi_f, d\theta_f, dm_f^*$ are the final values of the differentials of time and the states.

Since we know and specify a fixed final coordinate, the differentials of $\phi_f$ and $\theta_f$ equal zero:

$$H_f dt_f - \lambda_{m_f^*} dm_f^* = 0 \tag{25}$$

The differentials of final time and the final states are independent, requiring both terms of eqn. xx to equal zero independently of each other. Since $dt_f$ and $dm_f^*$ are unspecified, in general they are not zero, leaving us with our final boundary conditions:

$$H_f = 0 \tag{26}$$
$$\lambda_{m_f^*} = 0 \tag{27}$$

The combination of ODEs (eqns. 8-10, 17-19) and boundary conditions (eqns. 11-15, 26-27) form a well-posed Two Point Boundary Value problem. Matlab's built-in routine, bvp4c, is a Multi-point Boundary Value solver implementing the 3-stage Lobatto IIIa formula [Mathworks, 2016].

### 3.3 Numerical algorithm using BVP4C

In order to solve, bvp4c requires an initial guess of the trajectory. We use ode45 to solve the 6 ODEs out to a small arbitrary amount of time, generating a small initial guess. Then, we use the final states of the ODE guess as boundary conditions for bvp4c. The solution to

the sub problem from bvp4c gives us an initial guess for the next sub problem. We continue to solve sub problems, each time setting the final point closer to the true final point, in order to set up a well-conditioned guess for solving for the complete trajectory. To illustrate the procedure, we plotted sub trajectories for a flight from Paris to Miami in Figure 3.

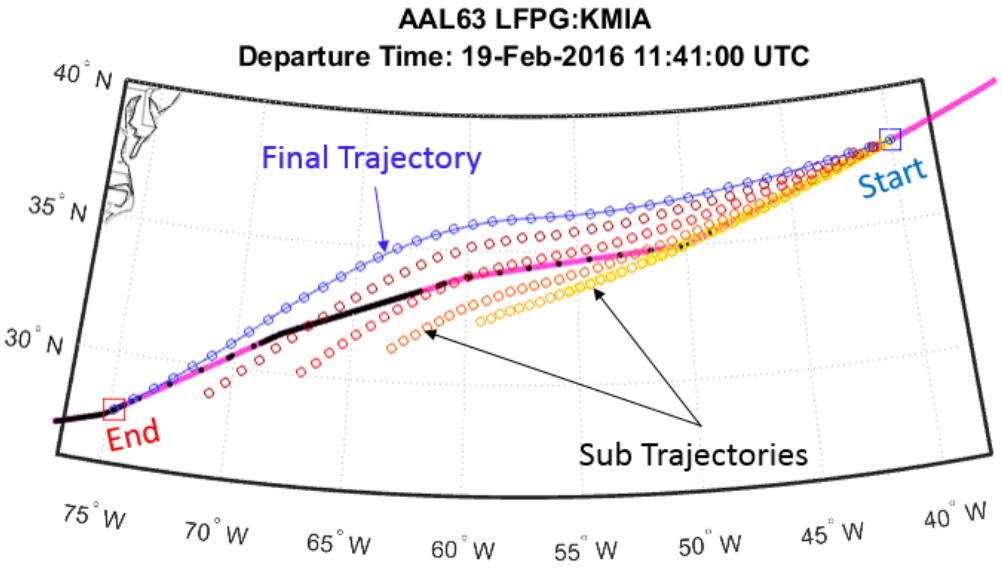


Figure 3: Example of trajectory solver

Figure 4 contains the wind field used for computing the trajectory.

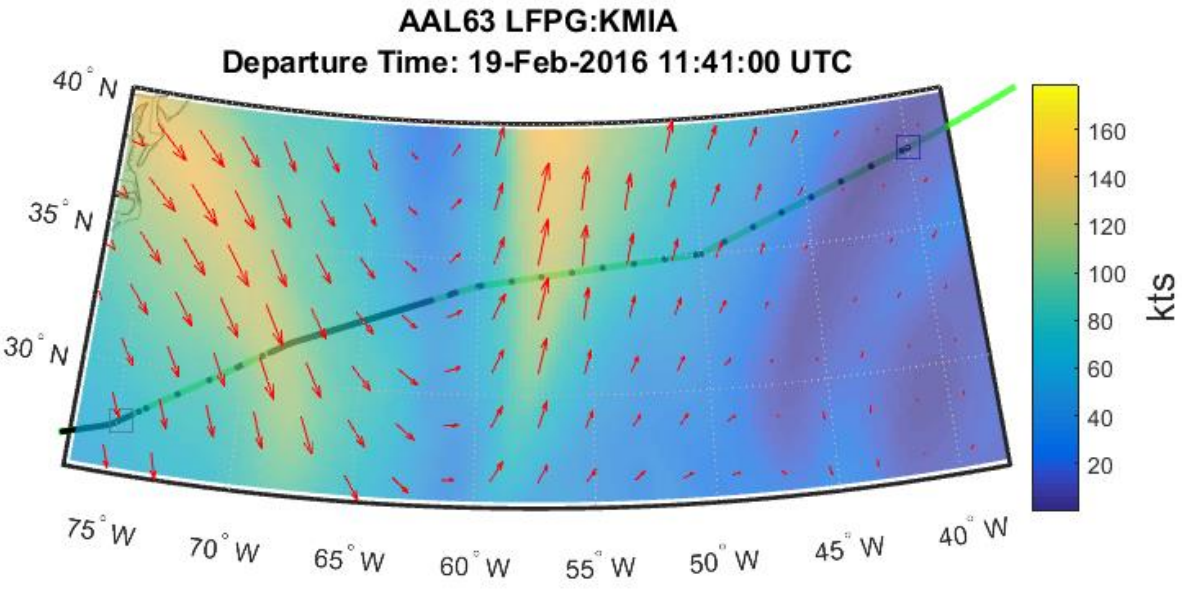


Figure 4: Wind field at altitude used in solver

## 3.4 Limitations of Solver

Ideally, we would be able to take the scaled mass history from the solver, multiply by initial mass and then have the fuel burnt on the wind-optimal trajectory. However, tests on a zero-wind, great circle flight showed a standing 3% difference between the fuel spent by the solver and the fuel calculated by passing the trajectory through the fuel burn estimator.

We resolved the issue by treating the raw trajectory as if we were computing optimal Mach. Using the coordinates and airspeed, we computed groundspeed and then generated a time history, all which are needed for fuel burn estimation.

Using the new time history removes the 3% positive bias from the inefficiency calculations. There remains a -0.25% to -0.05% bias after running a series of arbitrary range and direction zero wind test flights.

# CHAPTER 4. ALTITUDE AND SPEED INEFFICIENCY

The optimal cruise altitude of an aircraft changes as it loses weight. In an ideal situation, an aircraft would continuously climb during cruise. The problem with continuous climb is that it makes it hard for controllers to manage aircraft separation. Step climbs are a reasonable compromise. Comparing the fuel burn between actual and optimal flight tracks will show flight inefficiency for off-optimal altitudes.

We describe the optimization method we use to generate optimal trajectories in Section 4.1, then note some key limitations of the method when using the Base of Aircraft Data (BADA) performance model in Section 4.2.

## 4.1 Specific Ground Range

Our objective function for minimizing fuel burn is Specific Ground Range (SGR). SGR is the ratio between groundspeed and fuel flow at any point in time during cruise flight [Jensen 2007]:

$$SGR = \frac{groundspeed}{fuel\ flow} \tag{28}$$

Basically, the idea is to maximize the amount of distance covered per unit of fuel. Maximizing SGR minimizes cruise fuel burn. If we only care about minimizing fuel burn along the distance traveled in the *air* rather than with respect to the ground, then we should use Specific Air Range (SAR) which is the ratio of airspeed to fuel flow.

To optimize the SGR, we follow Jensen (2007) in using a brute force search for maximum SGR over a range of feasible altitudes and Mach numbers at each point in time over the cruise flight track. To calculate fuel flow at each sample point, we assume that the aircraft is in equilibrium cruise. We use the base trajectory mass to compute fuel flow at the SGR sample points, as shown in Figure 5.

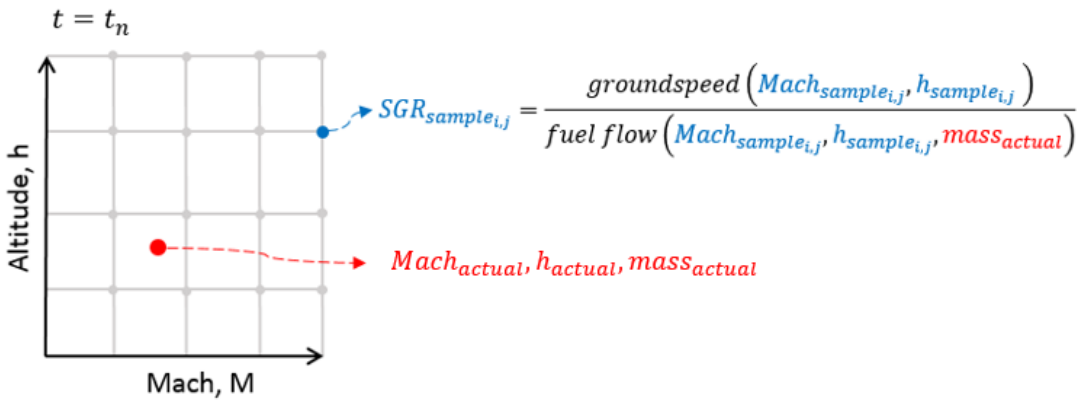


Figure 5: SGR Sampling Method

We select altitudes and Mach in a range based on limits for reasonable operations. BADA provides upper limits for altitude and Mach, but there are no defined lower operational limits, so we set the lower limits to encompass the majority of feasible operations.

Table 2: Flight parameter ranges

| | Minimum | Maximum | Step |
|---|---|---|---|
| **Mach** | *BADA nominal cruise Mach* – 0.1 | *BADA maximum operating Mach* | 0.005 |
| **Altitude** | 28000 ft | *BADA maximum operating altitude* | 250 ft |

Some combinations of altitude, Mach, and mass result in infeasible flight conditions. If a flight condition fails the following three criteria, we say the condition is infeasible. First, the aircraft must be able to perform a 300 ft/minute climb with the thrust difference between maximum cruise thrust and thrust used to oppose drag. Second, the Mach number must be greater than the low speed buffet Mach number. The relationship for calculating low speed buffet Mach is given by BADA as a function of mass, pressure, and aircraft specific constants. Third, calibrated airspeed (CAS) must be below the BADA maximum calibrated airspeed. Maximum operating Mach at high altitudes converts to airspeeds well below maximum CAS, so maximum CAS is rarely violated so we omit it from the collection of limiting parameters. Figure 6 shows an example SGR grid overlaid with feasible boundaries. There may be additional restrictions to performance issued by the FAA, the airlines, or the manufacturer, but we did not include any as the minimum climb and low speed Mach effect were the most relevant to limiting cruise altitude.

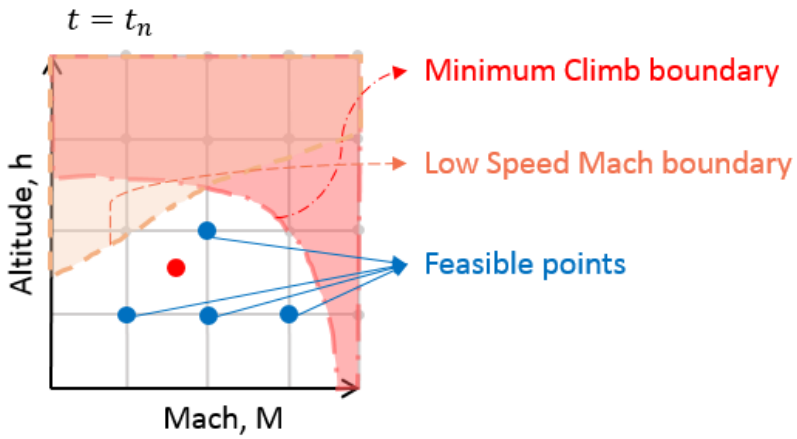


Figure 6: Feasible Flight Limits

There are some flights in our database that occasionally violate our feasibility constraints. Since the feasibility constraints are derived from estimated parameters we expect the occasional violation. To get a sense of how well our estimations are performing, we record the percent of cruise flight time spent outside the boundaries for each flight, as shown in Figure 7 for CEP flights. We use the feasibility cutoff percent as a filter for our results.

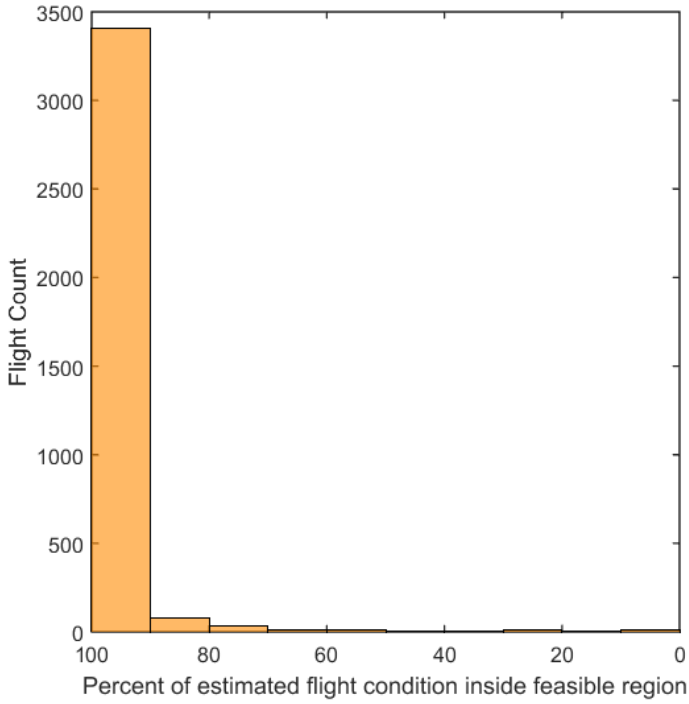


Figure 7: Distribution of CEP flight feasibility violations

Among the feasible SGR points, we are interested in three different maximum points: the point with optimal Mach and altitude, the point with optimal altitude given the actual flight Mach number, and the point of optimal Mach given the actual flight altitude. For each of the points with a different altitude than the base altitude, we compute a separate version that adjusts the optimal altitudes to respect the "Odd-east, Even-west" rule. In addition to the SGR optimal trajectories, we are interested in seeing how much fuel can be saved by flying a trajectory one available cruise altitude higher than the actual altitude.

Figure 8 shows an example of an SGR grid for a transatlantic flight. The red X on the grid is the actual flight condition, the red circle is the Best Overall point, the magenta square is the Best Altitude for the actual Mach, and the black triangle is the Best Mach for the actual altitude.

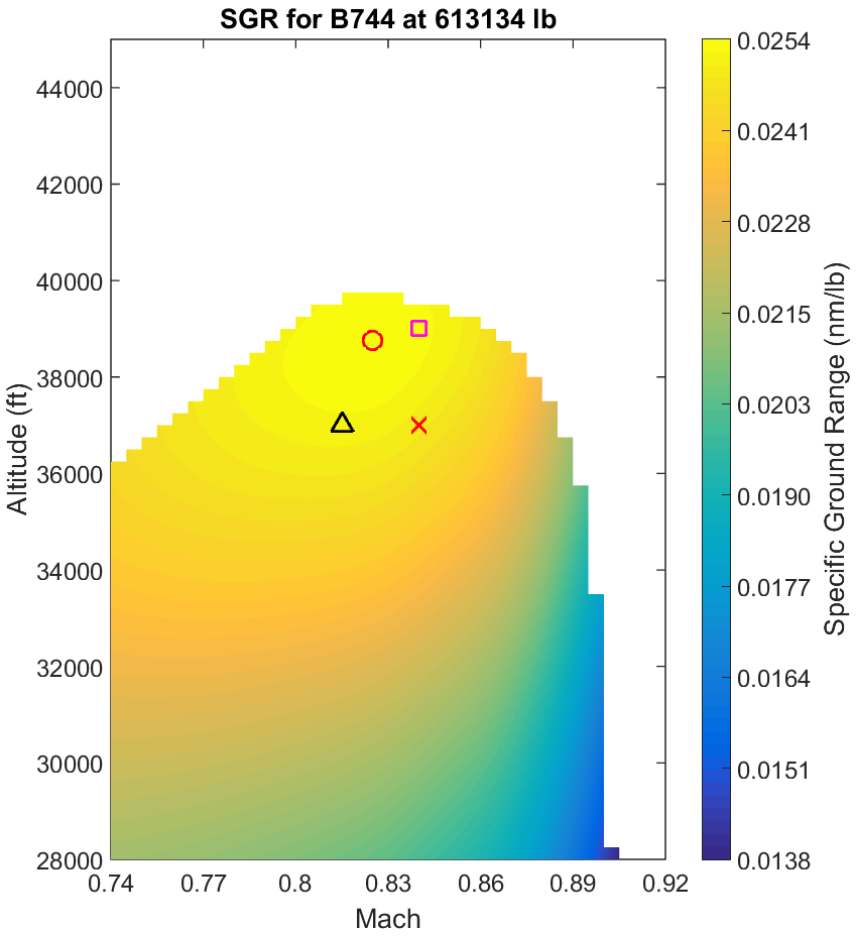


Figure 8: SGR grid and associated maximum points for a 747 at mid mission weight

To compute the fuel burned by the optimal trajectories, we swap out the actual altitude with the optimal altitude, re-interpolate the weather, and send the flight through the fuel burn estimator. To prevent changes in the flight path from affecting the initial mass, we carry the initial mass from the base case forward to use at the start of the other trajectories.

For trajectories with different Mach profiles, we have to adjust the flight time to match the new groundspeed. We calculate new groundspeed by converting Mach to true airspeed using the temperature data at altitude, and then using wind data to compute the groundspeed:

$$V_{TAS,opt} = Mach_{opt}\sqrt{\gamma RT} \tag{29}$$

$$G_{opt} = Course - \sin^{-1}\left(\frac{Wind_{mag} * \sin(Wind_{direction} - Course)}{V_{TAS,opt}}\right) \tag{30}$$

Once we have groundspeed, we compute the time to cross each track segment by dividing the great circle distance between segments with groundspeed:

$$\Delta t_{opt,segment} = \frac{D_{GC,segment}}{G_{mean,segment}} \tag{31}$$

The time differences are incremented from the timestamp at the start of the analysis region, $t_0$, to generate the new time profile:

$$t_k = t_0 + \sum_{i=0}^{k} \Delta t_{opt,i} \tag{32}$$

## 4.2 BADA Limitations

BADA has a key limitation when used for computing optimal altitudes. During the course of our investigation, we found that optimal altitudes derived solely from maximizing SGR

(without any limitations on climb rate) would return optimal altitudes significantly higher than Jensen's results. Jensen used Piano-X instead of BADA when developing the model, so we looked at the difference between the two models.

To get a rough comparison of the two performance models, we attempted to reproduce a graph from Jensen's thesis. His graph of SAR vs Flight Level was particularly reproducible because it is independent of weather. The narrow body airliner we chose to generate the comparison SAR is the Boeing 737-800, which best fits the mass range and cruise Mach limits in Jensen's graph. The BADA results are in Figure 9, and the Piano-X results are in Figure 10.

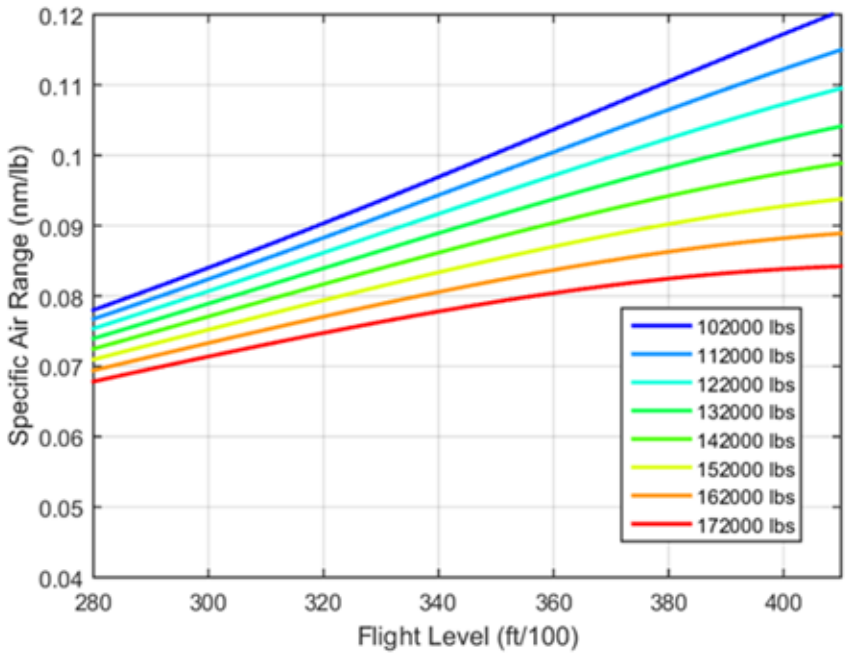


Figure 9: SAR against flight level using BADA. 737-800 at Mach 0.78

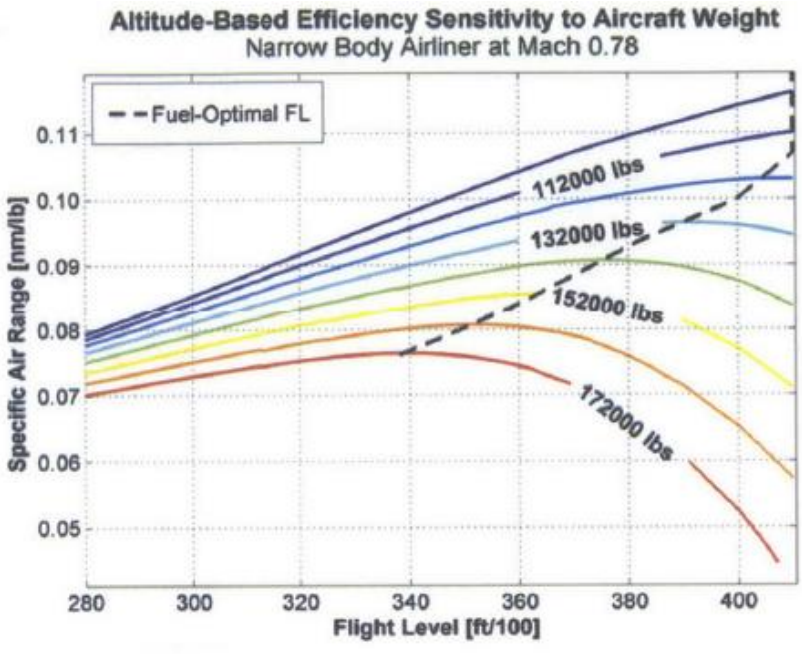


Figure 10: SAR against flight level using Piano-X, Figure 16 from [Jensen, 2014]

Our implementation of BADA lines up fairly well with the Piano-X results until the flight level becomes sufficiently large, after which our results do not show the sharp curvature present in the Piano-X implementation. Also notice that we do not have any points of maximum SGR within the range of operational altitudes, in contrast to Jensen's graph, where the optimal altitudes are feasible.

To determine whether the discrepancy might be due to our using BADA, we compared performance results with Piano-X for the 787. Lissys provides a demo version of Piano-X which comes with a few full scale models, including the 787-800, A340-600, and A380-800.

To generate performance results, we generated a series of aircraft parameters, such as weight, Mach, and altitude. We ran the parameters through Piano-X using the point performance tool and computed performance parameters like drag and fuel flow. The Piano-X standard operating weights for the aircraft model were set equal to the BADA numbers to get equal conditions.

Because drag directly factors into fuel flow by setting thrust equal to drag at steady state cruise, we compared the drag numbers. In Figure 11, the Piano-X drag curve shows a minimum at 37500 ft, versus the BADA drag curve which does not have a minimum in the region of operable cruise altitudes. Using BADA for the SGR methods generates too high optimal altitudes, so the drag curve indicates drag modeling is the source of the problem.

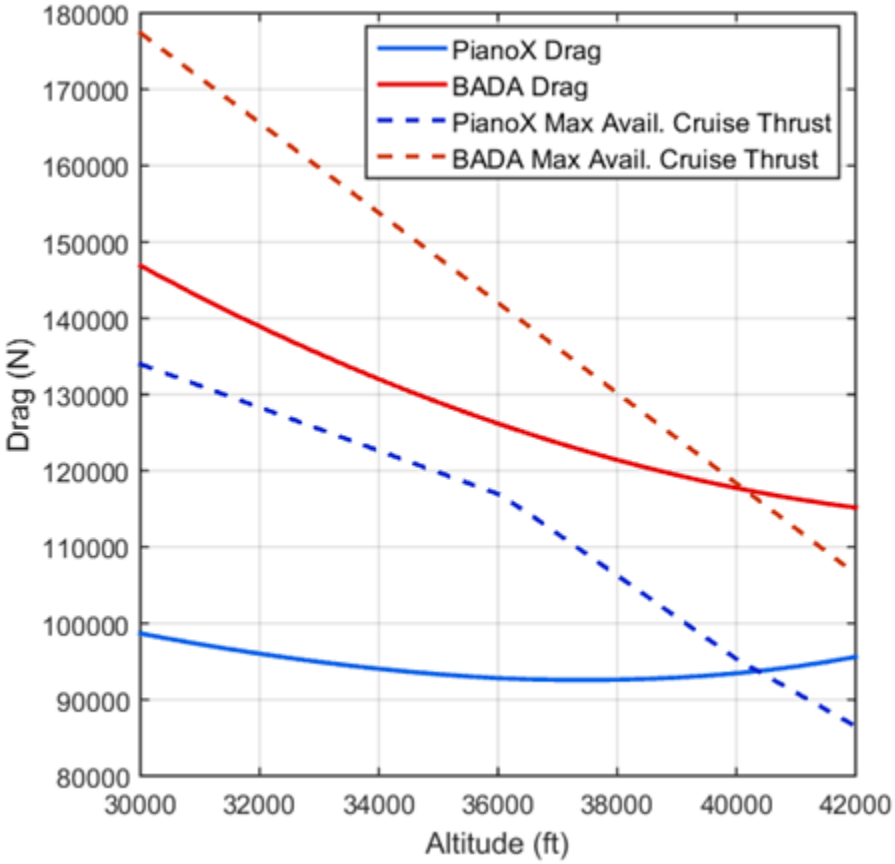


Figure 11: Drag vs altitude for B788 at Mach 0.84 and 200,000 kg.

For reference, the drag model in BADA is as follows:

$$Drag = \frac{1}{2}\rho V^2 S * C_D \tag{33}$$

Where $\rho$ is density, $V$ is true airspeed, $S$ is surface area, and $C_D$ is the drag coefficient, given by:

$$C_D = C_{D0} + C_{D2}C_L^2 \qquad (34)$$

Where $C_{D0}$ is the parasitic drag coefficient, $C_{D2}$ is the induced lift drag coefficient, and $C_L$ is the lift coefficient. Piano-X (2008) uses a drag model that includes extra drag coefficients, such as for compressibility and trim, and models the drag coefficients as functions of Reynolds number, Mach number, and angle of attack.

After simulation, the BADA and Piano-X $C_L$ results were within 1% of each other, so we checked the drag coefficients. In Figure 12, we plotted $C_{D0}$ and $C_{D2}C_L^2$ from BADA and the zero lift and induced lift coefficients from Piano-X. Both induced lift drag coefficients are very close to each other, (within 7%), but the parasitic and zero lift coefficients are about 50% different. Lissys (2008) refers to the zero lift drag coefficient as $C_{D0}$, which is used in BADA for the parasitic drag coefficient, thus we believe the Piano-X *zero lift* drag coefficient to be the same as the BADA *parasitic* drag coefficient.

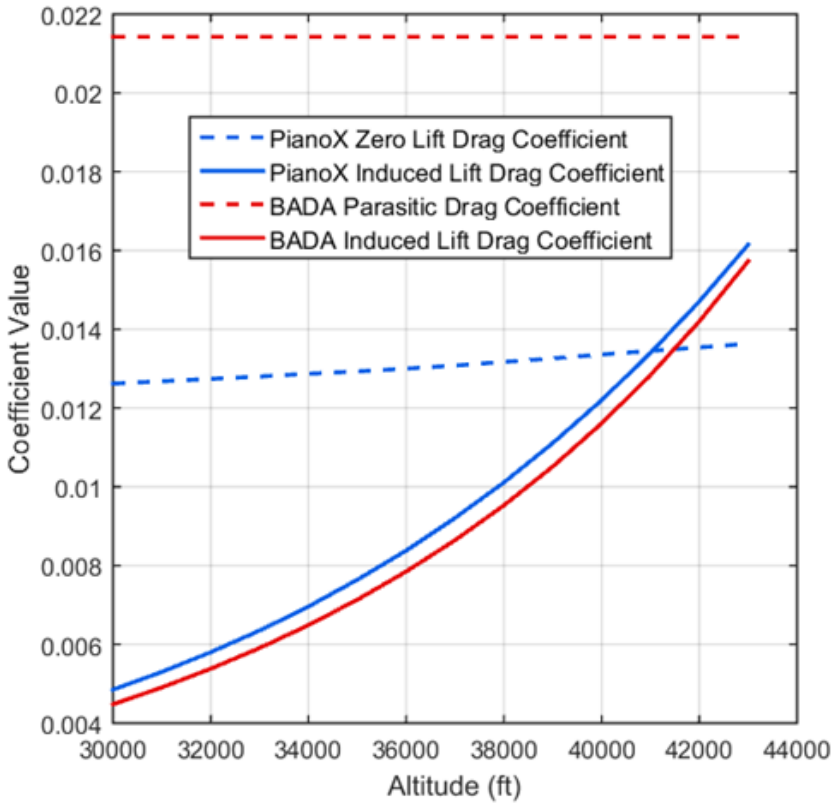


Figure 12: Drag coefficients from Piano-X and BADA.

Thus we can conclude that the large value of the BADA parasitic drag coefficient ends up over-weighting the effect of parasitic drag, which results in higher optimal altitudes because of the decrease in density with altitude.

# CHAPTER 5. BLOCKING INEFFICIENCY

To avoid mid-air collisions, air traffic control requires aircraft to be separated from each other by time or distance. In areas of low surveillance, such as oceanic airspace, larger separation standards are required. For example, longitudinal separation in airspace with radar coverage is 5–10 nautical miles, while longitudinal separation over oceanic airspace is at least 50 nautical miles when aircraft give position reports using Automatic Dependent Surveillance – Contract (ADS-C).

The larger separation standards can create a scenario in which nearby aircraft at different altitudes "sandwich", removing opportunities to climb or descend without violating lateral and longitudinal separation standards. In the case where a lower aircraft should climb to stay on the optimal altitude, the "sandwich" effect will block the aircraft from climbing and cause a net fuel burn inefficiency.

We discuss oceanic separation standards in Section 5.1, and set up our blocking analysis in Section 5.2.

## 5.1 Oceanic Separation Standards

The FARs require operators of US registered aircraft to comply with ICAO Annex 2 when operating over the high seas (14 C.F.R § 91.703). Annex 2 contains passages requiring aircraft to report position to the appropriate air traffic services unit (ICAO, 2005). Since the FAA provides air traffic services in the form of a Flight Information Region (FIR) in the regions we are interested in, they set the rules for providing separation.

FAA separation standards in oceanic regions depend on the equipage of the aircraft and the communication protocols used by the crew (FAA Order JO 7110.65 2015). For example, in CEP, aircraft using Automatic Dependent Surveillance – Contract (ADS-C) to provide position reports with flight crews using Controller Pilot Data Link Communications

(CPDLC) are provided 30 nm lateral and longitudinal separation given the maximum time between position reports is less than 14 minutes.

Table 3: CEP Longitudinal Separation standards for ADS-C equipped aircraft [FAA Order JO 7110.65, 2015]

| Minima | RNP | Maximum ADS-C Reporting Interval |
|---|---|---|
| 50 NM | 10 | 27 minutes |
| 50 NM | 4 | 32 minutes |
| 30 NM | 4 | 14 minutes |

The only difference with WATRS is that 30 nm minima require a 10 minute interval, rather than 14 minutes for CEP.

The FAA has been in the process of developing an air traffic control method that will allow aircraft to conduct climbs when within the separation minima listed in Table 3. The method is called the ADS-B In Trail Climb Procedure (ADS-B ITP) and was first used in operational trial in June 2011 (IPACG/40 IP/09). ADS-B ITP allows properly equipped aircraft to climb or descend when within no less than 15nm of another suitably equipped aircraft (FAA JO 7110.65W). Trials are still on-going although wording for the procedure was added to the main Air Traffic Organization Policy document (FAA JO 7110.65W) in June 2016 (Hemdal, 2016).

## 5.2 Blocking Algorithm

To determine whether aircraft are blocked, we check the distance between each time-coincident track point on a flight with every other time-coincident track points on all flights that possibly approach within separation standards. Computationally, a naïve search is infeasible. We make the problem tractable by using several steps to trim down the search space.

The first step is a rough sort by search time. We take all flights with the same search time plus/minus one search period. If a pair of aircraft is separated by more than two search periods, the aircraft should never meet unless one of the aircraft reverses course.

The second step is to select flights from the pool from the previous step and loop through the track points and identify time-coincident points, between which we compute distance. Assuming lateral and longitudinal separation standards are the same and follow a circular path around the main flight, we mark a potential blocking situation by comparing the computed distance to the separation standard distance.

At this point, we have a list of coincident track points between a flight and a proximate flight that pass within separation standards. We go through the set of points within separation distance and record the mean differences between the flight altitude, proximate flight altitude, and optimal flight altitude.

We call flights blocked when they have at least one pair of track points within separation for which the proximate flight comes between the optimal and the actual altitude. Figure 13 shows a case where a pair of track points would be designated as blocked. We let optimal altitude get within 500 ft. of the proximate track when flagging as blocked due to the noisy nature of the optimal altitude computation.

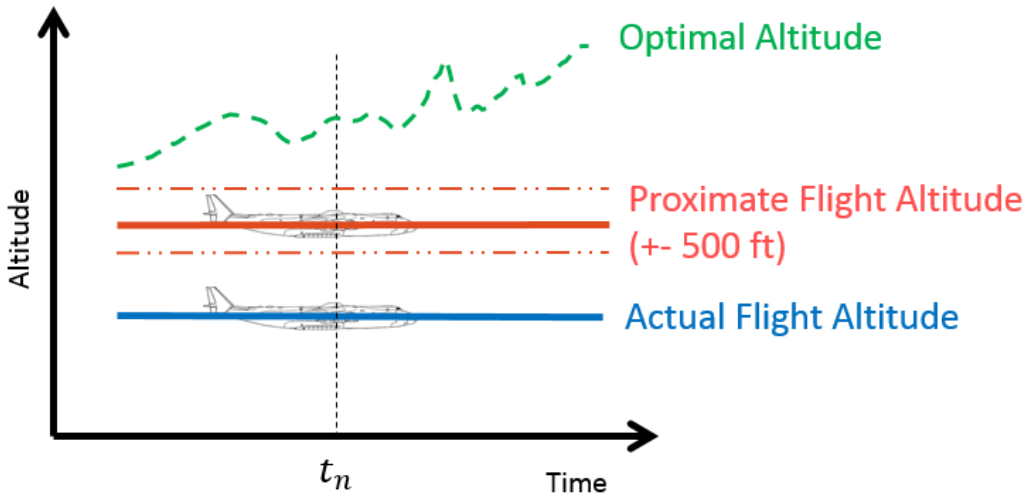


Figure 13: Blocking Scenario with tolerance on proximate altitude

The differences between the optimal, proximate, and actual altitudes allow us to take a look at how far the aircraft is held from its optimal altitude. In addition, we collect the total time that the aircraft is blocked, which includes blocking from all other potential proximate aircraft.

We take a weighted mean of the mean altitude differences from each proximate flight by weighting with the total time spent blocked by each proximate flight.

# CHAPTER 6. ESTIMATING AIRCRAFT FUEL BURN

Currently, the only publicly available research-grade data set with aircraft fuel consumption data and a model for computing fuel consumption is the Base of Aircraft Data (BADA). In Section 6.1, we discuss the core model used by BADA to simulate performance. In Section 6.2 we discretize the model for computation and then discuss corrections to the model in Section 6.3.

## 6.1 Total-Energy Model

The main feature of the model is an equation relating the change in potential and kinetic energy of an aircraft to the balance between thrust and drag:

$$(T - D)V_{TAS} = mg_0 \frac{dh_{Geod}}{dt} + mV_{TAS} \frac{dV_{TAS}}{dt} \qquad (35)$$

where $T$ is the thrust acting parallel to the aircraft velocity vector, $D$ is aerodynamic drag, $m$ is aircraft mass, $h_{Geod}$ is geodetic altitude, $g_0$ is gravitational acceleration, $V_{TAS}$ is true airspeed, and $\frac{d}{dt}$ is the first order derivative with respect to time.

Thrust specific fuel consumption (TSFC), $\eta$, can be computed using the following relation:

$$\eta = C_{f1}\left[1 + \frac{V_{TAS}}{C_{f2}}\right] \qquad (36)$$

where $C_{f1}, C_{f2}$ are aircraft specific fuel coefficients and $V_{TAS}$ is true airspeed.
Finally, fuel burn rate combines specific fuel consumption and thrust:

$$\dot{f} = \eta T \qquad (37)$$

## 6.2 Discretized Model

Our flight track data is given in discrete points in time, so the fuel burn is calculated over the segments connecting the track points. In Figure 14, $t_n$ represents time and $f_n$ represents the fuel burned traveling a track segment starting at time $t_n$.

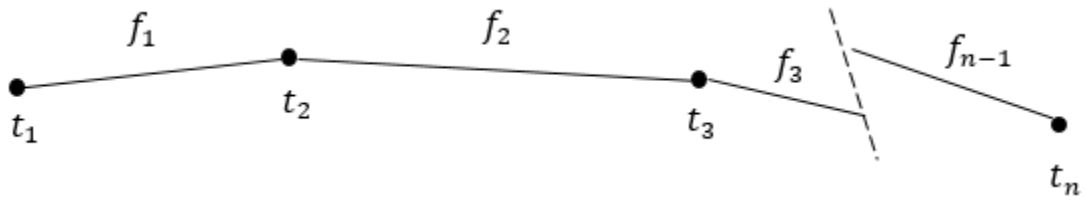


Figure 14: Discretized Flight Track

Since our flight data is discrete in time, equation (35) must be modified. Similar to Yoder (2007), we discretize the total-energy equation and solve for the necessary thrust at point *n* based on the change in airspeed, change in geopotential height, drag, true airspeed, and mass:

$$T_n = D_n + \frac{m_n g_0}{V_{TAS,n}} \frac{\Delta h_{geop,n}}{\Delta t_n} + m_n \frac{\Delta V_{TAS,n}}{\Delta t_n} \tag{38}$$

Where all subscripts $n$ represent the value of the subscripted variable at time $t = t_n$. Assuming small variation in the gravitational field allows for geopotential height to be substituted for geodetic height.

Then the fuel burned in segment *n* is given by the product of the specific fuel consumption, thrust, and time interval over which the fuel was burned:

$$f_n = \eta_n T_n \Delta t_n \tag{39}$$

Aerodynamic drag is computed in terms of aircraft-specific drag and lift coefficients provided by BADA:

$$D_n = \frac{C_{D,n} \rho_n V_{TAS,n}^2 S}{2} \tag{40}$$

Where $C_{D,n}$ is the drag coefficient, $S$ is the reference wing surface area, and $\rho_n$ is air density given by:

$$\rho_n = \frac{P_n}{R * Temp_n} \tag{41}$$

Where $Temp_n$ is the air temperature and $R$ is the real gas coefficient of air given by BADA. $C_{D,n}$ is the drag coefficient, given by:

$$C_{D,n} = C_{D0,n} + C_{D2,n}\left(C_{L,n}\right)^2 \tag{42}$$

Where $C_{D0}, C_{D2}$ are phase-of-flight specific drag coefficients and $C_{L,n}$ is the lift coefficient, given by:

$$C_{L,n} = \frac{2m_n g_0}{\rho_n V_{TAS,n}^2 S} \tag{43}$$

Since aircraft mass changes over the course of a flight, we use the fuel burn over segments to decrement the mass as follows.

$$m_n = m_0 - \sum_{i=1}^{n-1} f_i \tag{44}$$

where $m_0$ is initial aircraft mass.

Since we do not have initial mass, we must estimate it. We experimented with using the basic BADA reference mass, but that mass is best used as a mid-mission reference mass. A method by Chatterji (2012) estimates initial mass by iterating and storing successive flight fuel burns.

We start with a guess for zero-fuel weight (ZFW), essentially a guess for the loading of the aircraft, and then compute the fuel burn using ZFW as initial mass. Taking the difference between final and initial mass gives the amount of fuel burned, which we add to ZFW as our new starting mass. Chatterji found three iterations to be sufficient in stabilizing the initial mass. In lieu of actual payload data, we used 100% of the BADA payload mass as initial loading for each flight.

## 6.3 BADA Corrections

The BADA model does not take temperature or pressure variations into account when computing fuel burn. Yoder (2007) used data from a computer flight data recorder (CFDR) to make corrections to BADA's fuel burn computation method. He used regression to fit the CFDR data to a model that relates thrust specific fuel consumption to thrust, temperature, and Mach number:

$$\frac{\eta}{\sqrt{\theta}} = \alpha + \beta_1 M + \beta_2 e^{-\beta_3 \left(\frac{\tau}{\delta^{0.9}}\right)^{0.3}} \tag{45}$$

Where $\theta$ and $\delta$ are the ratio of temperature and pressure to their respective sea-level ISA standard values, $\tau$ is the ratio of thrust to sea-level maximum thrust, $\beta_{1,2,3}$ are regression coefficients, $C_{fl1,fl2,fcr}$ are BADA fuel flow coefficients, is the thrust specific fuel consumption, and $\alpha$ is an intermediate coefficient that is related to the BADA fuel flow coefficients, given by:

$$\alpha = \frac{C_{fl1}}{60000}\left(1 + \frac{1.9348(240)}{C_{fl2}}\right) C_{fcr} - 5.3(10)^{-6} \tag{46}$$

The regression relationship is dependent on the BADA coefficients used. Yoder derived the regression using BADA 3.6, and we used BADA 3.11. To test the validity of the regression, we computed fuel burn for a set of flights using the BADA method and the corrected Yoder method.

Table 4: Percent difference of BADA fuel to Yoder fuel

| | **Our BADA 11765 flights** | **Our corrected 11765 flights** | **Yoder BADA 218335 flights** | **Yoder corrected 218335 flights** |
|---|---|---|---|---|
| **Total Fuel (kg)** | 3.142e8 | 3.076e8 | 8.785e8 | 8.430e8 |
| **Percent Difference** | 2.12% | | 4.12% | |

The change in percent difference can be attributed to a change to the BADA coefficients in 3.7 (BADA 2009). Because the new coefficients still do not take Mach and temperature

effects into account, and since our percent change between the corrected and BADA models is similar to Yoder's, we elected to use the regression model for our inefficiency analysis.

Separate from the TSFC model, another limitation of BADA is that the included drag model does not account for compressibility effects, affecting results in the transonic regime. Klima (2005) adapted the Kroo Method to BADA coefficients to solve for the increase in total drag coefficient due to compressibility at high speeds. Following Klima, we disable $\Delta C_{Dc}$ effects for flight segments with computed Mach numbers above 104.6% of the BADA nominal cruise Mach.

$C_D$ is the corrected drag coefficient given by:

$$C_D = C_{D0} + C_{D2}(C_L)^2 + \Delta C_{Dc} \tag{47}$$

Where $\Delta C_{Dc}$ is the transonic drag rise coefficient given as a piecewise function by:

$$\Delta C_{Dc} = \begin{cases} 0.00100 + 0.02727Y - 0.1952Y^2 + 19.09Y^3 & X \geq 1.0 \\ 0.00100 + 0.02727Y + 0.4920Y^2 + 3.573Y^3 & 1.0 > X \geq 0.95 \\ 0.0007093 + 0.006733Y + 0.01956Y^2 + 0.01185Y^3 & 0.95 > X \geq 0.8 \\ 0.00013889 + 0.00055556Y - 0.00055556Y^2 & 0.8 > X \geq 0.5 \\ 0 & 0.5 > X \end{cases} \tag{48}$$

Where $X$ and $Y$ are intermediate coefficients based on Mach number, given by:

$$X = \frac{M}{M_{BADA}}, \qquad Y = X - 1 \tag{49}$$

Where $M$ is Mach number and $M_{BADA}$ is the nominal cruise Mach given by BADA.

Further uncertainty not covered by the BADA model is real world variation in engine types and winglet equipage.

# CHAPTER 7. OCEANIC AIRSPACE ANALYSIS

We tested our inefficiency system on flights in selected oceanic airspace. All of our data comes from publicly available sources, resulting in some unique challenges which we discuss throughout this chapter.

## 7.1 Data Sources and Preparation

Since the data necessary for computing inefficiency come from several different sources, there were many steps to formatting and pre-processing our data before input to our system. Here, we explain the different sources and methods we used to gather and prepare the data.

### 7.1.1 Flight tracks

We used FlightAware for flight data. FlightAware is one of the few public sources of flight track data that is cheap, easy to access, and which fuses ADS-B, radar, and oceanic position report data. Because only one type of data may be available at a time in a given region, the fusion of multiple sources allows us to obtain a more complete flight track.

Appendix A lists our collection methods for both WATRS and CEP flights. From our set of flights, we prepared subsets from the month of April to use for analysis. The data covers the full month of April for CEP and April 1-21 for WATRS.

### 7.1.2 Filtering tracks

Most raw tracks generally have well-sequenced data, where the track point times increase monotonically and the data update types are smoothly distributed. For the flights that did not have well-tempered data, there were three predominant sources of error.

First, some flights have segments of track points farther away from the optimal track than is likely feasible. These segments will lead to inaccurate results because speed and

horizontal track inefficiency computation relies on computing the time from point to point using the mean groundspeed and great circle distance. The out-of-place segments will skew the inefficiency higher because the base fuel burn will be higher than it should be. Figure 15 shows an example flight track with spurious points.

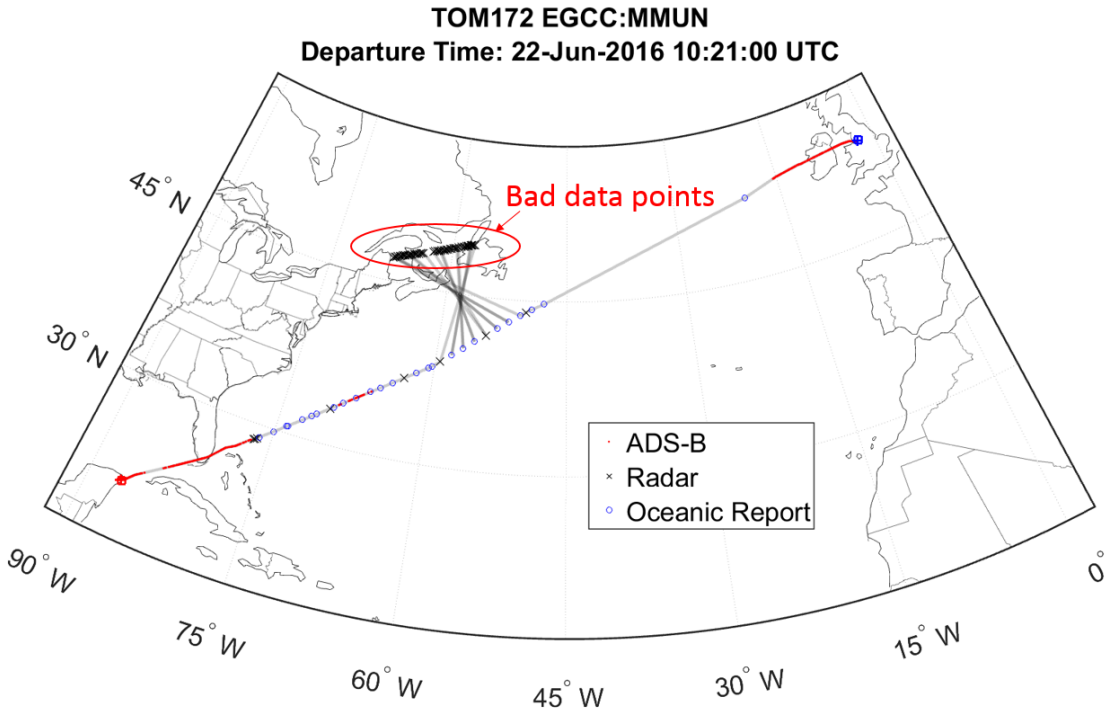


Figure 15: Flight with interlaced bad data

To resolve the errors in the data, we developed a filter algorithm, inspired by the work done on filtering Enhanced Traffic Management System (ETMS) data by Palacios (2013).

The filter is based on extra expected distance between two points. Expected distance ($E\_d$) is the distance implied by the groundspeed and time histories, i.e., expected distance is the estimate of the actual distance an aircraft has flown over the segment given that the information we have. We compute the expected distance from the mean of the groundspeeds ($G_{mean}$) and the difference in time ($\Delta t$) between any two track points:

$$E_d = G_{mean} * \Delta t \tag{50}$$

We decompose expected distance into two components: the geometric great circle distance (D_GC) and an extra expected distance ($\Delta$e_d). The extra expected distance represents distance that results from the aircraft performing actions between data points that do not fit our assumptions of a great circle path and a linear groundspeed profile. If a flight flies the great circle route with a linear groundspeed profile between points, then $\Delta e_d$ will equal zero. This is not a unique case; aircraft can fly longer/shorter routes than the great circle with a faster/slower than the mean groundspeed profile, also resulting in $\Delta e_d$ equaling zero.

$$(D_{GC} + \Delta e_d) = G_{mean} * \Delta t \qquad (51)$$

Our filter uses the ratio of $|\Delta e_d|$ to $D_{GC}$ (converted to a percentage) as the metric for deciding whether the gap between two points represents a feasible aircraft action. We derived the first set of limits from a population of $\Delta e_d$ and $D_{GC}$ computed from flights. After viewing results we set the ratio to 28% to fully remove the egregious data points in the example flight given in Figure 15. Since examining the effect of the ratio on all flights was unfeasible, we kept the ratio at 28% after visually verifying the performance of the filter on several flights.

The algorithm works as follows:

1. Iterate forward through the list of track points and compute $\Delta e_d$ and $D_{GC}$ for sequential pairs of data points.
2. If $\frac{|\Delta e_d|}{D_{GC}} * 100\% > trigger\ percentage$ (in our case 28%) then mark the $i$+1 track point as failed on a forward pass.
3. Keep the $i^{th}$ point fixed and iterate over successive points, computing $\Delta e_d$ and $D_{GC}$ between each point and the base $i^{th}$ point. As long as the trigger condition fails, continue to iterate until the failure condition is cleared.
4. Once the condition breaks, move the base point forward to the next non-failed point.

5. At the end of the list, repeat the process traveling backwards and mark a separate set of backwards pass failing points.
6. Remove only the points that failed **both** the forwards and backwards pass.

The red and blue circles in Figure 16 surround points that failed the forwards and backwards passes respectively.

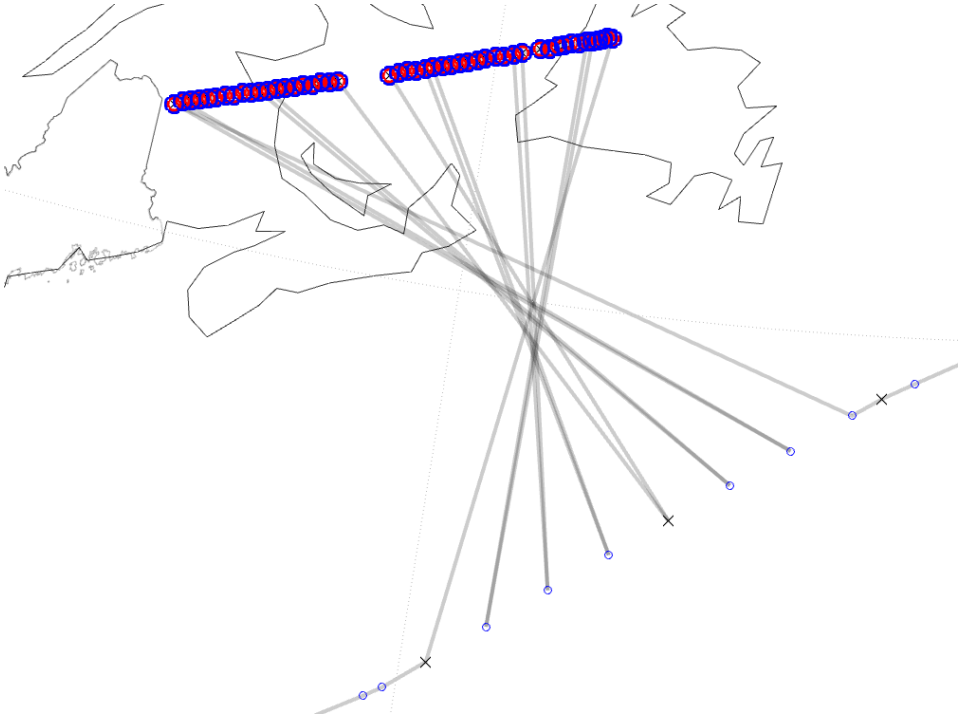

Figure 16: Points selected for deletion based on forward and backward filter passes

Figure 17 shows the flight with filtered points removed.

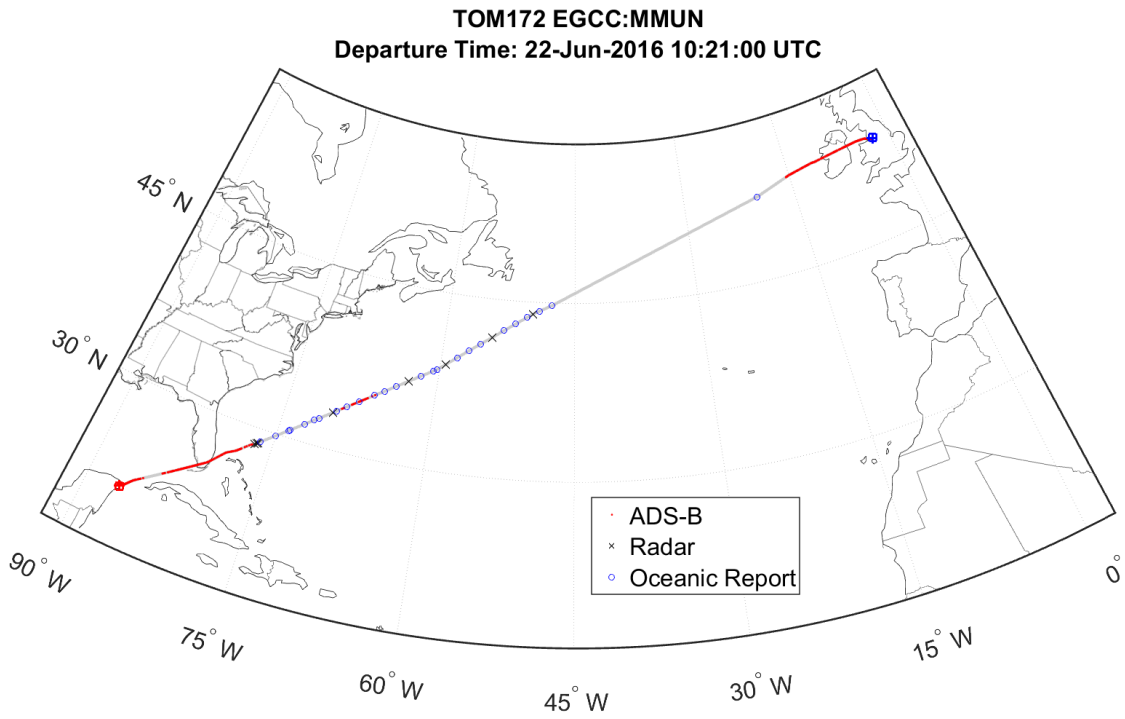


Figure 17: Filtered Result

Using a dual pass system allowed us to keep pairs of points that disagree solely because of a lack of knowledge of what happened between the points, e.g., a pair of points separated by a large gap in time and where the groundspeed over the gap varied significantly from the mean, from triggering the filter. This case happens often with ADS-B reported points, where the short update times result in short distances, making the ratio prone to large departures due to small $D_{GC}$. Figure 18 shows a case where both track points are retained.

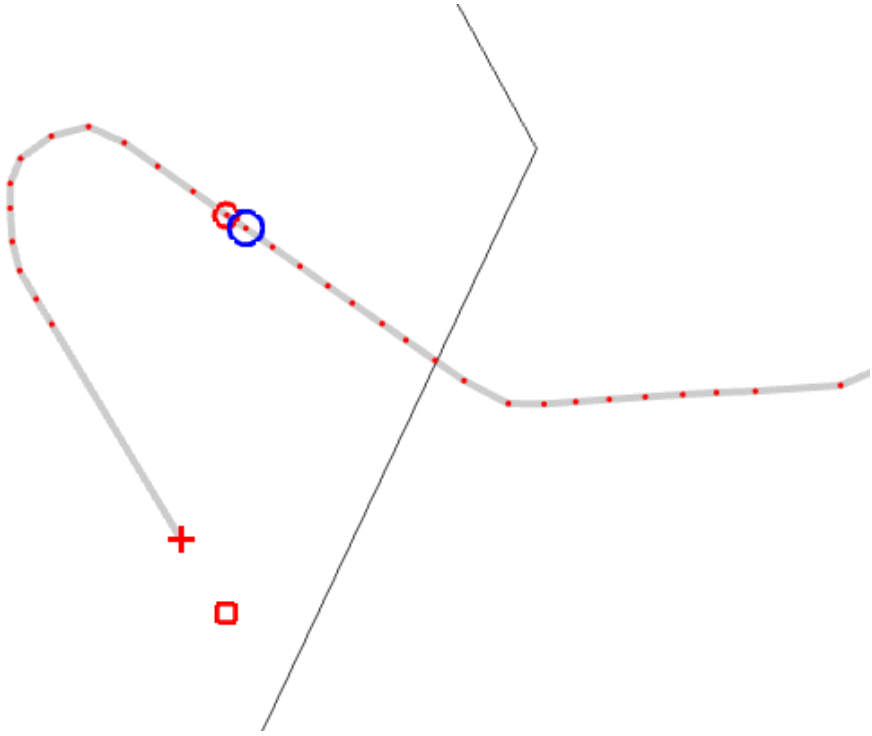

Figure 18: Non-removed pair of ADS-B points in disagreement with each other

The end result is that the filter is quite robust and capable of removing both series and singular erroneous data points.

Second, some errors can occur when ADS-B and radar data from the same region, most often over Europe, are mixed, as shown in Figure 19. Here, the mixed stream of points, sorted by time, make it appear as though the aircraft went backwards.

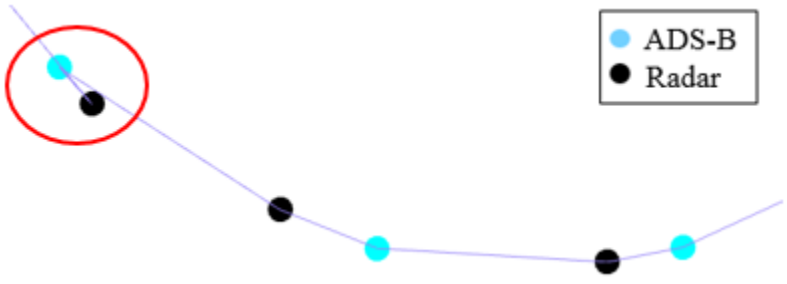


Figure 19: Data Point Reversal Error

To correct the ADS-B/Radar problem, we implement a data filter that identifies all ADS-B and radar points separated by less than 60 seconds and then discards the radar point in each pair. We take ADS-B points to be more authoritative because the position source for ADS-B is the aircraft's own navigation system, rather than a derived position from radar.

The last type of problem is when certain pairs of track points repeat, that is, the same position and time fix are recorded two or more times. We remove these duplicate points using a simple filter that checks for duplicate positions between sequential points and removes the duplicate points.

### 7.1.3 Interpolating tracks

To make statements about aircraft separation in Section 5.2, we need aircraft position at tighter intervals than provided by FlightAware. Oceanic position reporting intervals run from 2 to forty-five minutes. At an average cruising groundspeed of 470 knots, an aircraft can travel from 16 to 353 nm. On the upper end of the distance range, a short cross-track encounter that passes within separation distance with another aircraft would not be detected.

From our data, the time between raw track points mainly depends on the source of the track point. ADS-B sources provide the fastest updates, followed by Radar, and then Oceanic, as shown in Table 3.

Table 5: Update periods for track point data types

| Update Type | Time between updates |
|---|---|
| **ADS-B** | 15-30 seconds |
| **Radar** | 60 seconds |
| **Oceanic** | 2-45 minutes |

Variation in the update rate for oceanic data points comes from the different reporting systems used in oceanic airspace. Traditionally, position reports are provided by direct voice updates from the pilot over High Frequency (HF) radios. More advanced technology allows for automatic datalink transfer of position to air traffic control on a defined schedule, such as Automatic Dependent Surveillance-Contract (ADS-C) (ICAO 2013).

The closer the data points are to each other, the more confident we can be in an aircraft's interpolated position between the data points. Assured positions allow us more confidence in our estimate of how close two aircraft come to each other. To get an idea of the oceanic data time density, we tallied the time between oceanic updates for each flight track and took the mean over each flight. Figure 20 shows the resulting distribution of update times.

About half the flights through New York Oceanic have a mean time of 10 minutes or less between oceanic reports. In ten minutes an aircraft with a groundspeed of 450 knots will travel about 75 nm. While 75 nm is enough space to conduct significant turning maneuvers, we assume that most deviations from the great circle track would show up on larger length scales.

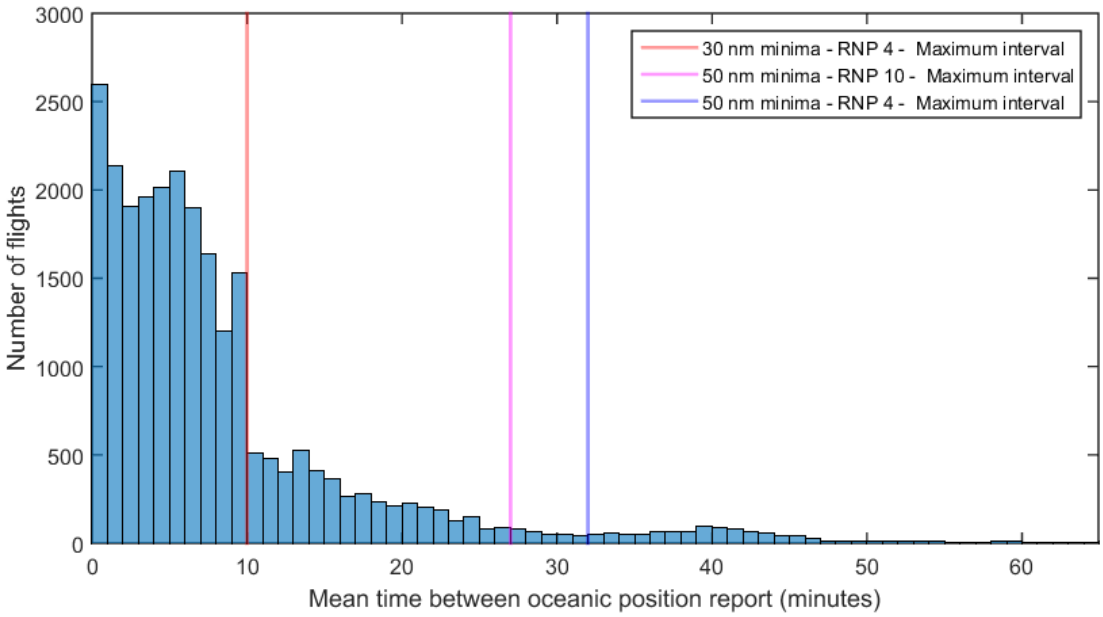


Figure 20: Distribution of oceanic reporting times in ZWY CTA

In CEP, the update requirement for 30nm separation is relaxed to 14 minutes. Figure 21 shows the distribution of CEP oceanic reporting times.

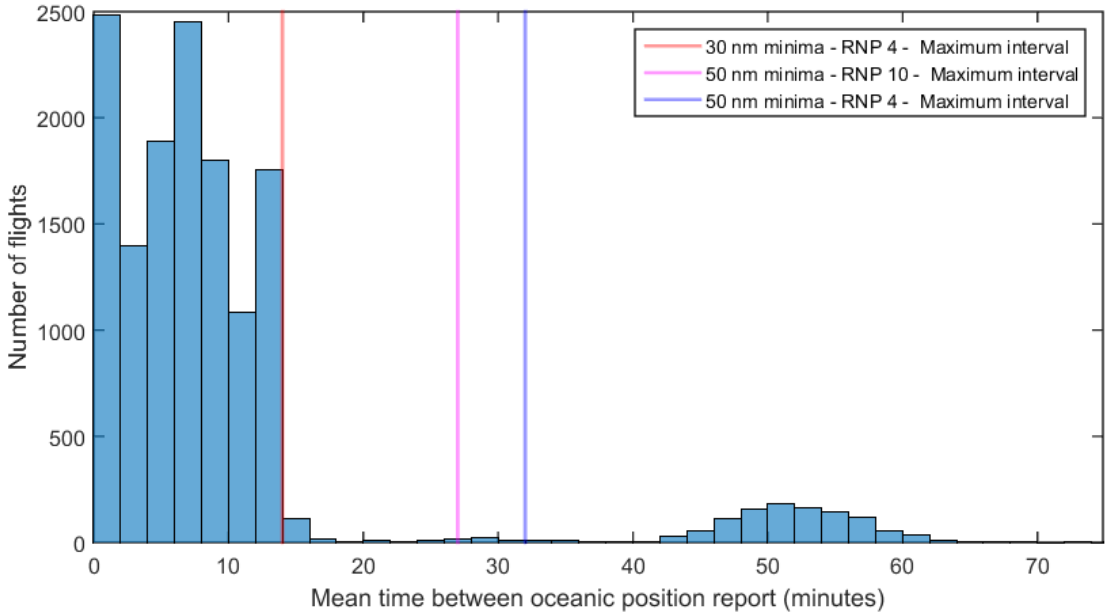


Figure 21: Distribution of oceanic reporting times in ZAK CTA

We interpolate new data points by assuming that aircraft follow a great circle route and that parameters such as altitude and groundspeed linearly interpolate from the first to the second data point. The error in making a great circle assumption is greater as time increases between the two end points, especially over the mid-Atlantic south of the North Atlantic Tracks where flights have more leeway to track to the best winds.

### 7.1.4 Compensating for missing data

True airspeed and heading data is not included in our flight track data so we had to estimate course to compute the true airspeed. Using MATLAB's "azimuth.m" function, which computes the course angle between two track points, we computed the course from any given point to the points just ahead and behind the main point in time. By assuming great circle paths, the computed courses represent arrival and departure course angles.

The course angle between two points close together in time is more likely to be the correct representation of course angle for a single point than the angle between two distant points. Since we compute course from the angles to the previous and subsequent points we use time-based weighting to average between the two computed course angles, as shown in

Figure 22. In the figure, the aircraft course at track point *b* is estimated using the course from *b* to *a* minus 180˚, and the course from *b* to *c*. The magnitude of the course vector is set by the groundspeed of the aircraft at the track point.

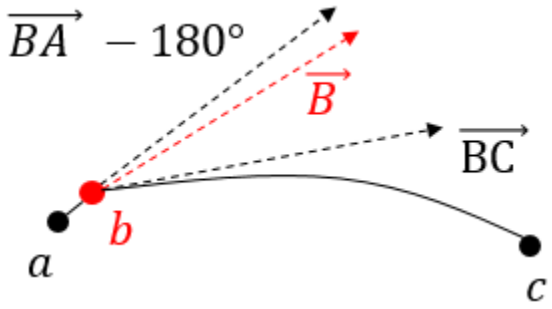


Figure 22: Estimated course

The resulting estimated course approximates the aircraft course, even during sharp turns, as would be found on approach. Figure 23 shows the estimated course vectors of a Boeing 757 on approach to Miami International.

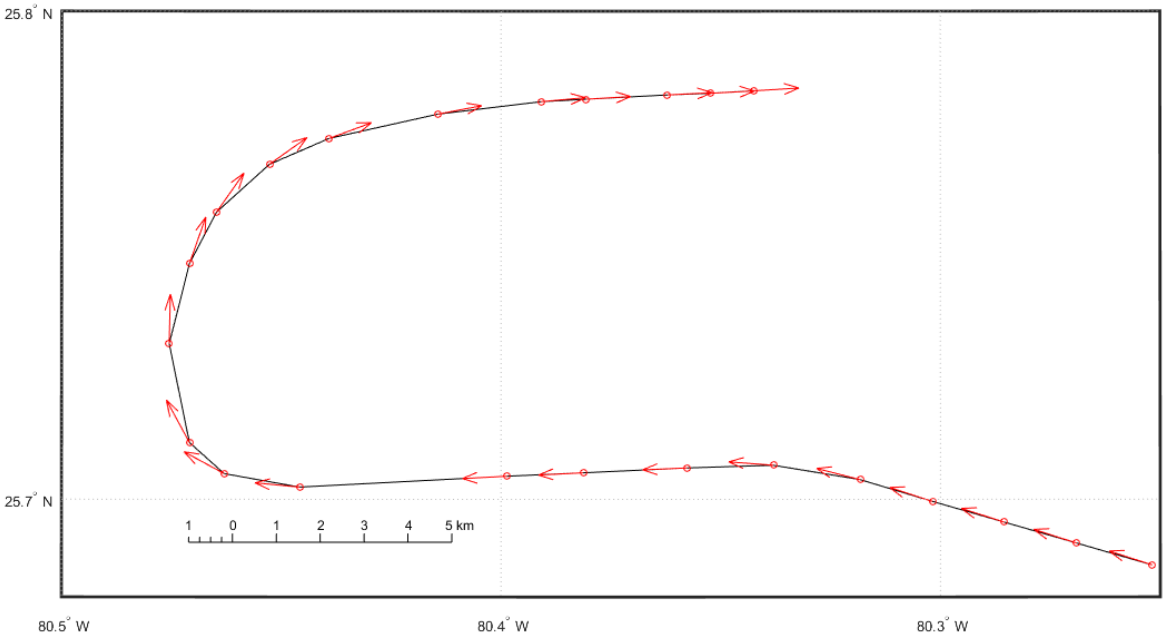


Figure 23: Estimated course vectors on approach to KMIA

### 7.1.5 Weather Data

Our weather data source is the Global Forecast System (GFS). GFS provides wind, temperature, and geopotential height data on latitude-longitude grids with global coverage. We discuss our procedure for collecting and formatting the weather data in Appendix B. To avoid unacceptable loading times, analysis is performed using weather grids fixed in time, i.e., weather

## 7.2 Central East Pacific

Central East Pacific (CEP) is a set of seven fixed routes connecting Hawaii and the US West Coast. Figure 24 shows the seven CEP routes.

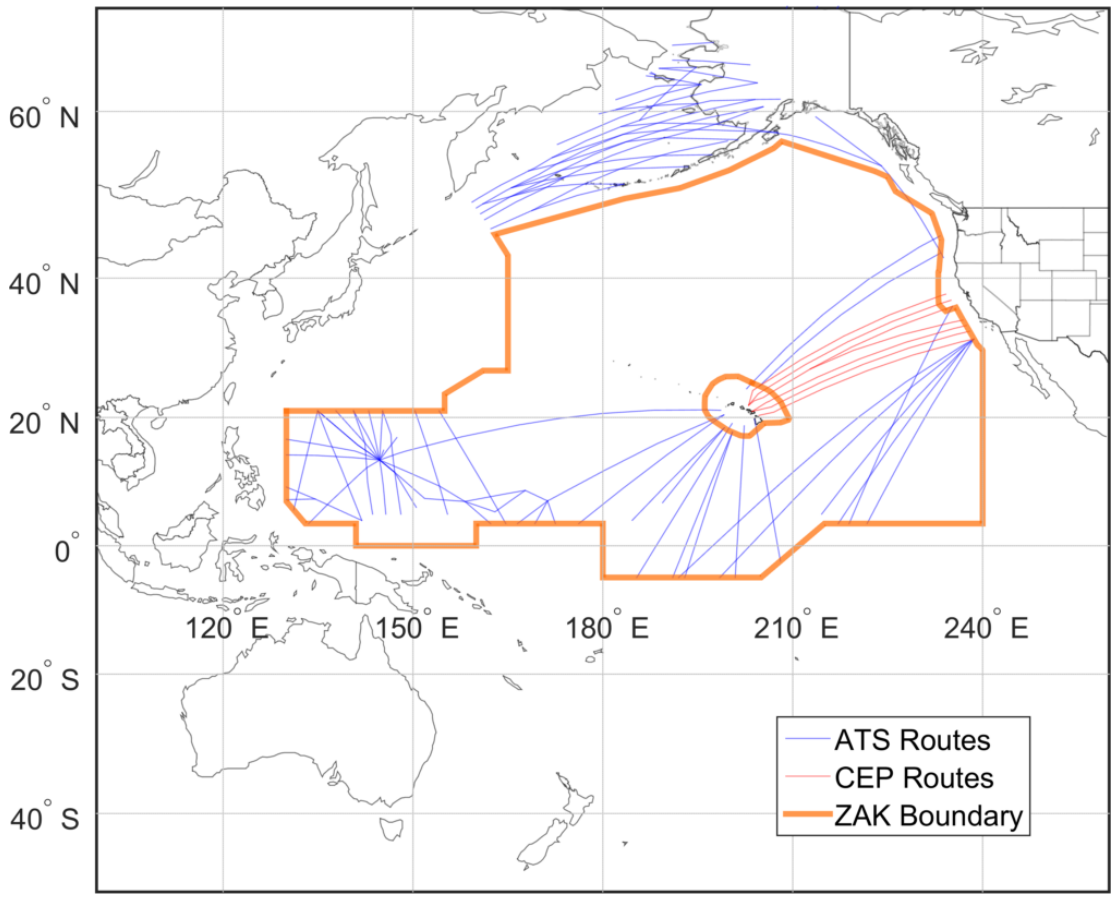


Figure 24: Structure of CEP, bounding airspace, and additional routes

Traffic on the CEP routes is almost completely comprised of flights between Hawaii and the Continental United States with the occasional flight to/from Sydney or Auckland. Figure 25 shows the paths of aircraft through the region.

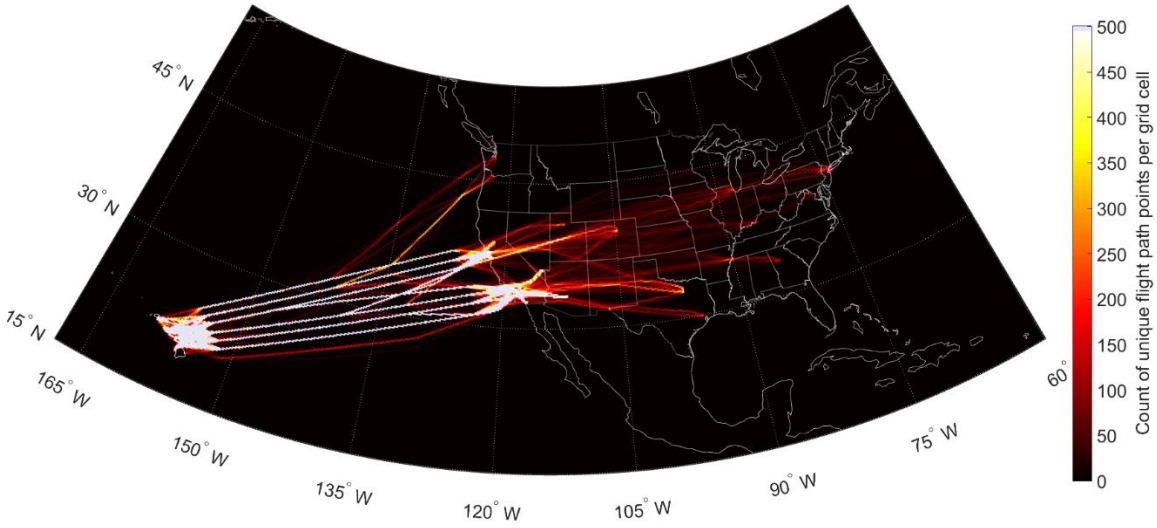


Figure 25: CEP Flight tracks from February 1st to August 1st aggregated

### 7.2.1 Data Set Selection

We selected flights from our database that flew through CEP during the month of April. In total, there were 5498 flights in the database for April, of which 5351 had complete tracks and performance files for their type in the BADA database.

As discussed in Section 4.1, certain regions of the flight envelope are unfeasible. If the estimate of initial mass is higher than reality, then the 300 ft/min climb rate ceiling could be lower than the actual altitude. Also, noisy groundspeed profiles can result in Mach profiles going below buffet Mach for the given conditions. Flight in unfeasible regions can skew or misstate inefficiency so we developed a filter to remove flights that are not feasible.

First, we measure the feasibility of a flight by comparing two flight parameters, altitude and Mach, against the limits we established in Section 4.1 for capping optimal altitude. We tally the total number of moments in flight that stay inside the feasible limit and compute

a “feasibility” percentage. We can then select all flights with a feasibility greater than or equal to some arbitrary cutoff value. Figure 26 shows the percent of flights dropped from the dataset as a function of the cutoff value.

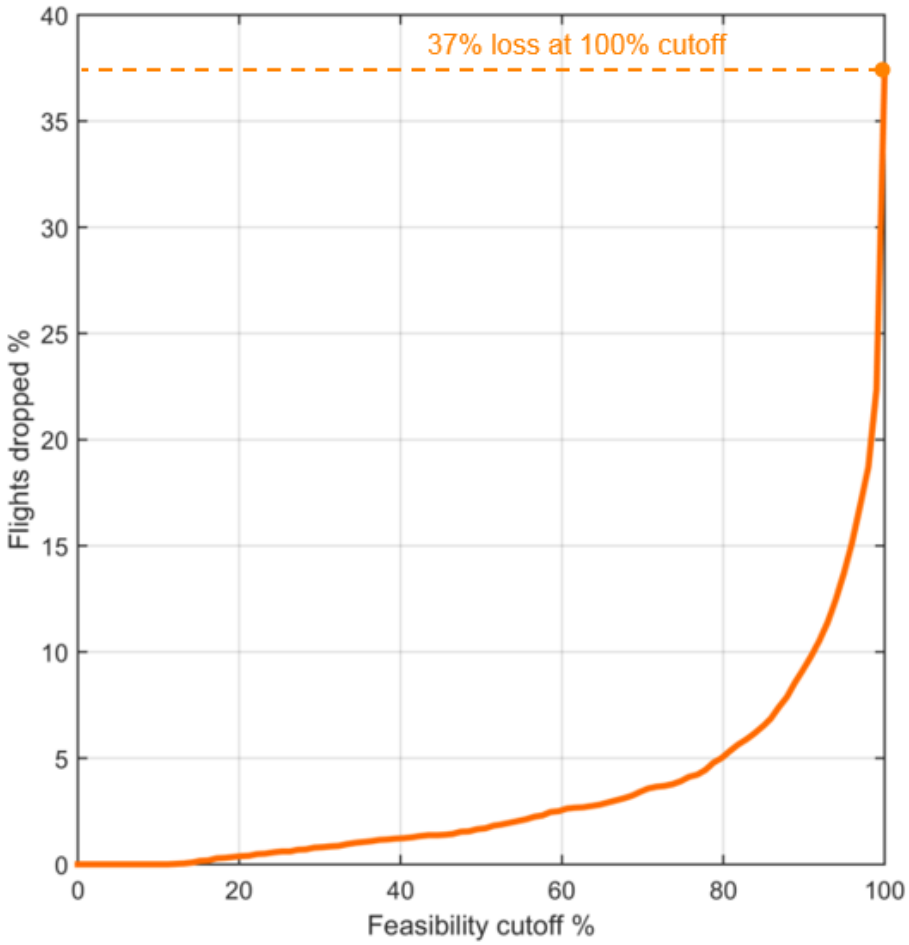


Figure 26: CEP Percent of flights dropped based on feasibility cutoff setting

To see the effects of removing infeasible flights, we computed the fuel burn inefficiencies for a range of cutoff values going from 0% to 100% and plotted the percent error with respect to the inefficiencies from the 0% cutoff group in Figure 27.

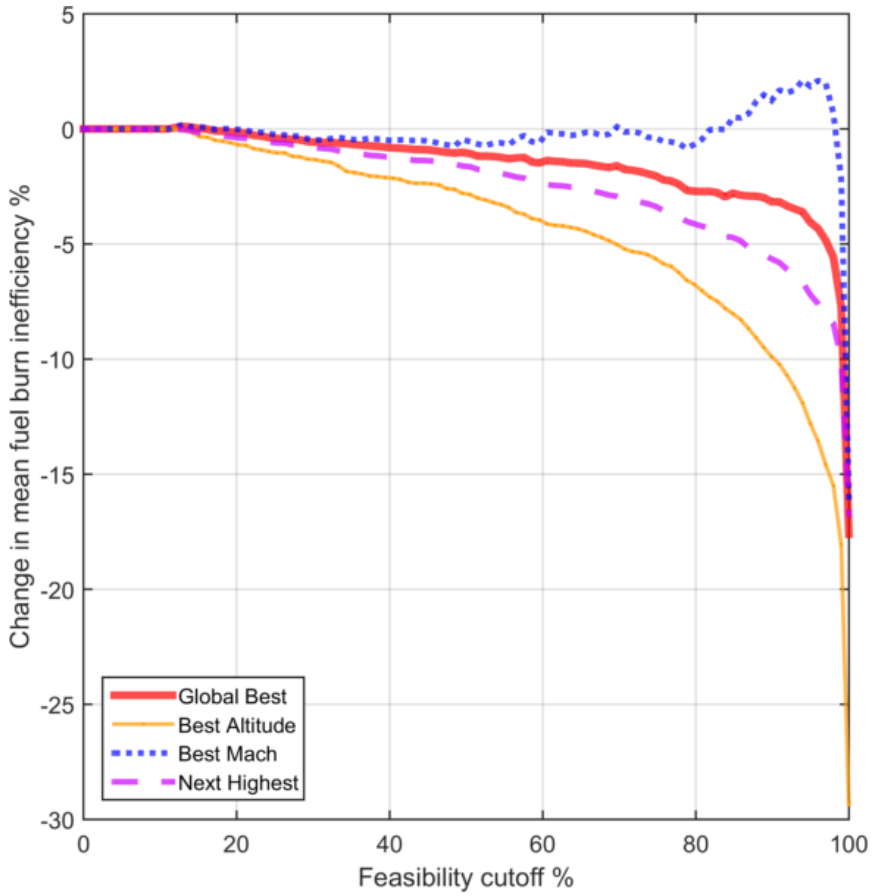


Figure 27: CEP Inefficiency variation with change in feasibility cutoff

The change in inefficiency allowed us to see the effect of keeping the infeasible flights on the mean inefficiency for each trajectory type. For example, if we selected 60% as our cutoff value, then using the unfiltered dataset would have underestimated Best Altitude mean inefficiency by roughly 4%. We selected a 100% feasibility cutoff since a 37% loss in flights indicated by Figure 26 was acceptable in light of the large change in Best Mach inefficiency right near the 95% cutoff.

Applying the feasibility criteria reduced the final dataset to 3084 flights.

### 7.2.2 Results

Table 6 shows the results after filtering against the feasibility criteria.

Table 6: Initial CEP Inefficiency Results

| 3084 flights | Global Best | Global Best - Legal | Best Altitude | Best Altitude - Legal | Best Mach | Next Highest | Horizontal |
|---|---|---|---|---|---|---|---|
| **Mean %** | 4.97 | 4.68 | 4.50 | 3.91 | 1.23 | 2.23 | -0.22 |
| **S.D. %** | 4.21 | 4.27 | 3.72 | 3.70 | 2.32 | 1.55 | 1.39 |

To our surprise, a significant portion of Best Mach and Horizontal inefficiencies resulted in a negative results. Taken at face value, the result appeared to indicate that our solvers were outputting sub-optimal trajectories. After further investigation, we found that most of the CEP flights had a similar problem that was causing an underestimate of the base fuel burn, resulting in exaggerated low inefficiencies.

The problem in the data is the same problem our $\Delta e_d$ metric was designed to eliminate, which was an inconsistency between the base trajectories and our between track segment assumptions of great circle path and linear groundspeed profile. The reason the problem still exists is that our fuel burn computation depends on time, rather than distance, so the $\Delta e_d$ metric is less applicable.

To solve the issue, we computed new time histories for the base track in the same way we did for optimal Mach trajectories in Section 4.1. The differences between the actual (timestamp) and computed time in the airspace were mostly on the order of a few minutes, which seemed insignificant on the surface. However, a few extra minutes are significant for common fuel burn rates, which can be on the order of one kg/sec, resulting in several hundred kilograms of extra fuel when comparing the computed time fuel burn to the timestamp fuel burn. Common total fuel burns for CEP are on the order of 10,000 kg so on average the error can add up to several inefficiency percent points. We plotted the percent change between base fuel burns in Figure 28.

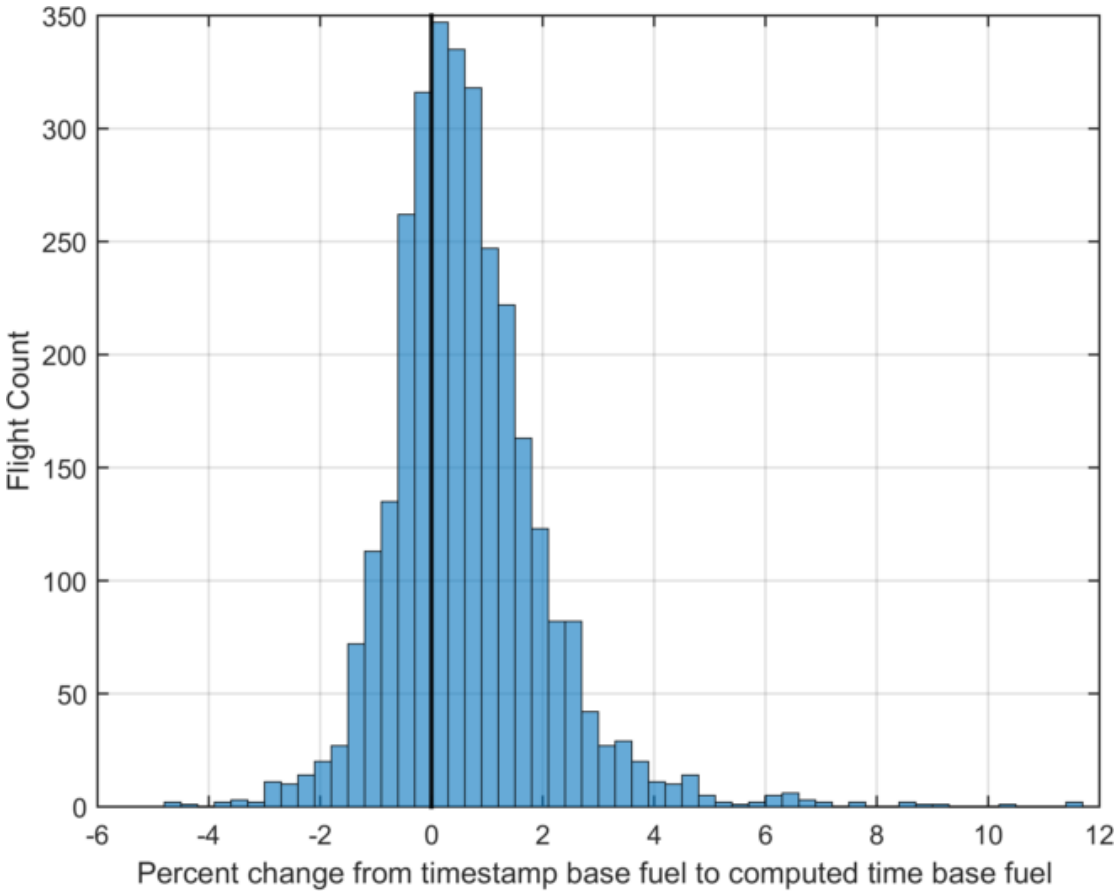


Figure 28: Change in basis fuels when computing time histories

The positive change indicates that using the timestamp base fuel for the inefficiency calculation will result in a decreased inefficiency. Flights with a larger difference in base fuels will see a decrease in inefficiency, possibly leading to negative inefficiencies if the gain from flying the fuel optimal trajectories is small.

Using the new base fuel burn, we recomputed inefficiencies for the affected trajectories. The only trajectories we computed time histories for are the Global Best, Best Mach, and Horizontal inefficiencies.

Table 7: Recomputed Time Basis: CEP Inefficiency Results

| 3084 flights | Global Best | Global Best - Legal | Best Altitude | Best Altitude - Legal | Best Mach | Next Highest | Horizontal |
|---|---|---|---|---|---|---|---|
| **Mean %** | 5.62 | 5.33 | 4.50 | 3.91 | 1.86 | 2.23 | 0.41 |
| **S.D. %** | 3.92 | 3.99 | 3.72 | 3.70 | 1.62 | 1.55 | 1.05 |

With the computed time basis, all affected trajectories return sensible inefficiency results, for example, Global Best showed the highest inefficiency. There still remains the issue of large inefficiencies for trajectories that modify altitude, but that is explained by BADA over-weighting parasitic drag, resulting in excessively reduced fuel burn at higher altitudes.

One thing of interest to us was if longer flights suffered from greater horizontal inefficiency as distance flown inside the airspace increased, which is plotted in Figure 29.

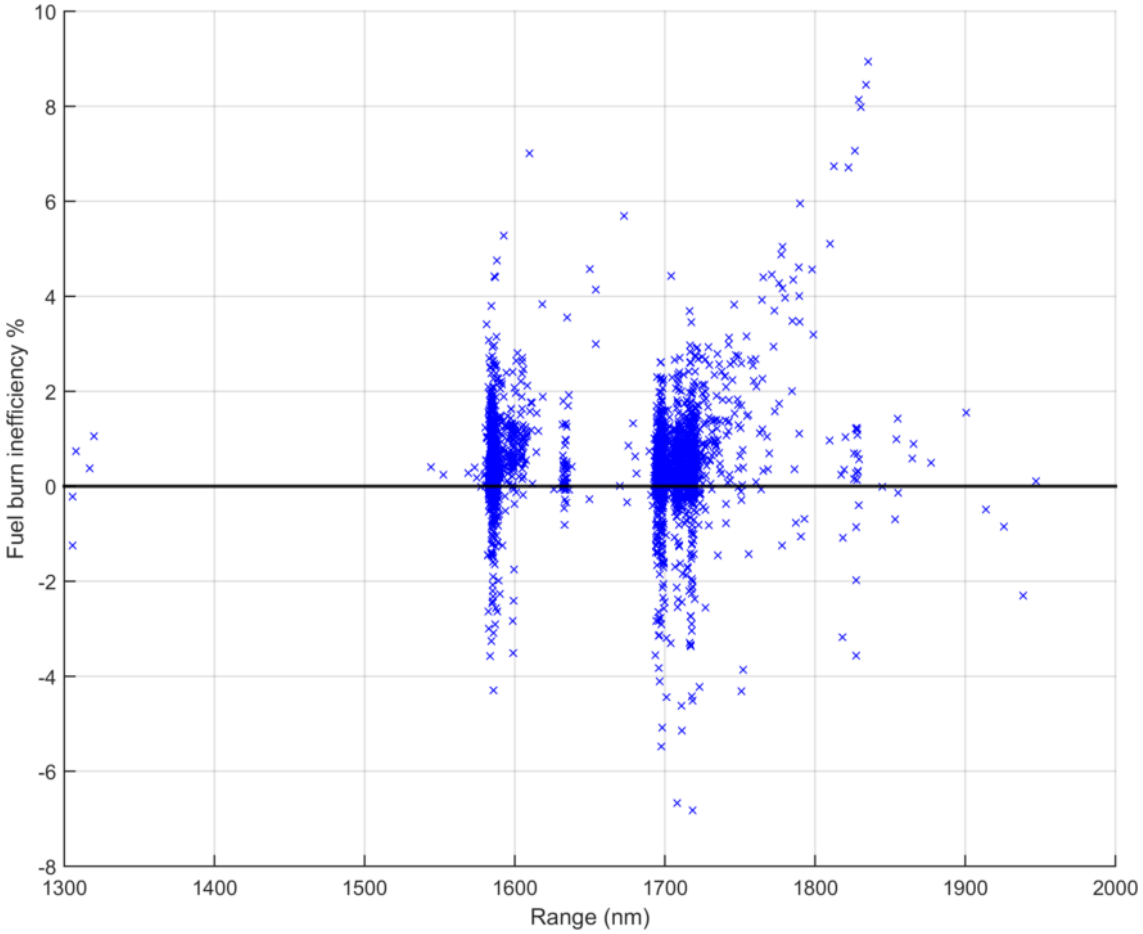


Figure 29: CEP Horizontal inefficiency vs distance traveled in airspace

Inside each of the main clusters, there did not appear to be much correlation with distance. A few flights at about 1800 nm showed some manner of a positive trend but the rest of the long range flights have average inefficiencies.

To obtain the effect of blocking on the inefficiencies, we used the blocking event as a filter to separate the dataset into two states, blocked and not blocked.

Table 8: Examining the effect of blocking on CEP inefficiency

| | Blocked, 1516 flights | | Not Blocked, 1581 flights | | Difference between means |
|---|---|---|---|---|---|
| | Mean % | S.D. % | Mean % | S.D. % | |
| **Global Best** | 6.24 | 4.13 | 5.03 | 3.62 | 1.21 |
| **Global Best L.** | 5.94 | 4.23 | 4.75 | 3.67 | 1.19 |
| **Best Altitude** | 5.12 | 4.00 | 3.91 | 3.33 | 1.21 |
| **Best Altitude L.** | 4.47 | 3.98 | 3.38 | 3.32 | 1.09 |
| **Best Mach** | 2.10 | 1.69 | 1.63 | 1.52 | 0.47 |
| **Next Highest** | 2.33 | 1.61 | 2.14 | 1.49 | 0.19 |

For Global Best and Best Altitude trajectories, the differences in means between the blocked and not blocked states was statistically significant when using the two-tailed t-test at an alpha level of 0.01. There is about a 1.2 increase in altitude-based inefficiency percentage for flights that pass within 50 nm of another aircraft and have optimal altitudes on the other side of the conflicting aircraft's altitude.

## 7.3 West Atlantic Route System

The West Atlantic Route System (WATRS) refers to a set of Air Traffic Service (ATS) routes contained with the western half of New York Oceanic FIR (KZWY.) Figure 30 shows the distribution of ATS routes through WATRS and ZWY.

Traffic through WATRS is a mix between predominantly north-south traffic between New York and the Caribbean (primarily Puerto Rico and the Dominican Republic), and east-west traffic between Florida and Western Europe. Figure 31 shows the paths of aircraft through the region.

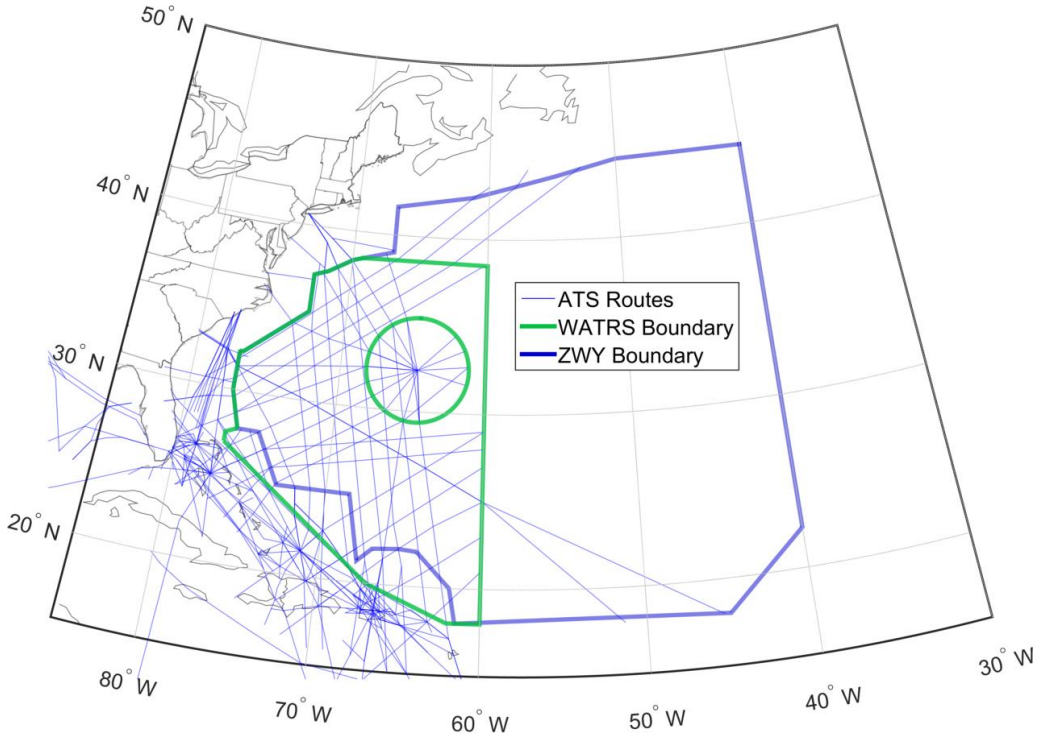


Figure 30: Structure of WATRS, bounding airspace, and additional routes

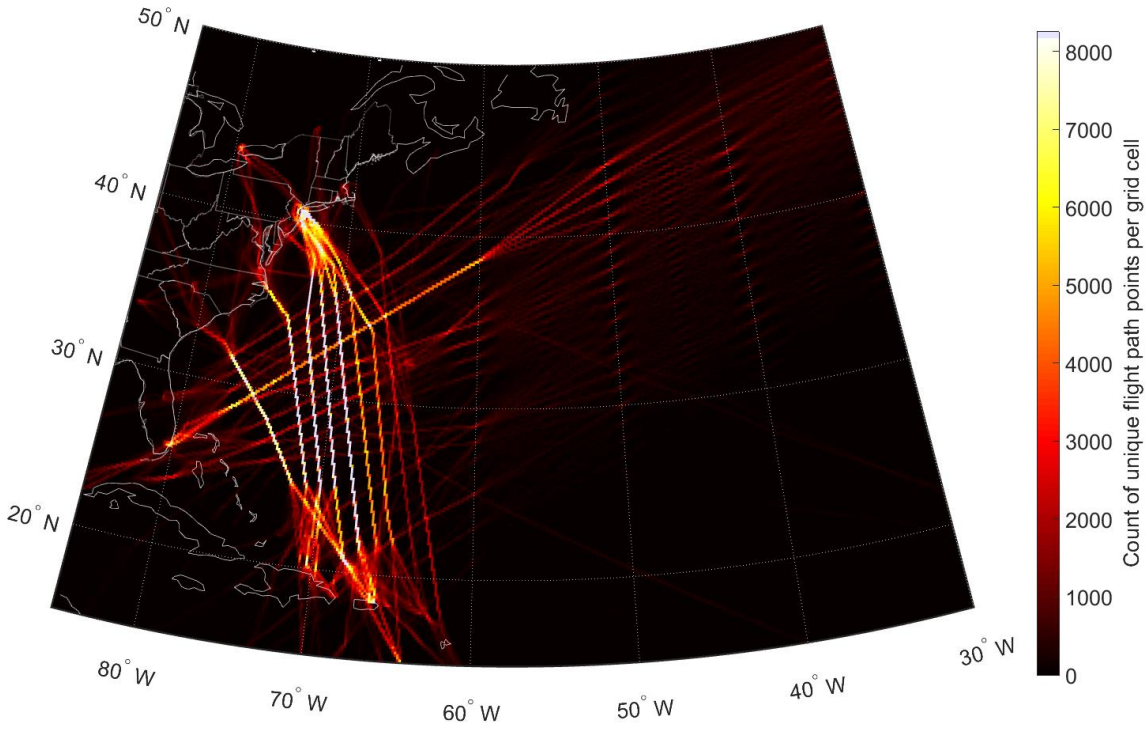


Figure 31: WATRS Flight tracks from February 1st to August 1st aggregatedData Set Selection

There is more traffic through WATRS than CEP so the initial dataset for April contains 9305 flights, of which 8908 flights have complete tracks and BADA performance files. Using the same criteria from CEP for the feasibility filter, the final dataset is reduced to 4535 flights.

Dropping the infeasible flights had about the same effect as in CEP by reducing underestimation for all trajectory types.

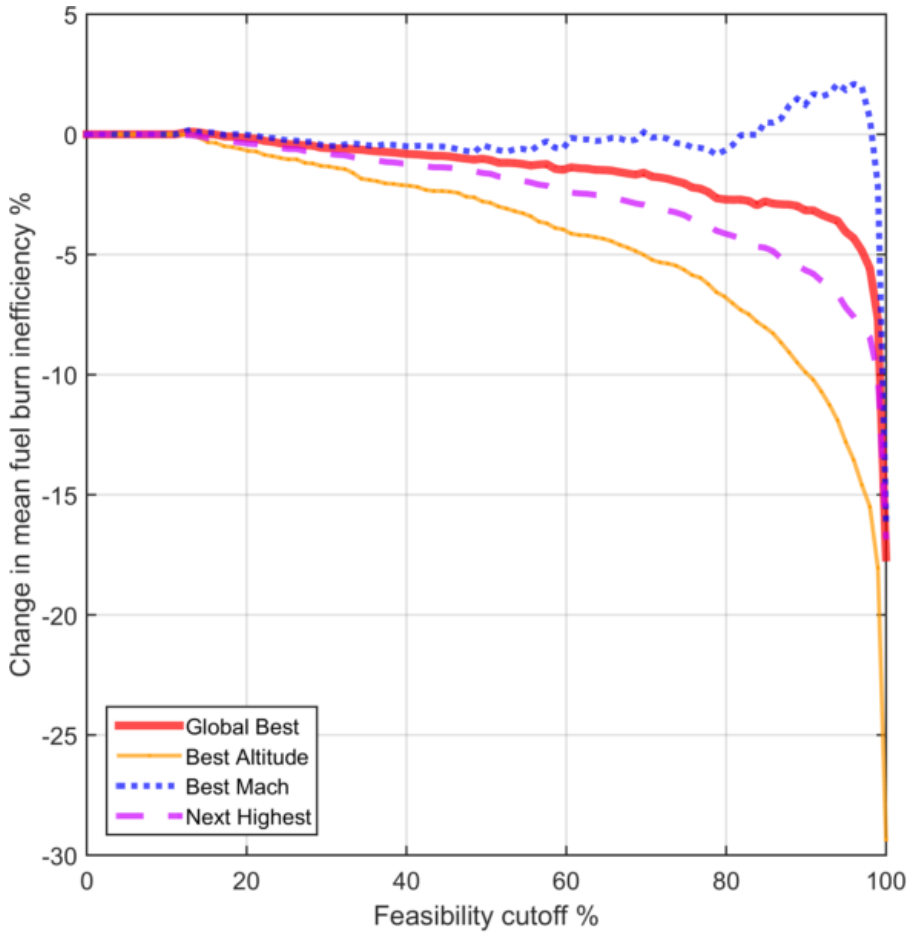


Figure 32: WATRS Inefficiency variation with change in feasibility cutoff

### 7.3.1 Results

Table 9: WATRS Inefficiency Results

| 4535 flights | Global Best | Global Best - Legal | Best Altitude | Best Altitude - Legal | Best Mach | Next Highest | Horizontal |
|---|---|---|---|---|---|---|---|
| **Mean %** | 5.97 | 5.51 | 4.75 | 3.43 | 1.90 | 2.46 | 0.94 |
| **S.D. %** | 4.72 | 4.70 | 4.00 | 3.98 | 2.75 | 1.66 | 2.20 |

Here we have a different result than CEP, where no inefficiencies were negative, and Global Best showed the greatest inefficiency even when using the timestamp base fuel as reference. WATRS flights did not suffer as much on average from unequal time bases as CEP. We still used recomputed fuel burns as a basis in order to minimize variation due to those flights that have unequal time problems.

Table 10: Recomputed Time Basis: WATRS Inefficiency Results

| 4535 flights | Global Best | Global Best - Legal | Best Altitude | Best Altitude - Legal | Best Mach | Next Highest | Horizontal |
|---|---|---|---|---|---|---|---|
| **Mean %** | 6.27 | 5.80 | 4.75 | 3.43 | 2.18 | 2.46 | 1.24 |
| **S.D. %** | 4.27 | 4.24 | 4.00 | 3.99 | 1.83 | 1.66 | 1.79 |

The differences between inefficiency percentages between fuel bases averaged out to about 0.2. The major effect of changing bases was to tighten up the distributions, due to removing the relatively randomly distributed time errors. Beyond correcting for model biases, we have uncertainties in our results which we cannot quantify because we do not have real fuel burn data with which to perform a proper model validation. Knowledge of actual initial mass, wind, and temperature data would allow a comparison with model estimates to generate uncertainty in the final result.

Figure 33 shows range based inefficiency in WATRS.

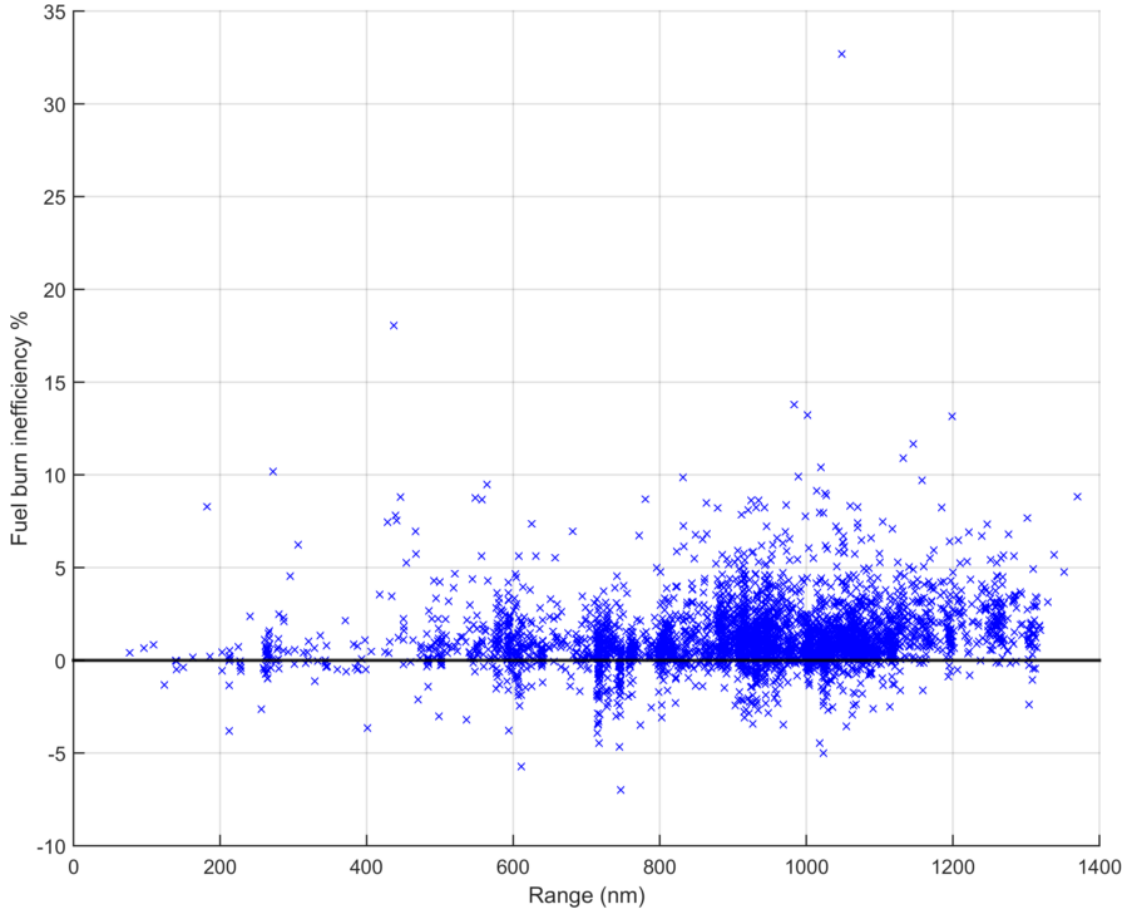


Figure 33: WATRS Horizontal inefficiency vs distance traveled in airspace

Surprisingly, there did not seem to be a correlation of inefficiency with range. We expected a positive trend of inefficiency with range because the longer the flight, the greater the potential savings. A 20 kts boost to groundspeed will make a larger difference in the total fuel burn of a 1500 nm flight than a 500 nm flight because time savings scale over distance. In addition to scaling, the wind-optimal track in a constant gradient wind should be the same as in a zero wind situation, which is the great circle track. Put simply, gains from following a crosswind away from the great circle track will be lost when steering back to the destination. The longer the distance of a flight, the less chance the gradient of the winds will remain constant, implying the wind optimal track diverges from the great circle track.

A potential physical explanation for a lack in correlation is that, on average, wind patterns may align better with WATRS tracks used for longer distance flights. In this case, these

long range tracks are naturally “optimized” compared to the tracks used for shorter range flights. CEP inefficiency against range in Figure 29 shows a series of long range flights following a positive trend, implying that certain combinations of winds and CEP tracks results in worse inefficiencies.

A confounding factor is airspeed and altitude variation. The wind optimal trajectory we generate has constant altitude and airspeed, so the longer the flight, the less the optimal and actual flights will match in fuel burn if we only examined altitude and speed savings. In addition to fuel results, we checked the time savings against distance in Figure 34 and found similar behavior to the fuel inefficiencies but with a more pronounced upper limit that increased with distance.

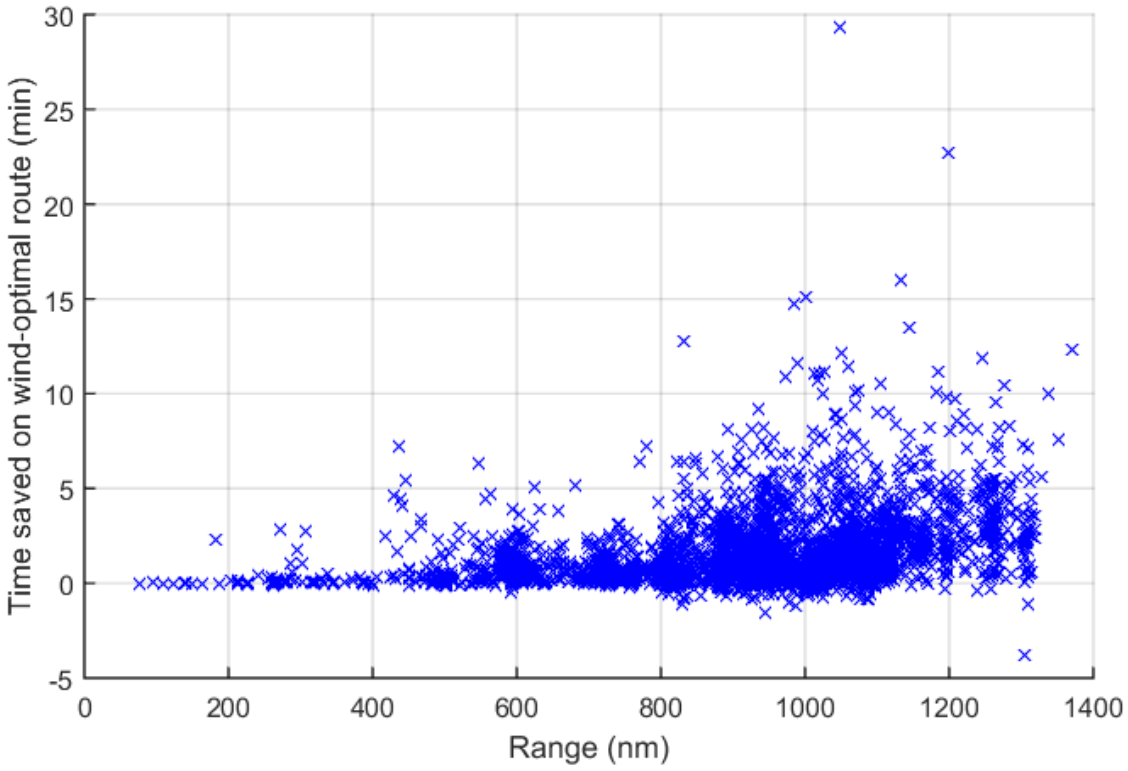


Figure 34: WATRS time savings on optimal route vs distance traveled in airspace

Checking blocking effects, we used the recomputed time fuel as the basis for the inefficiency calculation.

Table 11: Examining the effect of blocking on WATRS inefficiency

| | Blocked, 3833 flights | | Not Blocked, 702 flights | | Difference between means |
|---|---|---|---|---|---|
| | Mean % | S.D. % | Mean % | S.D. % | |
| **Global Best** | 6.70 | 4.26 | 3.90 | 3.41 | 2.80 |
| **Global Best L.** | 6.22 | 4.24 | 3.51 | 3.43 | 2.71 |
| **Best Altitude** | 5.15 | 4.00 | 2.56 | 3.17 | 2.59 |
| **Best Altitude L.** | 3.78 | 4.01 | 1.56 | 3.23 | 2.22 |
| **Best Mach** | 2.31 | 1.84 | 1.48 | 1.61 | 0.83 |
| **Next Highest** | 2.57 | 1.64 | 1.84 | 1.64 | 0.73 |

Similar to CEP, blocking has a statistically significant impact on all trajectories.

## 7.4 Comparison

Directly comparing WATRS inefficiencies against CEP by subtracting means and standard deviations, we can see that most trajectories indicate a higher inefficiency in WATRS along with greater spread.

Table 12: Recomputed Time Basis: WATRS minus CEP mean inefficiency percent

| | Global Best | Global Best - Legal | Best Altitude | Best Altitude - Legal | Best Mach | Next Highest | Horizontal |
|---|---|---|---|---|---|---|---|
| **Mean (%-%)** | 0.65 | 0.47 | 0.25 | -0.48 | 0.32 | 0.23 | 0.83 |
| **S.D. (%-%)** | 0.35 | 0.25 | 0.28 | 0.29 | 0.21 | 0.11 | 0.74 |

One of the significant differences between the airspaces is the effect of blocking. 85% of WATRS flights recorded a blocking event, in contrast to 49% of CEP flights. The increase in the number of blocked flights is accompanied by increase in inefficiency. The difference in inefficiency percent in WATRS due to blocking is about two and a half times that of CEP.

The first reason for the large increase in both blocking counts and inefficiency is that traffic in WATRS is denser than in CEP. Structurally, crossing tracks increase opportunity for conflicts. Figure 35 shows the change in airspace load with time.

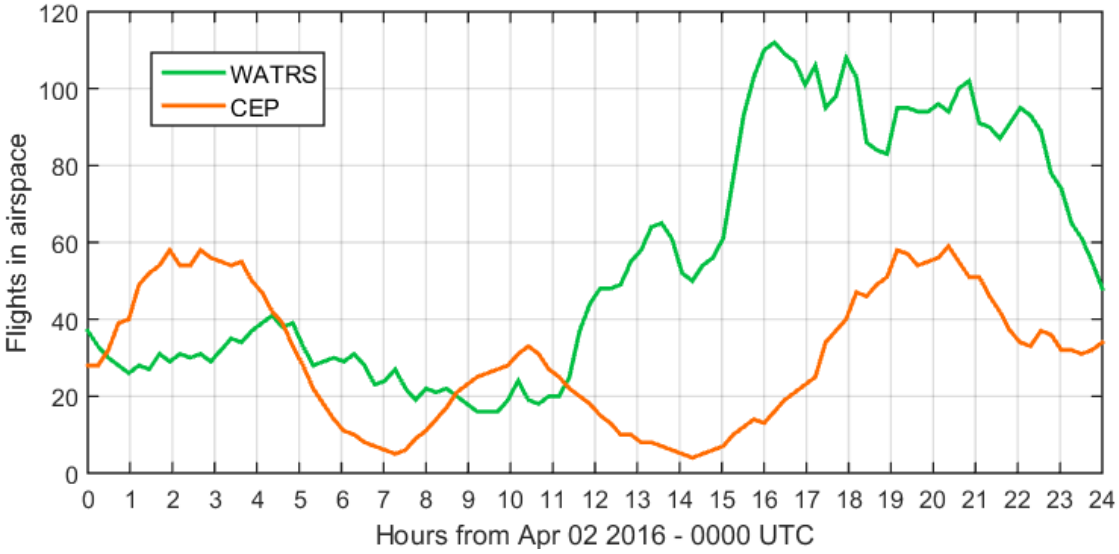


Figure 35: Flights in airspace on April 2

We would expect that an increase in the amount of time spent blocked would result in an increase in inefficiency. Figure 36 and Figure 37 show the time spent in a blocked state against Best Altitude inefficiency for CEP and WATRS respectively.

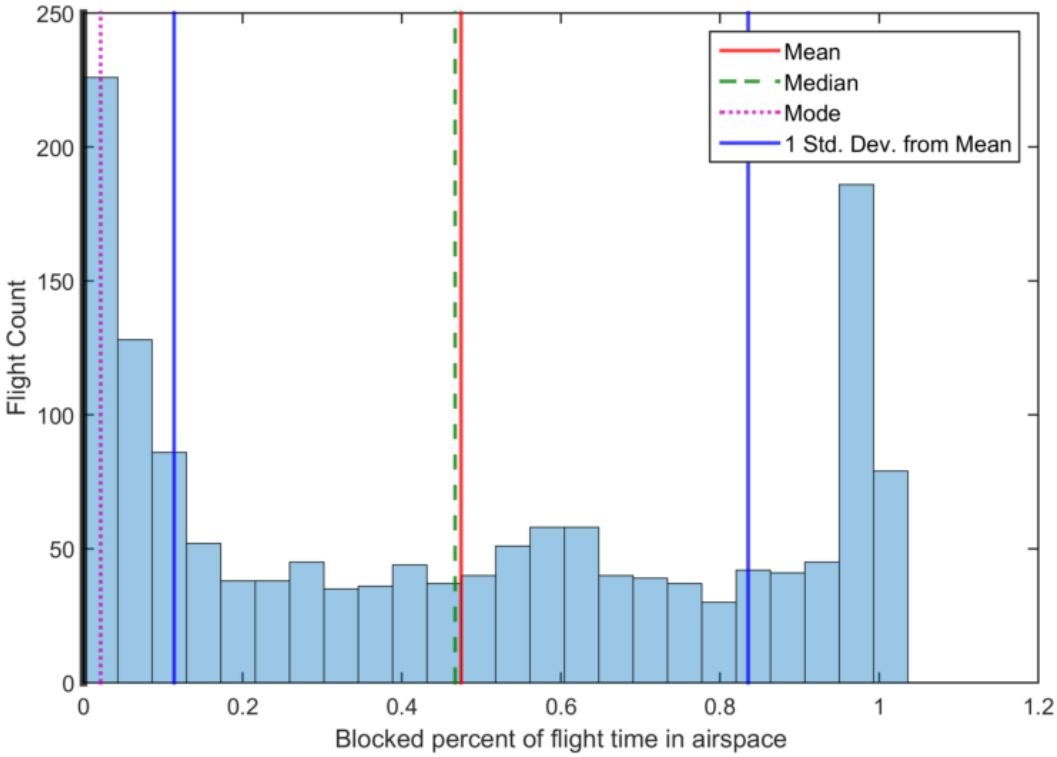


Figure 36: CEP Blocked Time (decimal percent)

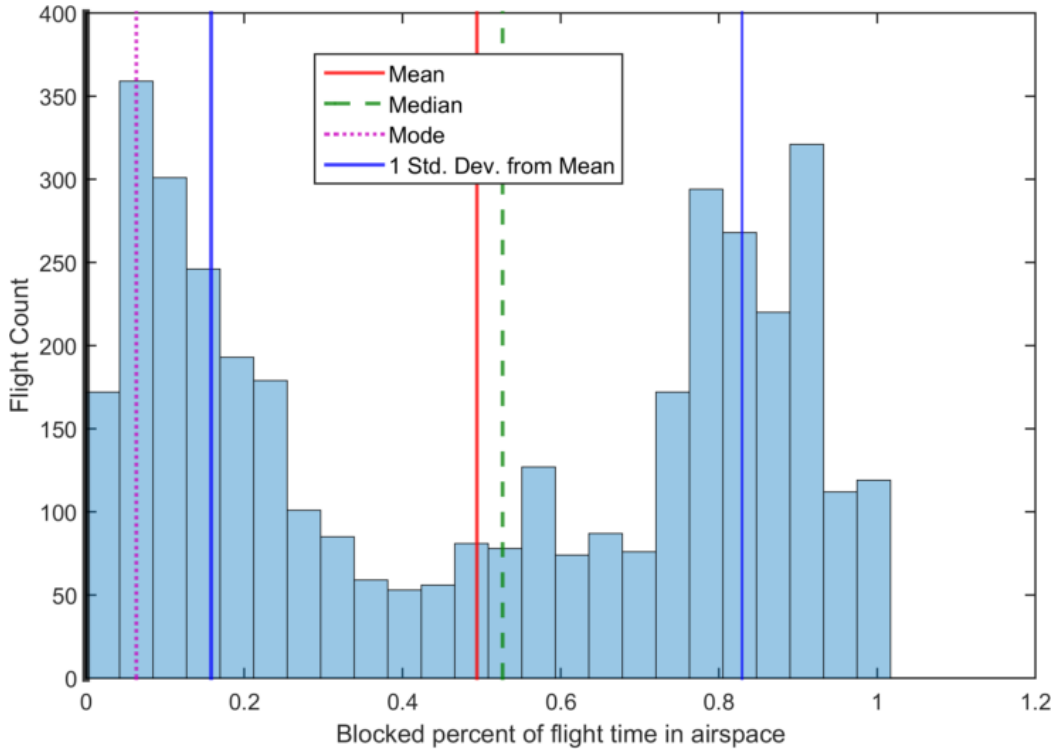


Figure 37: WATRS Blocked Time (decimal percent)

In CEP, about half of the flights are either blocked for their entire flight or not at all, with a relatively uniform distribution over the intermediate blocking percentages. WATRS is a different story, where a large segment of flights is blocked anywhere from 80% to 100% of the time. Increasing from 0%, the amount of flights decreases more slowly than in CEP, implying more flights are blocked for a shorter time. This follows from our suspicion that crossing tracks cause more momentary blocking events than in CEP, which is made up of mostly parallel routes.

We plot the relationship between blocked time and Best Altitude inefficiency in Figures 38 and 39, for CEP and WATRS. The mean difference between the Best Altitude and actual altitude is added as colors to show the effect of altitude separation on inefficiency.

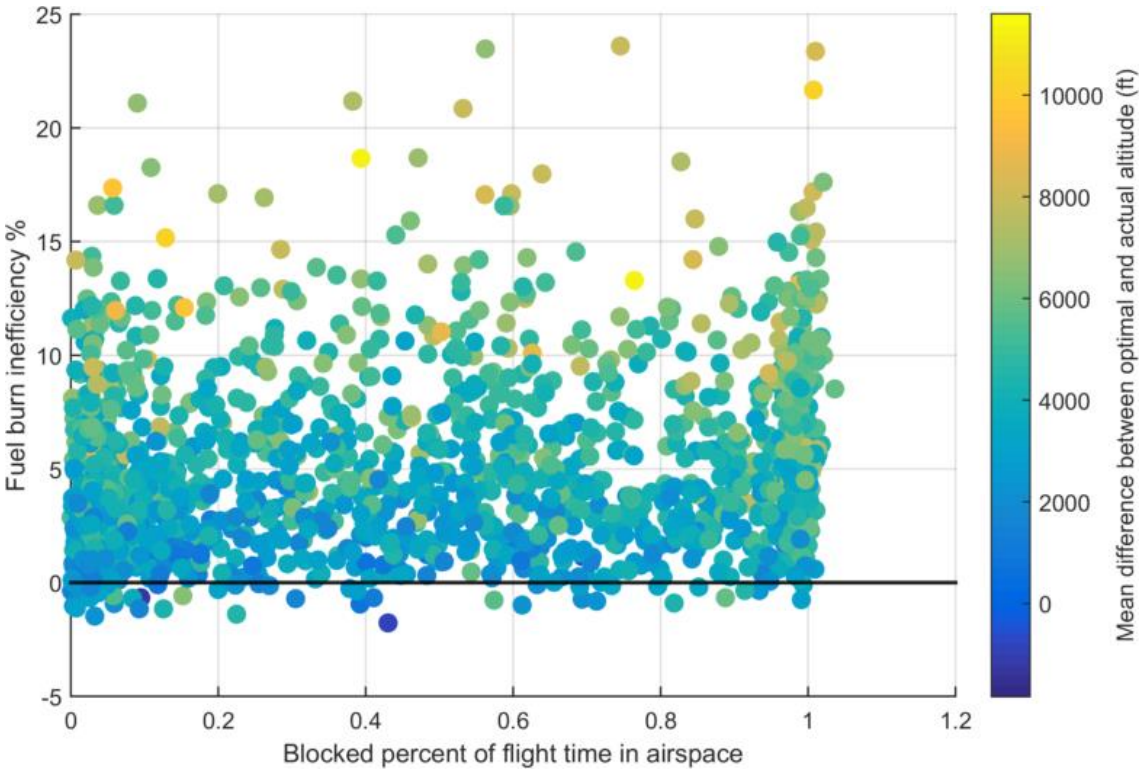


Figure 38: CEP Best Altitude inefficiency vs blocked time (decimal percent)

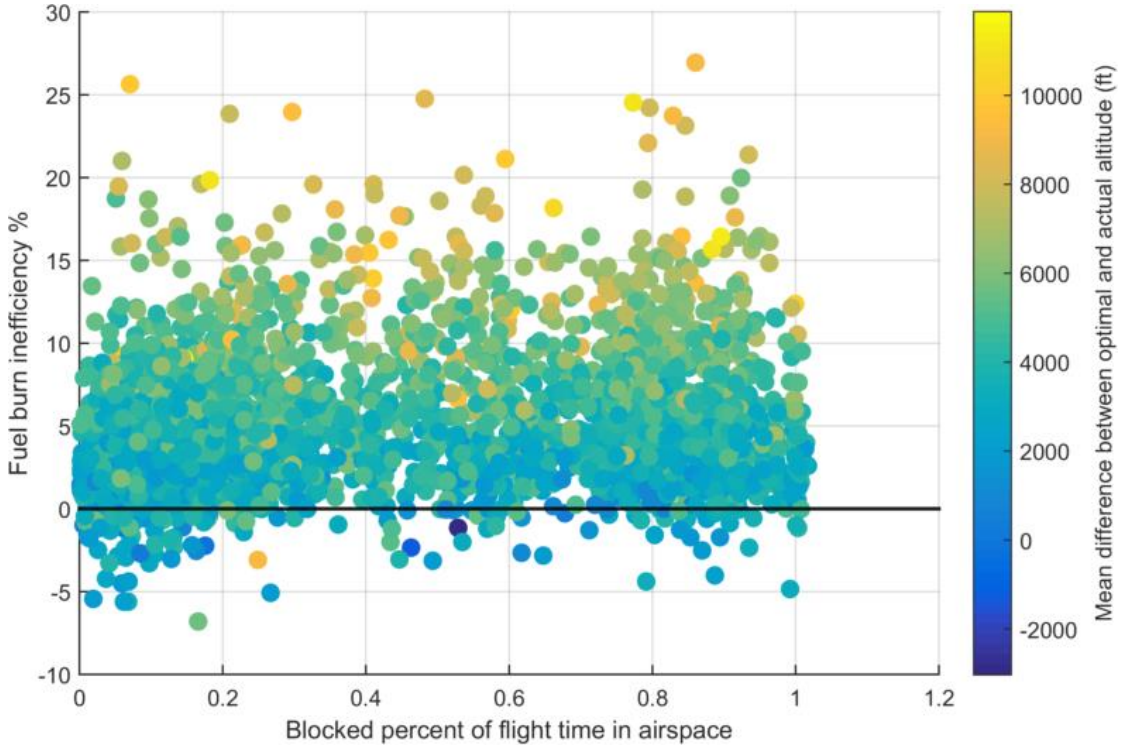


Figure 39: WATRS Best Altitude inefficiency vs blocked time (decimal percent)

We do not see any correlation between Best Altitude inefficiency and blocked time in either airspace. As expected, we still see a positive relationship between distance from optimal altitude and inefficiency.

# CHAPTER 8. CONCLUSION

Here, we will conclude with a real world comparison with our results and then a discussion on future improvements to the model and directions for future study.

## 8.1 Experimental Comparison

SESAR conducted a real world fuel efficiency experiment in 2011 called ENGAGE (SESAR, 2011). The real world test allowed 37 flights traversing the North Atlantic Tracks to freely vary their altitudes and speeds to better match their optimal trajectories. Fuel burn reduction was measured as the difference between the actual observed fuel and the planned fuel burn at fixed altitude and Mach.

The ENGAGE flights were allowed a free 2000 ft block of altitude and a 0.02 Mach range that they could traverse with no restrictions. These permissions were only allocated during the lowest traffic periods to avoid overloading controllers. Out of the 37 trials, only 23 qualified as complete tests.

Our Next Highest trajectory fits closest to the 2000 ft block limit for the ENGAGE flights so we directly compared our results with the ENGAGE results. It is important to note that the 2000 ft block altitude limits of the ENGAGE flights are not the same as adding 2000 ft to the base trajectory, so we expected to see a higher fuel burn reduction from our results compared to ENGAGE due to higher altitudes of the Next Highest trajectories. Figure 40 overlays the distribution of our Next Highest fuel reduction over the distribution from ENGAGE.

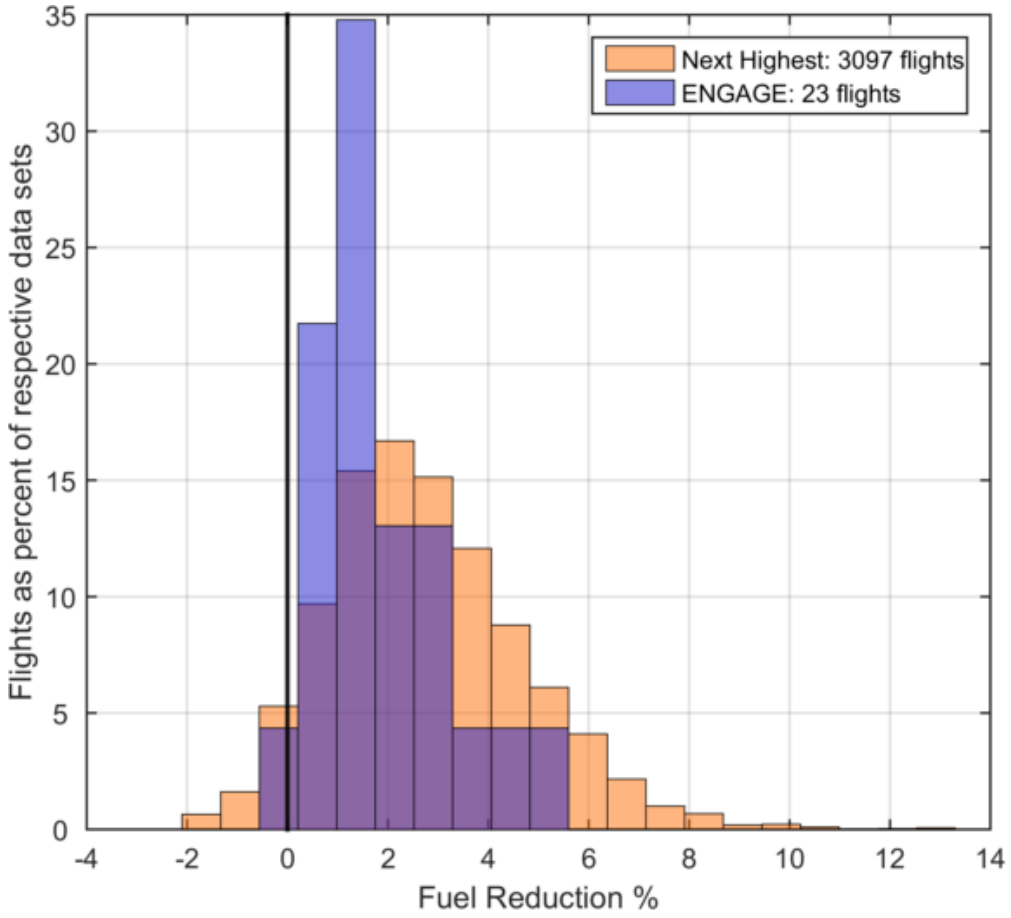


Figure 40: Distribution of CEP Next Highest and ENGAGE fuel burn reduction

Our data set falls slightly higher than the ENGAGE results, per our expectations.

As discussed in Section 4.2, BADA overestimates optimal altitude. Because of the altitude overestimate, optimal fuel burn is underestimated, leading to an overestimate of fuel burn inefficiency. Jensen's work indicated a fuel burn reduction of about 1.98% when optimizing altitude, while our altitude optimization resulted in mean reductions of 4.83% and 4.50% for WATRS and CEP respectively. When optimizing for Best Mach, Jensen got a reduction of 1.94% and we got 2.11%, indicating that the BADA overestimation affects Mach optimization less than altitude optimization.

## 8.2 Future Work

There are several tasks that would enhance the accuracy of this study. The first would be to use a more accurate, and hence more costly, performance model. The (free) BADA model overestimates optimal altitude, leading to excessively large altitude inefficiency estimates. By contrast, use of the Piano-X model returns optimal altitudes that are closer to other studies (Dalmau 2015, Jensen 2011).

Next, the blocking analysis could be improved in several ways. The first would be to enhance the separation model from a simple radius check to a rectangular model. This would allow different lateral and longitudinal separations to be used in the blocking criteria. The usefulness of checking different separations would be to see how often aircraft reach different minimums, and if the smaller minimums would increase or decrease inefficiency.

Flights are planned around weather, especially areas with turbulence. Currently, we cannot see whether or not deviations from the wind optimal track are made because of track or congestion related sources or if they are deviations from bad weather. Flights avoiding bad weather will show large inefficiencies which are not directly attributable to the design of the airspace.

The BVP4C solver has the capability to handle multistage TPBVPs, implying that we could expand the solver to handle changes in altitude or airspeed in the future. This would allow us to combine optimal altitudes and speeds with wind optimal tracks to estimate an upper limit to total inefficiency.

We have generated hundreds of new optimal flight tracks, but we do not know if the tracks would cause an unacceptable increase in the number of traffic conflicts. Grabbe (2007) used scheduling algorithms to try and schedule the optimal tracks so that they can be deconflicted. Beyond enhancing the results of the current study, we suggest an examination of the interactions between wind-optimal tracks in order to assess their feasibility from an air traffic control perspective.

Once the In Trail Climb procedure is fully implemented, the method defined in this thesis may be used to check the effectiveness of the procedure in reducing inefficiency due to blocking.

# APPENDIX A. FLIGHT TRACK SOURCE

The FlightAware API is named FlightXML2.0 and offers a host of access options for a small fee per server query. One of the options provides a snapshot-like search of a user-defined area, meaning that all flights in the FlightAware database within the search parameters are captured and returned at the specific moment the FlightAware database is queried. Data is removed from the servers after 24-48 hours so we created a Python script to automatically collect data on a schedule.

We defined search parameters by latitude, longitude, and altitude limits and used one search region per airspace region. The definitions of the search regions are defined in Table 13. We set the timing periods for querying the server based on the amount of time it would take an average aircraft to traverse an edge of the search region. To capture the correct traffic, we set the edges of each search box to contain the routes of the airspace such that airways of interest traversed an edge or longer distance. Figure 41 shows the placement of the search boxes relative to the airways.

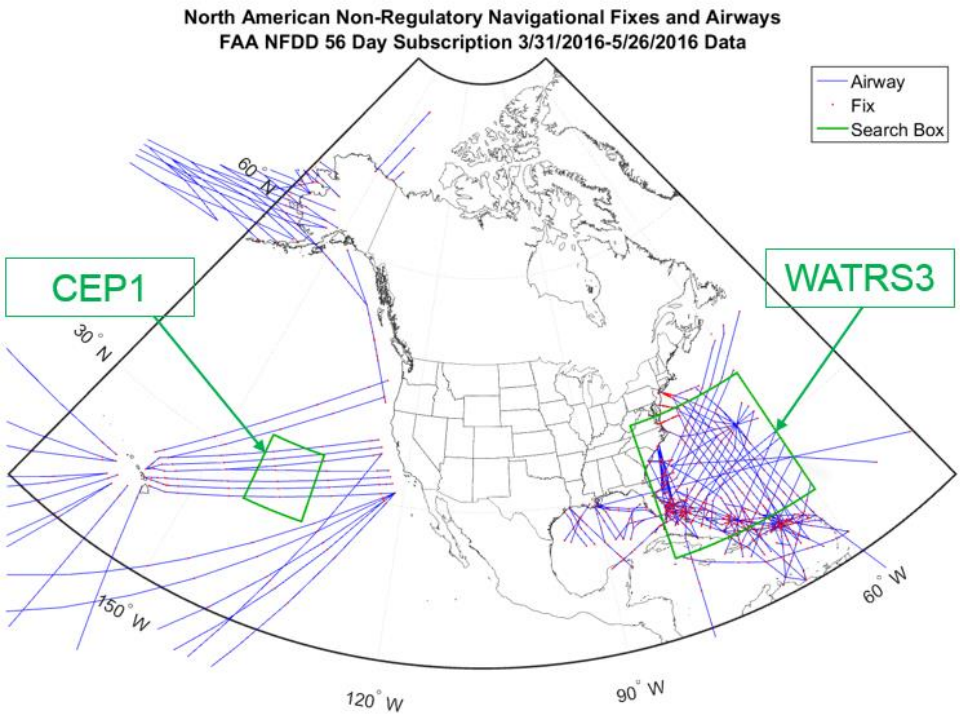


Figure 41: Search Box Locations

Table 13: Search Box Definitions

| Region Name | Latitude | Longitude | Altitude | Polling Period |
|---|---|---|---|---|
| WATRS3 | 20˚N - 38˚N | 81˚W - 60˚W | Above FL 290 | 2 hours |
| CEP1 | 25˚N - 34˚N | 143˚W - 134˚W | Above FL 290 | 1 hour |

After each search call, we transfer the search data into a software queue in addition to saving a file copy. We wait 16 hours to ensure all the searched flights have landed, after which we pull the data from the queue and poll the server's GetHistoricalTrack function with the flight IDs contained in the queue to obtain a track for each flight. Each flight track point contains the data shown in Table 14.

Table 14: Flight track point data format

| Data Type | Description |
|---|---|
| Timestamp | POSIX timestamp (seconds since 0000 UTC Jan. 1 1970) |
| Latitude | Degrees |
| Longitude | Degrees |
| Altitude | Thousands of ft.<br>(Pressure Altitude if above FL180 over USA) |
| Groundspeed | Knots |
| Altitude Status | Indicates if climbing or descending |
| Update Type | Indicates FlightAware's data source. |

.

# APPENDIX B. WEATHER DATA SOURCE

Our source for wind data is the Global Forecast System (GFS), a public and free data source that generates a gridded forecast and analysis for the entire globe. The National Centers for Environmental Prediction host the output from GFS on servers, which include the data from the latest run of the model to roughly two weeks before the day of access. Each model run outputs a zero-time analysis as well as forecasts for every 3 hours out to 180 hours after model runtime. The data is organized in 3-D grids of varying resolution with latitude, longitude, and pressure level as the grid axes.

Initially, we chose the 0.5˚x 0.5˚ grid output due to its increased vertical resolution of 47 pressure layers versus the 0.25˚x 0.25˚ grid with a lower vertical resolution of 26 pressure layers. After working with the datasets for some time, we realized we could use the 0.25˚x 0.25˚ grids by up-sampling and shuffling in the extra vertical layers from the 0.5˚x 0.5˚ grids.

The GFS output is provided in a native binary format, GRIB2, so we access the data through an external MATLAB module called NCTOOLBOX. To mitigate slow access times due to the large file size, we load and shape the data into grids which we use with MATLAB's native griddedInterpolant format, which allows for simple interpolation across latitude, longitude, and pressure level.

Aircraft use altimeters that convert pressure into an altitude reading. Indicated altitude therefore changes with local atmospheric pressure even when an aircraft maintains a fixed geometric height above the surface. For this reason, aircraft are required to set their altimeters to a common datum of 29.92 inHg when climbing above 18,000 ft. to maintain consistent altitude readings between locally situated aircraft. When altimeters are set to 29.92 inHg, the indicated altitude is referred to as Pressure Altitude and can be converted to atmospheric pressure using (National Weather Service 2016):

$$P = 101325e^{\frac{1}{0.190284}\ln\left[1-\frac{h_{press}}{145366.45}\right]} \quad (51)$$

Where $h_{press}$ is the pressure altitude in ft. and $P$ is the pressure in Pa.

Conversion of altitude to pressure allows us to place flight track points vertically in the weather grids, enabling simple interpolation.

# APPENDIX C. CEP INEFFICIENCY HISTOGRAMS

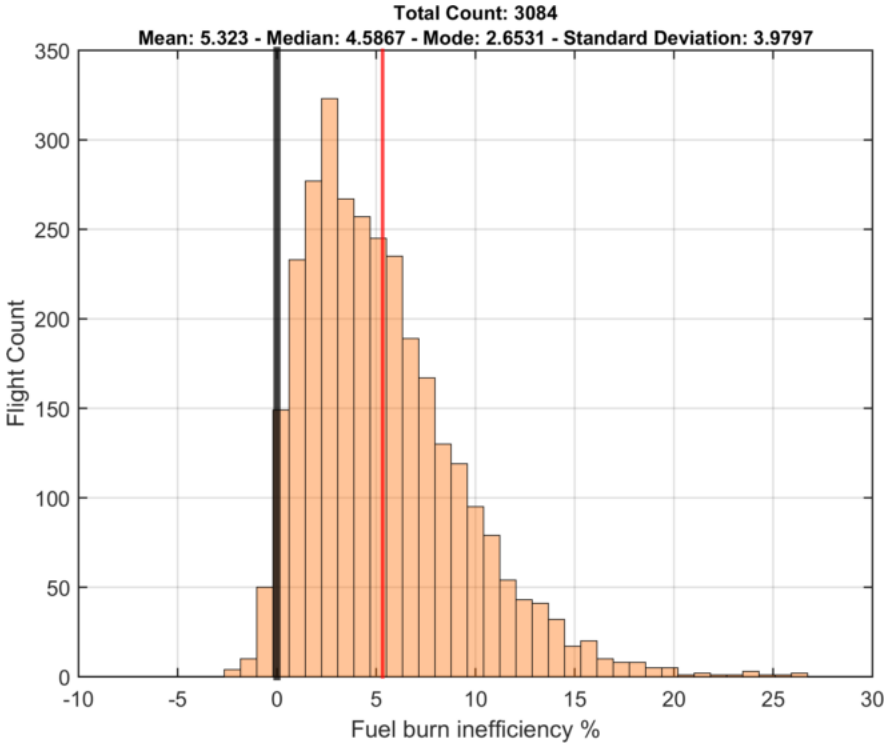


Figure 42: CEP Global Best inefficiency distribution

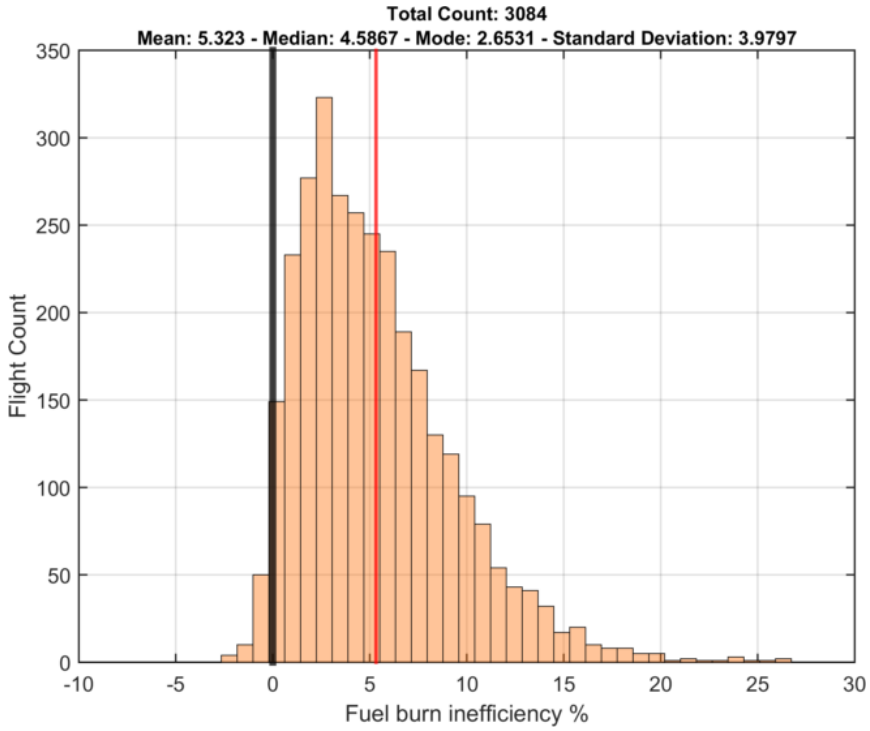


Figure 43: CEP Global Best Legal inefficiency distribution

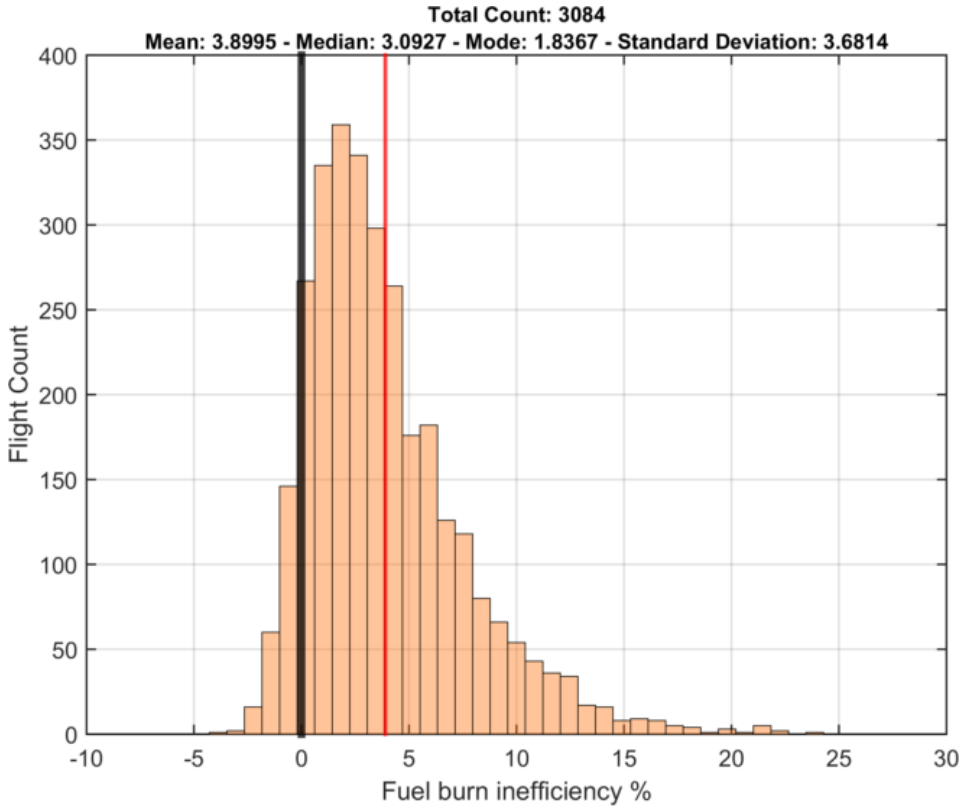


Figure 44: CEP Best Altitude inefficiency distribution

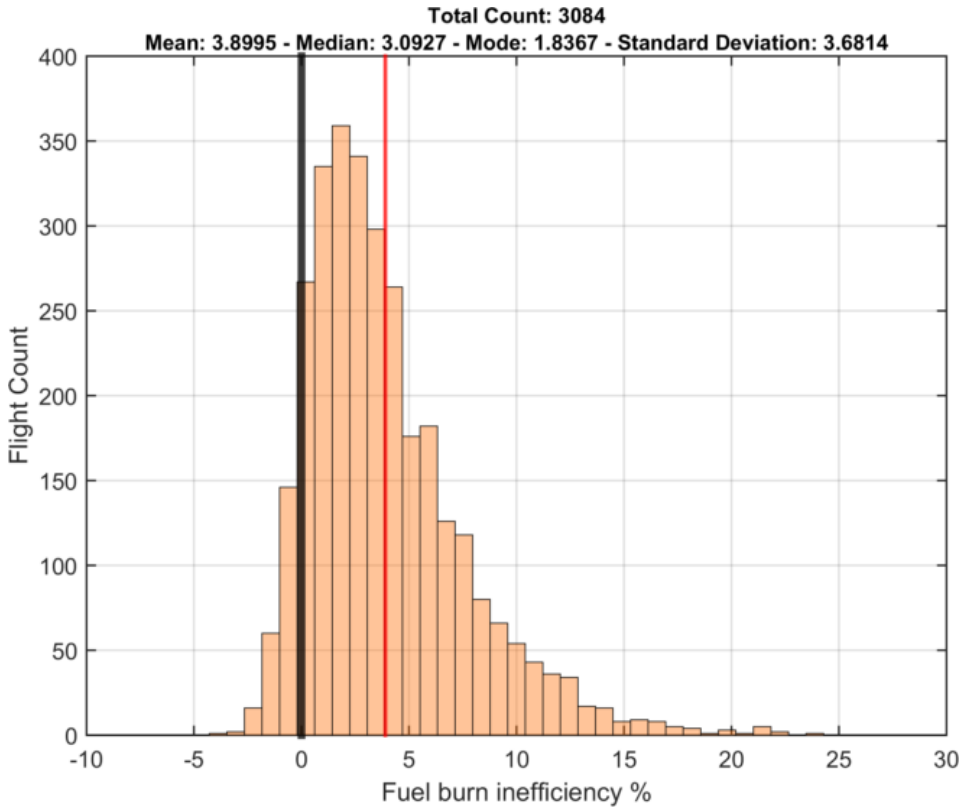


Figure 45: CEP Best Legal Altitude inefficiency distribution

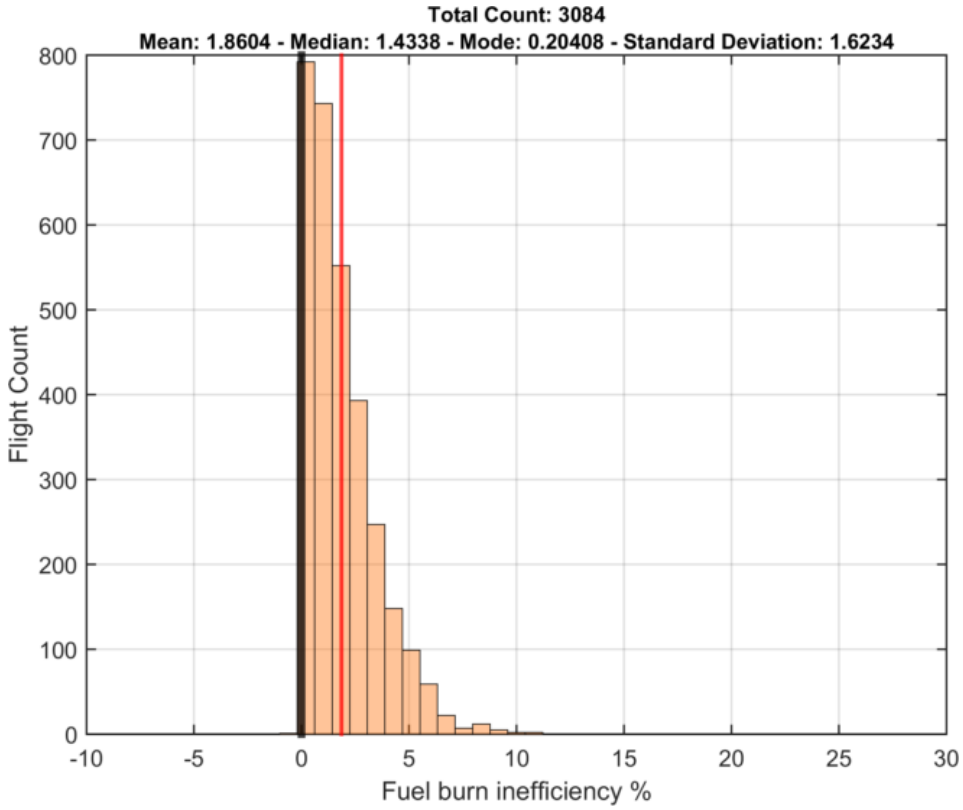


Figure 46: CEP Best Mach inefficiency distribution

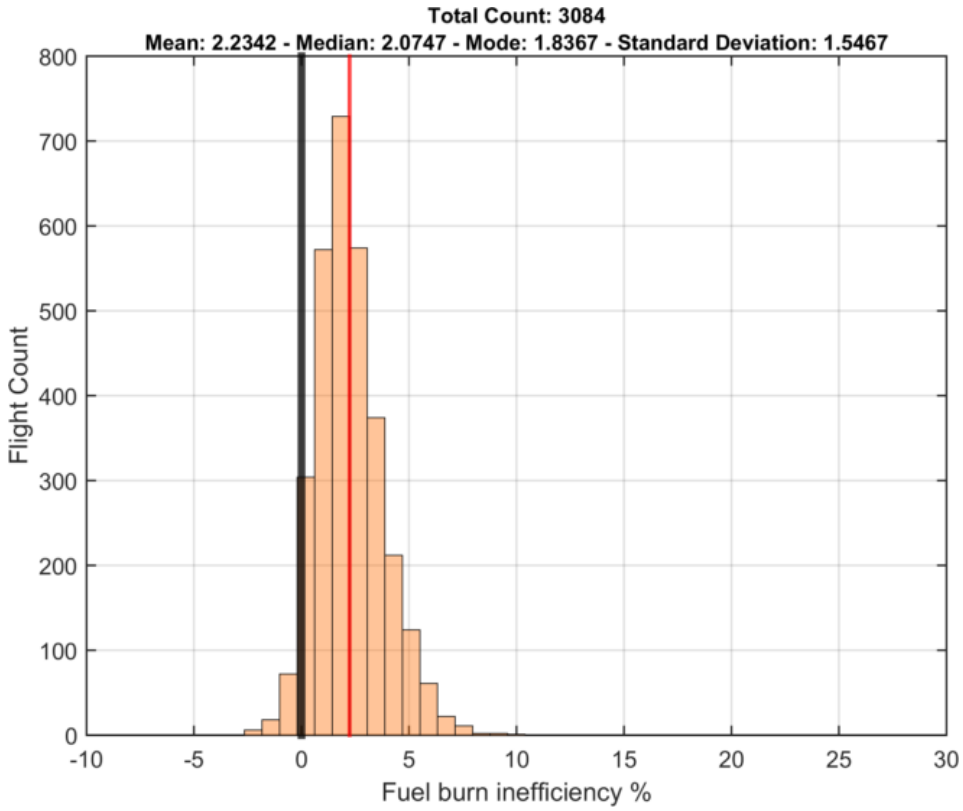


Figure 47: CEP Best Next Highest inefficiency distribution

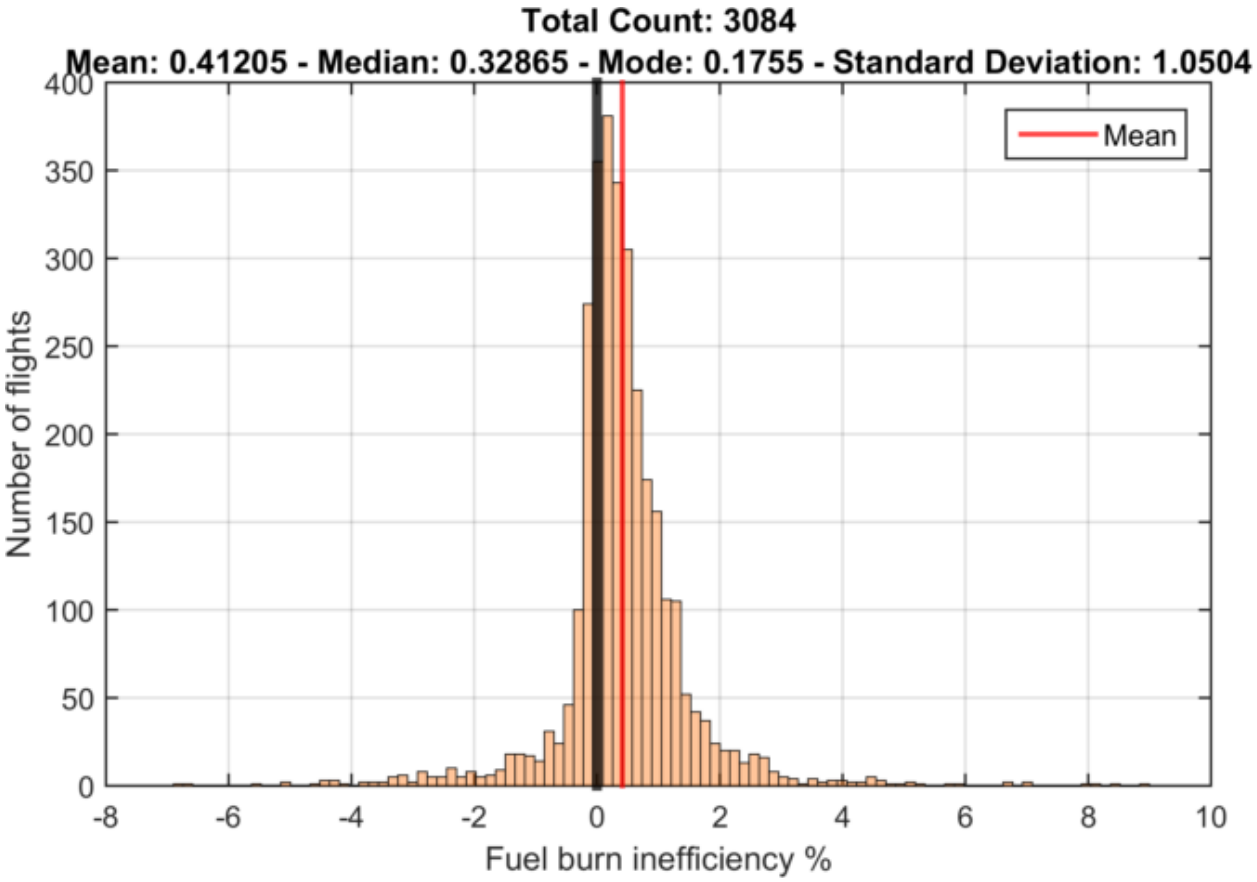


Figure 48: CEP Horizontal inefficiency distribution

# APPENDIX D. WATRS INEFFICIENCY HISTOGRAMS

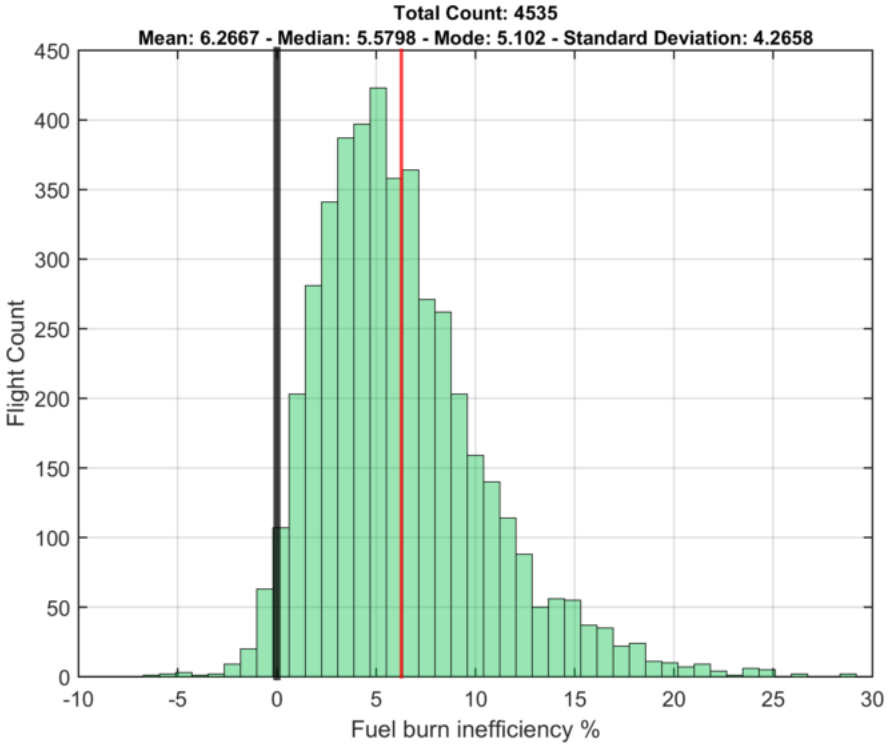


Figure 49: WATRS Global Best inefficiency distribution

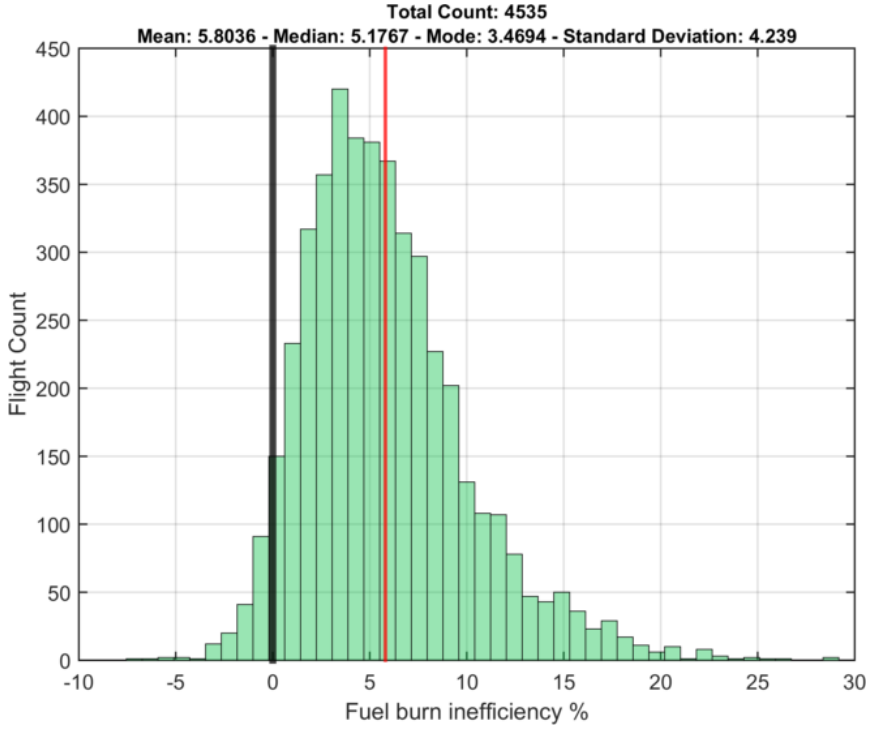


Figure 50: WATRS Global Best Legal inefficiency distribution

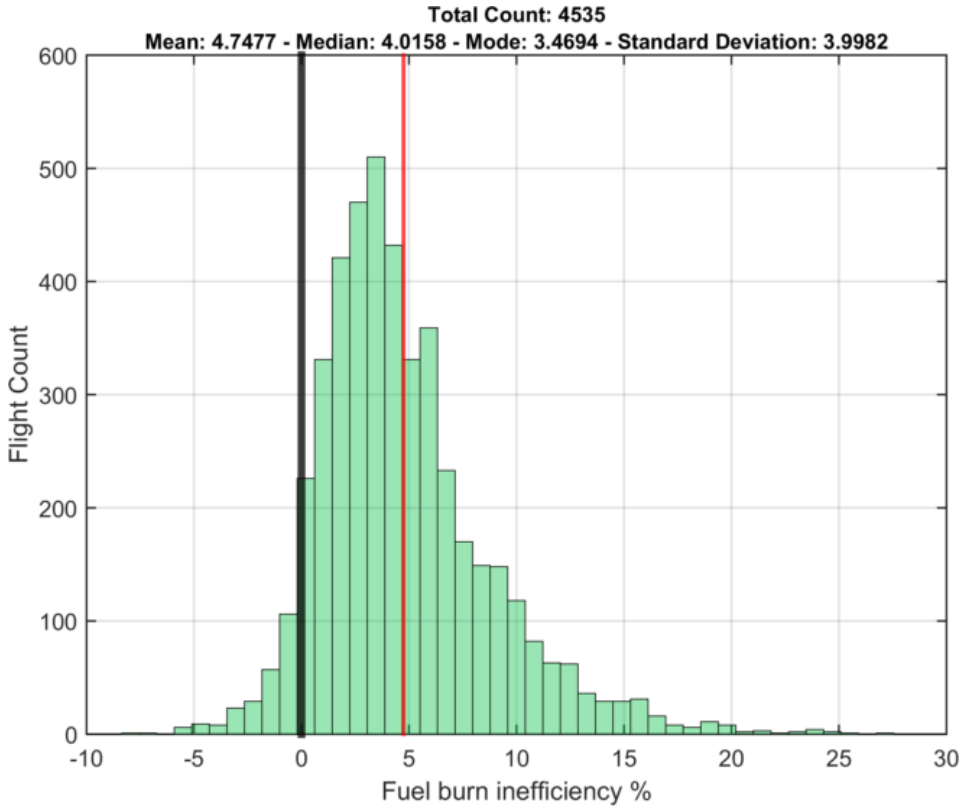


Figure 51: WATRS Best Altitude inefficiency distribution

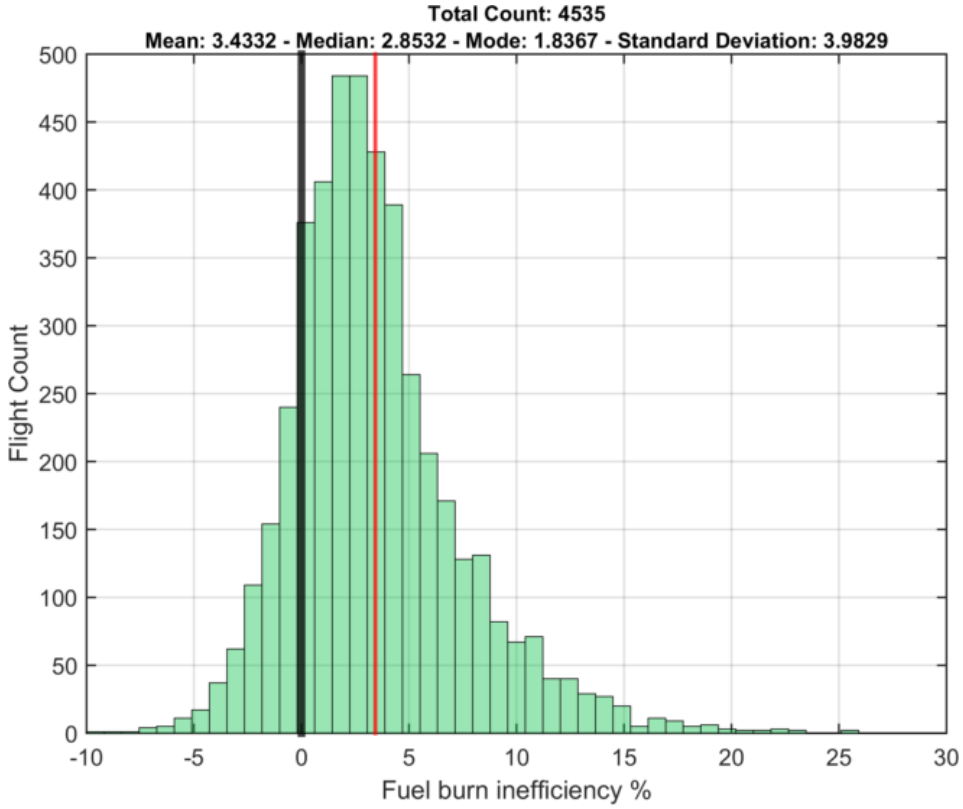


Figure 52: WATRS Best Legal Altitude inefficiency distribution

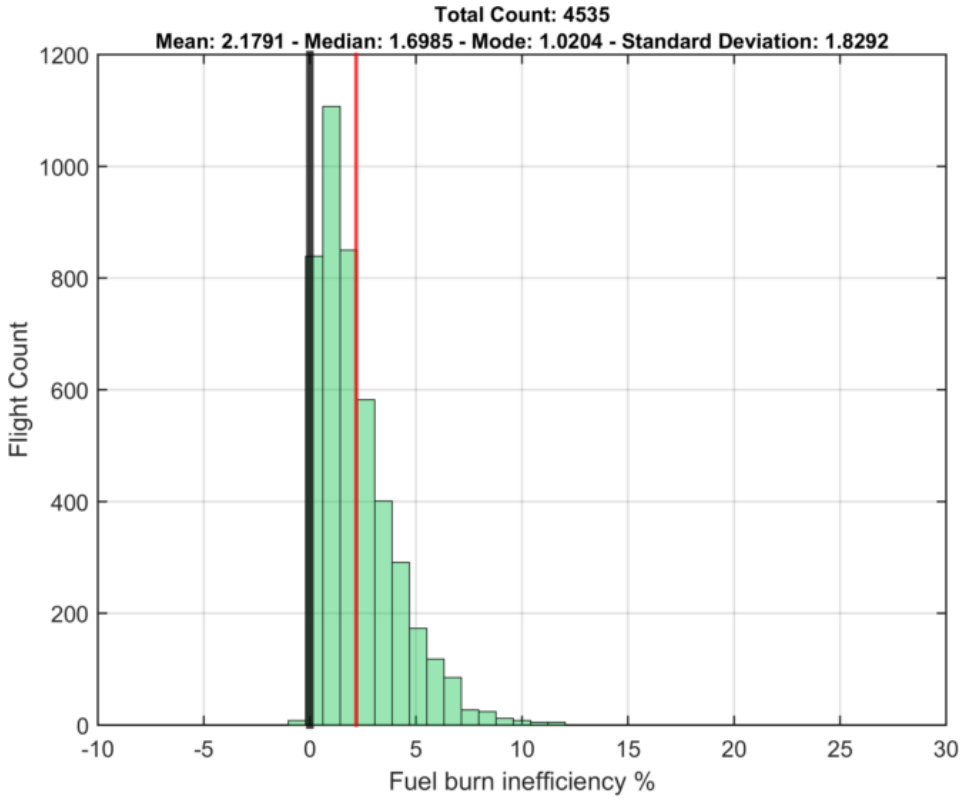


Figure 53: WATRS Best Mach inefficiency distribution

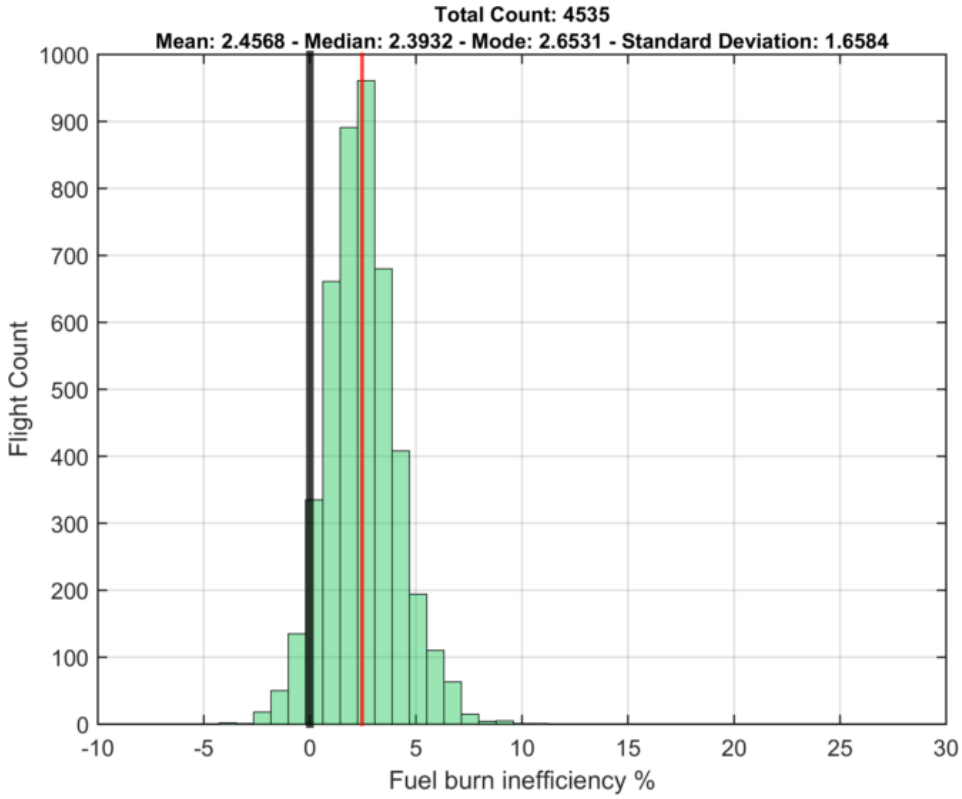


Figure 54: WATRS Best Next Highest inefficiency distribution

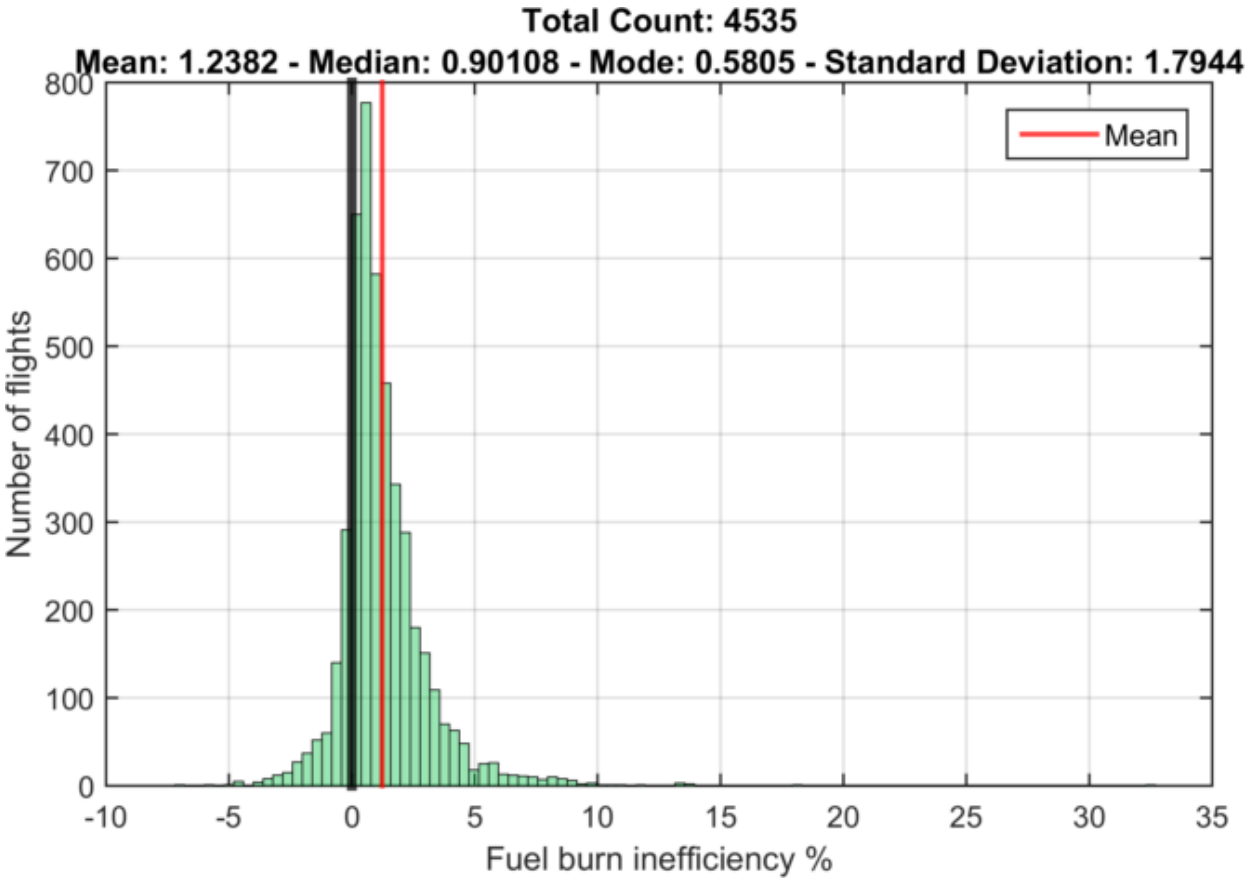


Figure 55: WATRS Horizontal inefficiency distribution

# REFERENCES

Belobaba, P, Odoni, A. R., Barnhart C., Eds., The Global Airline Industry, vol. 23. John Wiley
& Sons, 2009.

Bijlsma S J. Optimal Aircraft Routing in General Wind Fields. Journal of Guidance, Control, and Dynamics. 2009;32:1025-1028.

Bilimoria K, Lee H. Analysis of Aircraft Clusters to Measure Sector-Independent Airspace Congestion. AIAA 5th Aviation, Technology, Integration, and Operations Conference, Sep 2005.

Bryson, A. E., Ho, Y. C., Applied Optimal Control. Taylor and Francis, Levittown, PA, 1975.

Burrows, J. W., Fuel-Optimal Aircraft Trajectories with Fixed Arrival Times. Journal of Guidance, Control, and Dynamics, Vol. 6, No. 1 (1983), pp. 14-19.

Campbell S E, Bragg M B, Neogi N A. Fuel-optimal Trajectory Generation for Persistent Contrail Mitigation. Journal of Guidance, Control, and Dynamics. 2013;36:1741-1750.

Chatterji, G., Fuel Burn Estimation Using Real Track Data. 2012, 11th AIAA ATIO Conference.

Cook, A., Tanner, G., Williams, V., Meise, G., "Dynamic cost indexing - Managing airline delay costs," *J. Air Transp. Manag.*, vol. 15, no. 1, pp. 26–35, 2009.

Dalmau, R., Prats, X., Fuel and time savings by flying continuous cruise climbs: Estimating the benefit pools for maximum range operations. Transportation Research 2015;Part D 35:62-71

Delahaye D, Puechmorel S. Modeling and Optimization of Air Traffic. John Wiley & Sons, 2013. ISBN: 978-1-84821-595-5.

Federal Aviation Administration, "Air Traffic Control," Order 7110.65W, Oct. 27 2015.

Federal Aviation Administration (FAA). System for assessing Aviation's Global Emissions: Technical Manual (FAA-EE-2005-01). 2005.

Grabbe, S., Sridhar, B., Cheng, N., Central East Pacific Flight Routing, AIAA Guidance, Navigation, and Control Conference and Exhibit. Aug. 2006

Grabbe S, Sridhar B, Mukherjee A. Central East Pacific Flight Scheduling. AIAA Guidance, Navigation and Control Conference and Exhibit. Aug 2007

Green S, Bilimoria K, Ballin M. Distributed Air/Ground Traffic Management for En Route Flight Operations. Air Traffic Control Quarterly, Vol. 9, No. 4, 2001, pp. 259–285.

Gwiggner C, Nagaoka S. Data and queueing analysis of a Japanese air-traffic flow. European Journal of Operations Research. 2014;235:265-275.

FAA, Automatic Dependent Surveillance – Broadcast (ADS-B) In-Trail Procedures (ITP) Operational Flight Trial Project Status. IPACG/40, IP/09, Sep. 2014

Hansen M, Nikoleris T, Lovell D, Vlachou K, Odoni A. Use of queuing models to estimate delay savings from 4D Trajectory Precision. ATM2009.

Hemdal, H. Cancellation of FAA Order JO 7110.661, Automatic Dependent Surveillance Broadcast (ADS-B) In-Trail Procedure (ITP) [Memorandum], Washington, DC: Federal Aviation Administration. June 6, 2016.

IATA. Economic Performance of the Airline Industry. June 2016. http://www.iata.org/whatwedo/Documents/economics/Central-forecast-mid-year-2016-tables.pdf Last accessed 10/27/2016

ICAO, Annex 2 Rules of the Air. Tenth Edition, July 2005. http://www.icao.int/Meetings/anconf12/Document%20Archive/an02_cons%5B1%5D.pdf Last accessed 11/2/2016

ICAO, Global Operational Data Link Document (GOLD), Second Edition, 26 April 2013. http://www.skybrary.aero/bookshelf/books/2411.pdf Last accessed 10/27/2016

Jelinek, F., Carlier, S., et. al, "The EUR RVSM Implementation Project Environmental Benefit Analysis," EEC/ENV/2002/008, October 2002.

Jensen L. Fuel Efficiency Benefits and Implementation Considerations for Cruise Altitude and Speed Optimization in the National Airspace System. MIT 2011.

Kelly K. Assessment of a Global Contrail Modeling Method and Operational Strategies for Contrail Mitigation. MIT 2005, https://dspace.mit.edu/handle/1721.1/32460, Last accessed, 10/27/2016

Korn B, Edinger C, Tittel S, Kügler D, Pütz T, Hassa O, Mohrhard B. Sectorless ATM – A concept to increase en-route efficiency. Oct 2009. Digital Avionics Systems Conference.

Laudeman I, Shelden S, Branstrom R, Brasil C. Dynamic Density: An Air Traffic Management Metric. NASA/TM – 1998-112226.

Lee K, Feron E, Pritchett A. Air Traffic Complexity: An input-output approach. American Control Conference, 2007. 474-479.

Longuski J, Guzmán J, Prussing J. Optimal Control with Aerospace Applications. New York. Springer, 2014.

Lissys, Piano-X User Guide, 2008, http://www.lissys.demon.co.uk/piano-x-guide.pdf, Last accessed, 10/27/2016

Lissys, Piano 5 User Guide, http://www.lissys.demon.co.uk/pug/, Last accessed, 10/27/2016

Malwitz A, Yoder T, Balasubramanian S, Fleming G, and Waitz I. Assessment of the impact of reduced vertical separation on aircraft-related fuel burn and emissions for the domestic United States. Partnership for AiR Transportation Noise and Emissions Reduction. Nov 2007. Report No. PARTNER-COE-2007-002.

Marais K B, Reynolds T G, Uday P, Muller D, Lovegren J, Dumont J-M, Hansman R J, "Evaluation of potential near-term operational changes to mitigate environmental impacts of aviation," *Proc. Inst. Mech. Eng. Part G J. Aerosp. Eng.*, Jul. 2012.

Masalonis A, Callaham M, Wanke C. Dynamic Density and Complexity Metrics for Realtime Traffic Flow Management. 2003. MITRE Corporation.

Mathworks. bvp4c. http://www.mathworks.com/help/matlab/ref/bvp4c.html. Last accessed 10/27/2016

National Weather Service, Southern Region Headquarters. Pressure Altitude. https://www.weather.gov/media/epz/wxcalc/pressureAltitude.pdf, Last accessed on 10/27/2016

Ng H, Sridhar B, Grabbe S, Chen N. Cross-Polar Aircraft Trajectory Optimization and the Potential Climate Impact. 30th Digital Avionics Systems Conference. October 2011.

Ng H, Sridhar B, Grabbe S. Optimizing Aircraft Trajectories with Multiple Cruise Altitudes in the Presence of Winds. Journal of Aerospace Information Systems, 2014.

Palacios, Rafael, and R. John Hansman. "Filtering Enhanced Traffic Management System (ETMS) Altitude Data." Metrology and Measurement Systems 20, no. 3 (n.d.). © 2013 Polish Academy of Sciences

Prandini M, Piroddi L, Puechmorel S, Brázdilová. Toward Air Traffic Complexity Assessment in New Generation Air Traffic Management Systems. IEEE Transactions on Intelligent Transportation Systems, Vol. 12, No. 3, Sep 2011.

Puechmorel S, Delahaye D. New Trends in Air Traffic Complexity. EIWAC 2009. Tokyo, Japan.

Revision Summary Document for the Base of Aircraft Data (BADA) Revision 3.7, EUROCONTROL EEC Technical/Scientific Report No. 2009-004, Brussels, March 2009.

Reynolds T G. Air traffic management performance assessment using flight inefficiency metrics. Transport Policy 2014;34:63-74

SESAR, The ENGAGE Corridor – Phase 2 Deliverable Report, 2011, http://www.sesarju.eu/sites/default/files/documents/reports/AIRE_-_The_Engage_Corridor.pdf?issuusl=ignore, Last accessed 10/27/2016

Sridhar B, Chen N, Ng H, Rodionova O, Delahaye D, Linke F. Strategic Planning of Efficient Oceanic Flights. Eleventh USA/Europe Air Traffic Management Research and Development Seminar, 2015.

User Manual for the Base of Aircraft Data (BADA), Revision 3.11, EUROCONTROL EEC Technical/Scientific Report No. 13/04/16-01, Brussels, May 2013.

Williams A, Greenfeld I. Benefits assessment of reduced separations in North Atlantic organized track system. Presentation. CSSI Inc., Advanced Programs, 400.

Yoder T. Development of Aircraft Fuel Burn Modeling Techniques with Applications to Global Emissions Modeling and Assessment of the Benefits of Reduced Vertical Separation Minimums.
MIT 2007, https://dspace.mit.edu/handle/1721.1/39713

Zermelo E. Über die Navigation in der Luft als Problem der Variationsrechnung. Jahresbericht der Deutschen Mathematiker-Vereinigung. Vol. 39, 1930, pp. 44–48.

Operations of civil aircraft of U.S. registry outside of the United States, 14 C.F.R. § 91.703 (2016)